2002

Markov-like models for nonlinear loads in distribution systems

Feng Chen
Iowa State University

Markov-like models for nonlinear loads in distribution systems

by

Feng Chen

A dissertation submitted to the graduate faculty

in partial fulfillment of the requirements for the degree of

DOCTOR OF PHILOSOPHY

Major: Electrical Engineering (Electric Power)

Program of Study Committee:
Subrahmanyam S. Venkata, Major Professor
Vedula V. Sastry
James D. McCalley
Venkataramana Ajjarapu
William Q. Meeker

Iowa State University

Ames, Iowa

2002

UMI Number: 3051451

UMI Microform 3051451

ProQuest Information and Learning Company
300 North Zeeb Road
P.O. Box 1346
Ann Arbor, MI 48106-1346

Graduate College
Iowa State University

This is to certify that the doctoral dissertation of

Feng Chen

has met the dissertation requirements of Iowa State University

Signature was redacted for privacy.

Major Professor

Signature was redacted for privacy.

For The Major Program

Find Wonder at the Apex

——My father, Minghui

TABLE OF CONTENTS

LIST OF FIGURES

LIST OF TABLES

ACKNOWLEDGEMENTS

First of all, my sincere thanks must go to my major professor Dr. S.S. (Mani) Venkata for providing me the opportunity to work with him, for offering me his valuable advice, guidance, patience and for continuously supporting me during my stay at Iowa State University.

I would also like to express my gratitude to my co-advisers, Dr. Krishna B. Athreya and Dr. Vedula V. Sastry, who grant me their inspiring ideas, helpful comments, feedbacks, time and efforts during the course of the research project. I am also very grateful to my graduate committee members—Dr. James D. McCalley and Dr. Venkataramana Ajjarapu and Dr. William Q. Meeker. Their thoughtful suggestions and generous assistance are of great help to this research.

My fellow students, Nagaraj, Jang, Qiming, Jun, Xuezhen, Wenzhen, Yuan and many others in my memory, made my stay here even more enjoyable and fruitful. Thank you, guys.

Specially, I wish to say thanks to my wife, Fen. Her encouragement, support, understanding and precious love equip me to meet every difficulty. I also owe thanks to my mother Xiuying, my sister Ling and my brother Ping, who stand behind me all the time, despite the physical distance.

I would like to dedicate this dissertation to my dear father. Although he is at the other end of the world, I know he still cares for me, loves me.

This is a research project sponsored by National Science Foundation, to whom grateful acknowledgement is due. It is jointly undertaken with Arizona State University (ASU). Thanks to Professor G. T. Heydt and Professor E. Kostelich of ASU for their useful suggestions and discussions during the course of this investigation.

1 INTRODUCTION

Most of the systems in this world are nonlinear systems. By definition [1], a nonlinear system refers to a set of nonlinear equations (algebraic, difference, differential, integral, functional, or abstract operator equations, or a combination of some of these) used to describe a physical model (device, process, or structure) that otherwise cannot be well defined by a set of linear equations of any kind. Such a system may also depend on some variable parameters. If there is a unique consequence to every change of the system parameters or initial states, the system is deterministic. On the other hand, it is random or stochastic according to some probability distribution if there is more than one possible consequence for a change in its parameters or initial states. When the nonlinear system is deterministic and simple, it can be approximated by linear equations around an equilibrium point without losing too much of an accuracy. But for some complex systems such as nonlinear electric circuits, weather forecasting, orbits of satellites, chemical reactions, and spread of diseases, people have difficulty to find ways of formulating the nonlinear puzzle. Even worse, sometimes a nonlinear system is very difficult to be represented with equations and parameter identification. The only information that may be available about the system is its structure and time/frequency domain measurements. For example, current and voltage data for some highly nonlinear loads, such as Electric Arc Furnace (EAF), can be measured, but a precise mathematical model is hard to formulate. The observations on such a nonlinear system are generally called "nonlinear time series".

Developing a proper model that could accurately represent highly nonlinear loads under various operating conditions is very useful for power system planning and operation. It can help understand the mechanisms that govern their operation, and design effective controls to improve their performance [2]. Classical models with constant parameter representation, such as $R(t)=v(t)/i(t)$ for a resistor and $v(t)=d/dt\ [(L(t)i(t)]$ for an inductor, have been long used for power system studies. But for large, nonlinear, highly varying industrial loads such as steel rolling mills, plasma torches, EAFs, adjustable speed drives under certain loads and pumps under varying physical loads, it is difficult to describe them in such a straightforward form

because of their non-linearity. The current through and voltage cross these loads have variations in magnitude and/or even in frequency, which may cause flicker and introduce harmonics, and significant power quality problems in a power system [3]. Therefore, the task of modeling such a kind of load is challenging and an approach for a nonlinear time series based analysis making use of stochastic/statistical theories is considered to be novel for this purpose. In all, modeling, analysis and prediction of highly varying time series that appear in power systems will be addressed in this dissertation, taking EAF load as an example.

1.1 Power System Load Models

In general, power system load models can be divided into three categories, static load models, dynamic load models and composite load models (static and dynamic). Static load model is suitable for the condition when the system frequency f and bus voltage magnitude V do not vary abruptly. It expresses the active and reactive powers (P_s and Q_s) at any instant of time as functions of V and/or f at the same time. Here is an exponential model [4].

$$P_s = P_0 (V / V_0)^{\alpha_s} [1 + K_{pf} (f - f_0)] \tag{1.1}$$

$$Q_s = Q_0 (V / V_0)^{\beta_s} [1 + K_{qf} (f - f_0)] \tag{1.2}$$

where f_0 and V_0 are nominal values for frequency and voltage

α_s (0.5~1.8), β_s(1.5~6), K_{pf}(0~3) and K_{qf}(-2~0) are coefficients

On the other hand, dynamic load model expresses the active and reactive powers at any instant of time as functions of the voltage magnitude and/or frequency at past instants of time and in general the present instant of time as well. These models represent real power (P_d) and reactive power (Q_d) of the load as the functions of voltage or frequency or their combination. Since motors consist of 60% to 70% of the total loads in a power system, their dynamic characteristics are the most significant aspects of the dynamic load and should be studied with greater detail. One of these models is a first order recovery model that captures load restoration characteristics. It is expressed in state space form [5]:

$$\dot{x}_p = P_s(V) - P_d \tag{1.3}$$

$$\dot{x}_q = Q_s(V) - Q_d \tag{1.4}$$

$$P_d = x_p / T_p + P_t(V) \tag{1.5}$$

$$Q_d = x_q / T_q + Q_t(V) \tag{1.6}$$

where T_p, T_q are recovery time constants.

x_p, x_q are state variables, such as voltage and current of the load.

$P_s(V)$, $Q_s(V)$ and $P_t(V)$, $Q_t(V)$ are real power and reactive power for the static and transient load characteristics respectively.

$$P_s(V) = P_0(V / V_0)^{\alpha s}, \qquad Q_s(V) = Q_0(V / V_0)^{\beta s} \tag{1.7}$$

$$P_t(V) = P_0(V / V_0)^{\alpha t}, \qquad Q_t(V) = Q_0(V / V_0)^{\beta t} \tag{1.8}$$

here α_t, β_t, α_t and β_t are exponential parameters for transient load model.

The composite load models are actually based on the combination of the previous two models. Figure 1.1 shows such a model for an industrial load (a electric fan may need such a model).

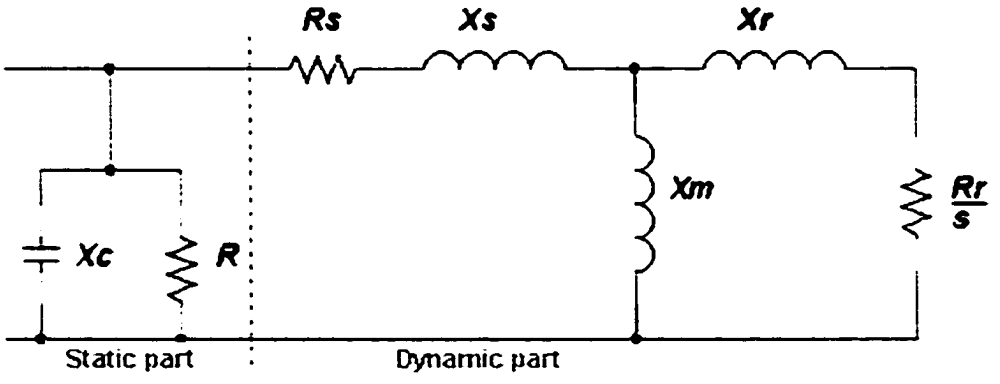

Figure 1.1 Composite load model for an industrial load

To determine the load model, there are two traditional approaches [6]: component based approach and measurement based approach. Component based approach models the

load on the basis of familiarity with static and dynamic behavior of all the individual loads and load components of a particular load bus. While measurement based approach uses system identification technology to estimate a proper model and its parameters. The component based approach maybe efficient in modeling a single load or a small number of loads. But it will encounter difficulties when evaluating the characteristics of a large variety of components. Moreover, there exist some difficulties even when the same type of load operates under different conditions (voltage level, load level). Measurement based approach requires measurement at various load buses to determine the appropriate model structure and parameters. It comes from direct measurement of real load behavior and may give better modeling results than the component based one.

1.2 EAF as a Highly Non-linear Load

The previous models may be weak when encountering the highly non-linear loads, such as EAFs. EAFs are widely used in today's steel, aluminum and other industries. They can be either alternating current (ac) or direct current (dc) type. The dc units consume less energy and need fewer electrodes, but they are more expensive than the ac units. Building an electric furnace is much cheaper and faster than to build a green-field integrated steel plant (which uses coke ovens, blast furnaces, or the more recent technology—Corex—to produce liquid iron). However, when the EAFs are used for melting scrap and/or pre-reduced metals such as aluminum, copper, lead and high-grade alloy steel, the position and length of the electrodes change frequently and the arc-length is time variant with the random movement of scrap. Thus the consumed power is also varying with time and the current waveform looks quite non-sinusoidal. Figure 1.2 shows how real power varies to bus voltage variation in an EAF. Each point in the figure symbolizes the voltage magnitude and real power of a cycle. The relationship between them is pretty confusing and beyond any algebraic expression.

In addition, arc furnace operation may be classified into stages, depending on the status of the melt and the time lapse from the initial energization of the unit. During the melting period, scraps of steel nearly create a short circuit on the secondary side of the furnace transformer. This creates large fluctuations on current. Consequently, the current fluctuations

cause variations in reactive power, which lead to flicker or a momentary drop in voltage, both at the supply bus and at nearby load centers in an interconnected system. The arc currents are more uniform during the operation of the refining period, and have less of an impact on the power quality of the system. Arc furnaces are also responsible for injection of harmonic load currents and asynchronous spectral components, which in turn cause excessive losses in transformers. The complex arcing process is assumed to be stochastic in nature [7-9] based on its features above. As a consequence, the EAF load cannot be adequately represented by a deterministic load model. Due to this reason, although the electric arc furnace has been studied for many years, a complete representation of such a load and its impact on the power system still appears to be an unresolved problem. Accordingly, stochastic/probabilistic modeling techniques become more and more important to study the behavior of an EAF in a power system.

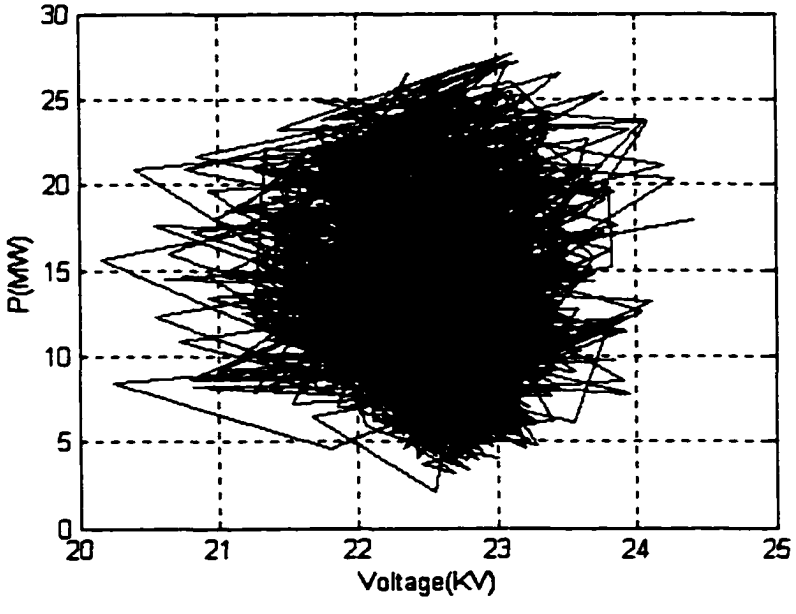

Figure 1.2 Real power as a function of bus voltage for an EAF

1.3 Problem Statement

As indicated in preceding sections, the nonlinear systems are complex and their time series look quite chaotic. For instance, Figure 1.3 shows a simplified circuit equivalent of an ac electric arc furnace, and Figure 1.4 illustrates a representative waveform of an arc current during the melting period [10]. Irregular characteristics of a highly nonlinear time series in a power system (such as EAF current) waveform include:

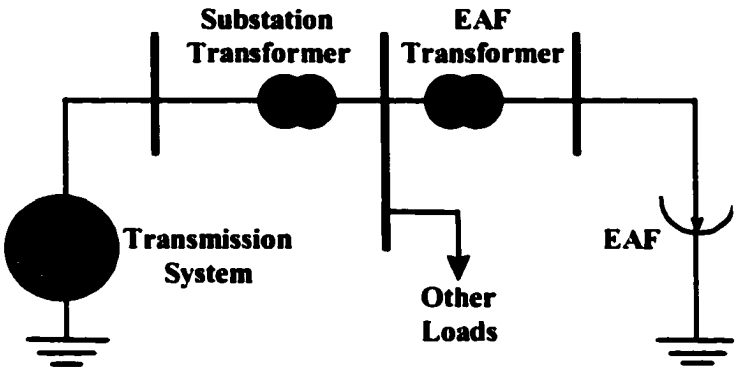

Figure 1.3 Pictorial of an EAF installation

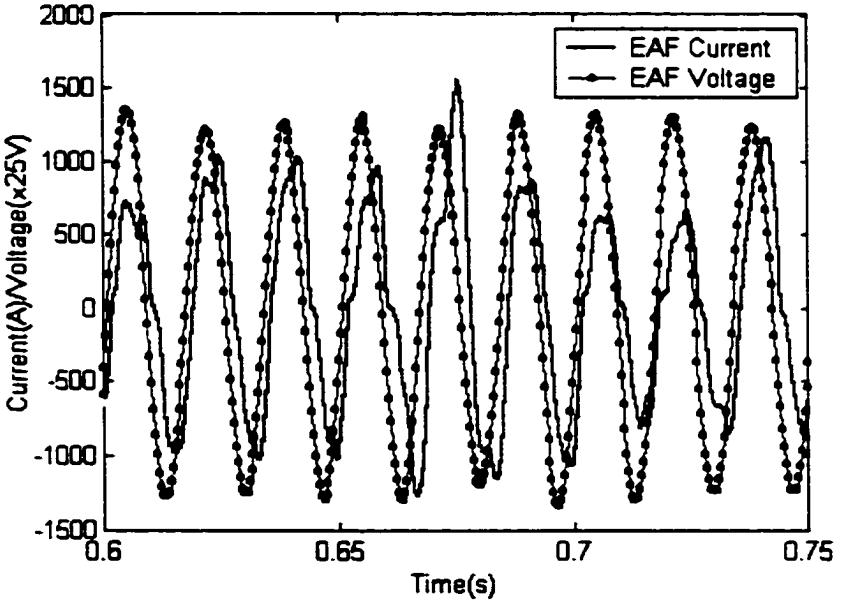

Figure 1.4 Measured current/voltage time series in an ac EAF

- There is some kind of periodicity due to the ac power source (with 60 Hz of system frequency in the Unite States).
- The amplitudes (or peak values) of all the cycles during the whole process are different from each other. Sometimes they reach to a very high value, sometimes they may be closer to zero.
- The frequency (or period) of each cycle changes randomly, but the average frequency is not very much different from the frequency of driving source voltage (such as 60Hz). For the EAF current, it fluctuates around system frequency 60 Hz with the range of ±15%, while the average frequency is 60 Hz.
- The shape of time series waveform also varies from time to time. It is far from a normal sinusoid waveform, and no pattern can be easily found.

Summarizing, the characteristics of the nonlinear time series in a power system are similar to that of a white noise in the respect of randomness. However, it has a dominant periodicity because of the driving power source.

But accurate modeling of such a nonlinear system is indeed necessary even without resorting to deterministic equations, as described in Section 1.2. The dynamic behavior underlying time response of an electric arc furnace is an important application area because of the impact of these large, highly varying loads on the power quality of an interconnected power system. There is a need for an accurate and versatile model for a highly varying load, because most current models only address to a specific phenomena under narrow operating conditions. New and improved models will help in dealing with the problems caused by the operation of an EAF. The study of electric arc furnaces has potential benefits for electric power utilities. A model that could represent these loads for a wider range of operating conditions in the power system would be very useful for power system analysis, planning and operation. The model would be used in power system analysis software to study the impact of the loads in the system. Mitigating techniques for power quality problems can be designed based on the simulations results of the program. Minimization of the impact of EAFs can improve electrical system efficiency and voltage fluctuations in the distribution system. EAF operators and customers near the EAF site can also benefit from the mitigation of the adverse

effects of EAF operation. When supply voltage is low due to a flicker, EAF current rises for a given operating power level. This rise in current reduces the expected life of EAF electrodes. Therefore, reducing flicker, i.e., reducing the fluctuations that cause flicker, also benefits EAF operators since electrode consumption is less. Reducing the impact of these loads implies that less reactive power is demanded, and more active power can be used in the melting period. This results in an improved load factor and economies of production. Customers nearby the EAF site may also see an improvement in the quality of supply to their house-hold/entertainment systems.

1.4 Organization

The organization of the dissertation is as follows: Chapter 2 gives a review of literature on this topic. The previous approaches with their advantages and disadvantages are presented. Chapters 3 to 5 describe the proposed models for an EAF in detail. After a brief presentation of the Markovian principles and non-parametric techniques, two basic models—a first order Markov-like model and a second order Markov-like model—are discussed in Chapter 3. The models are further generalized to the formulation of a function space approach in Chapter 4 for the purpose of short-range prediction of EAF current/voltage over a few cycles. While Chapters 3 and 4 mainly analyze the characteristics of EAF current, Chapter 5 considers EAF current and voltage together and extends the Markov-like model to such coupled current and voltage phenomenon. In addition, a harmonic compensation scheme based on the proposed model with the best performance is presented in Chapter 6, taking advantage of the previous approach available according to the model. Finally, in Chapter 7 one sees the conclusions of the whole dissertation and suggestions for future work in this area.

2 LITERATURE REVIEW AND RESEARCH OBJECTIVES

A seemingly random behavior that characterizes a nonlinear system makes it difficult to formulate an explicit mathematical model for it. There are standard methods for linear systems, but none for time series relating to such a nonlinear system so far. The latest methods for modeling nonlinear systems are evaluated in the following sections, using EAF load as an example. Thereafter the research objective will be stated.

2.1 Previous Methods For Nonlinear (EAF) Loads

Although electric arc furnace has been an area of study for a few decades and a lot of models have been proposed, a generic model for the analysis of this phenomenon is not available. So far, the methodologies used are: time domain analysis (including stochastic processes [9,12] and algebraic approximations [13,14]), frequency domain analysis [15-17], neural networks and fuzzy logic [18,19], and chaos theory [10,20-25]. These shall be discussed to some detail in the following sections.

2.1.1 Algebraic Approximation Based Model

The classical and empirical modeling of arc furnace has broadly classified the arc operation into two modes [13]. One is the "arcing" mode in which arc length may change due to magneto-hydrodynamic effects. The other is the "extinction" mode of arc, which causes a larger possible fluctuation in load. It is assumed that the ignition voltage is determined by arc length. Then the empirical voltage-current characteristic is approximated by some linear or nonlinear functions.

Trying to follow the same expression style as for parametric models, Acha et.al. proposed nonlinear differential equations for the EAFs and solved them in frequency domain [26]. This approach gives basic simulation results for an EAF. But since it is based on experimental formula, the solution of the nonlinear equations depends on system topology and its operating conditions.

A time domain controlled voltage source based on a piece wise linear approximation of the v-i characteristic of the EAF was proposed in [8]. The active power consumed by the load is also considered in this model. This makes the model dependent on the operating conditions of the load.

Advantages: The principles are simple, direct and can be easily implemented. In some particular operating conditions, this approach may give a good approximation.

Drawbacks: The equations and parameters used are arbitrary. In peculiar to the experimental setup, in most of the cases they didn't reflect the nature of the phenomena. In addition, the v-i characteristic of an EAF is not deterministic and subjects to change during an arcing process. Even for one specific voltage value or change in rate of voltage dv/dt, there exist a wide range of current values corresponding to it, as illustrated in Figure 2.1, which shows 20000 points of v-i characteristics. This cannot be solved by these methods.

2.1.2 Stochastic Process Based Model

The stochastic ideas had originated from the non-periodic, seemingly random and unpredictable behavior of these loads. A common approach is to generate white noise, and modulate it such that it resembles the behavior (current or voltage) of a given EAF. The modulation can be performed through empirical formulae that relate to the arc process for chosen voltage and current levels, or a related v-i characteristic of an actual load [9,27-30]. The dynamic variations of the arc are modeled through a combination of sinusoidal as well as random laws. This approach intends to cover both the deterministic and stochastic nature of the EAF operation. Some researchers have also used the actually recorded terminal quantities or nonlinear time varying resistor models where band-limited white noise and a periodic sinusoidal signal are combined to represent variations in arc length [31,32]. Further, in these models, stochastic process is used to represent the nonlinearity of arc furnaces based on the thought that harmonics are largely due to the arc characteristic, and voltage flicker is the results of a dynamic change in arc length [9].

Besides, system identification technique was used by Collantes and Gómez to study voltage disturbance of an EAF with a stochastic model [33]. Rather than focusing on the

detailed modeling of the v-i characteristic curves of the EAF operation, they concentrated on the modeling of the time dependent signal that modulates the curves. The main conclusion of their study was that the type of used model, static or dynamic, depends on the nature of the analysis desired.

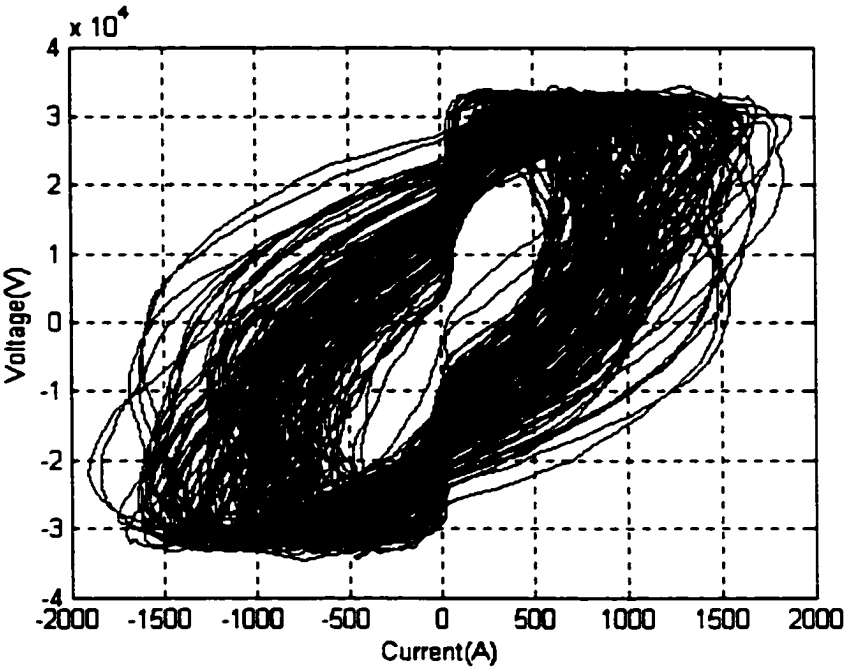

Figure 2.1 Related voltage and current characteristic of an EAF

- Advantages: Most of these approaches use deterministic stochastic process. They can be easily implemented, and requires shorter time for computer simulation. Also, this study recognized that the arc process is stochastic by nature.
- Drawbacks: It cannot accurately represent normal ac arc furnace operation. Most of the techniques use white noise or other stochastic process to approximate the arc voltage, hence, the accuracy cannot be guaranteed. Although some features of arc voltage are similar to white noise, both the driving power source and melting status of the arc furnace affect the nature of arc voltage makes it somewhat different from

white noise. Besides, from the picture shown in Figure 2.1, the relationship between arc current and voltage is not so simple. It needs more justification.

2.1.3 Frequency Domain Model

For the convenience of an iterative harmonic analysis of the voltage disturbance in power systems, Mayordomo et. al. proposed a frequency domain EAF model [15,16]. Using a critical operating point that is defined to discriminate continuous and discontinuous modes of operation, it is claimed to be capable of analyzing arc current for both single-phase and three-phase configurations. Wu et. al. also used frequency domain method to perform harmonic analysis for EAFs [17]. Describing the v-i characteristics of arc in the form of differential equations, the study is performed in frequency domain to avoid the unexpected transients and deviations caused by time domain calculation.

Some current injection model in frequency domain is also integrated in a power systems simulations program [34] using the actually recorded terminal quantities.

The effect of different arc furnace models on voltage distortion was then investigated by Zheng et. al. [35]. It was found that the time domain method was more accurate than the frequency domain methods, but the latter one is more computationally efficient.

- Advantages: It is convenient for harmonics analysis after a transformation to frequency domain. The simulation results can be reasonably correct if the formula derived from experimental data are accurate.
- Drawbacks: It is assumed that the arc furnace loads draw the maximum power at the fundamental frequency to determine the phase angle while transforming the time domain response to a frequency domain one. This can hardly be true. Also, the v-i characteristics are still a problem, just as discussed for the previous approaches.

2.1.4 Neural Network and Fuzzy Logic Based Model

After trying neural network approach to model an EAF with the application of radial basis functions [18], Sadeghian et. al. [19] continued to propose a fuzzy logic model for the

EAFs. This approach treats the EAF as a nonlinear black box. A classic fuzzy logic system was claimed to be fast in the training of neural nets while an adaptive fuzzy logic system was demonstrated to be more accurate.

- Advantages: It shows that neural networks and fuzzy logic may have capability to deal with nonlinearity. Such approaches to this problem are natural and easy to understand. Good results maybe achieved if a nonlinear system has some deterministic nature, or it is operating under stable conditions.
- Drawbacks: The design of the neural networks and fuzzy logic structure for the black-box modeling of EAF is somewhat difficult because of the complexity of the EAF system. In the black-box, nonlinear response is linearized by algebraic equations, which could introduce errors. The trail-and-error process may fail (and may not converge) since the EAF current and voltage may not show a significant regression pattern.

2.1.5 Chaos Theory Based Models

Recently, deterministic chaos has been detected in the time series of an arc current [20,21]. Chaos theory has been applied to model the arc furnace and to represent its highly varying and nonlinear nature of arc impedance. Application of nonlinear analysis and chaotic dynamics has felt to be the solution for several problems of power engineering that have been investigated in the past. Various studies have dealt with the relationship of chaos with conditions such as voltage collapse [22], operation and control of power systems [23], the modeling of various phenomena such as ferro-resonance [25] and high impedance faults [36]. In [31] and [37], evidence of chaotic behavior is attributed to the current drawn by an ac arc furnace. This irregular and a-periodic behavior is quantified by the use of the Largest Lyapunov Exponent (LLE). The calculation of the largest Lyapunov exponent of arc furnace data provides a mathematical support for the modeling of arc furnace using chaos theory. Further investigation reported that there are strange attractors in pseudo-phase-plane plot and Poincare map; the auto-correlation function approaches zero when its lag becomes very large; the power spectrum is continuous as to frequency and the index of Kolmogorov

entropy is positive. Thus the EAF phenomenon may have some kind of chaos features. Previous attempts to use deterministic ideas in the study of arc furnaces did not represent accurately the aperiodic behavior of the arc process. Chaotic dynamics seem to overcome this problem [10,31]. Ozgun and Abur combined the determined v-i characteristic with a chaotic element for arc voltage [38]. In this process, the time-varying harmonics spectrum of the arc voltage has been obtained.

- Advantages: Indeed there are some chaotic components in the EAF system according to the chaos theory. Proper models can generate time series data that are statistically similar to the EAF data and thus one can obtain satisfactory power quality results.
- Drawbacks: The first disadvantage of this technique is that people have not fully understood chaos theory yet. Available chaos models are very few. It is sometimes difficult to fit a suitable model/parameter to the EAF data. Accurate short-time prediction may not be easily achieved due to uncertainty aroused by the model's sensitivity to initial points.

Table 2.1 shows a summary of common techniques that have been used to model EAF.

2.2 Research Objectives:

For load modeling, power system engineer would like to know if the model could be represented in real-time power flow calculation as simple as an admittance. This thought is not so realistic for a highly nonlinear load such as the EAF because its power consumption is varying randomly, as illustrated in Figure 2.2. On the other hand, since the EAF current and voltage contain some significant harmonic components, steady state power flow calculation based on the fundamental component of current/voltage may lead to loss of accuracy. But it is possible to do a snap shot of off-line transient study using a software like EMTP (Electromagnetic Transients Program) through TACS (Transient Analysis of Control Systems, which interacts with the rest modules of the EMTP through a Fortran code) interface. In this dissertation, a novel Markovian model for EAFs will be first developed

based on time series data of EAF current and voltage for this purpose. This model will be based on a first or second order Markov chain. It can predict one step ahead and apply the predicted current and voltage to related EMTP states. Then EMTP continues to do the next step simulation with the state information of other components.

Table 2.1 Common modeling principles used for electric arc furnaces

Technique used		*Purpose of study*	*First author*	*Reference*
Algebraic approximation	Empirical formula	Harmonics	Acha	[26]
	Rated v-i curve	Flicker	Varadan	[13]
Stochastic processes	Nonlinear resistor	Power quality	Montanari	[9]
	Reactive power signal	Flicker	Manchur	[12]
Frequency domain	Current injection	Harmonics	VHARM	[34]
	Voltage source	Voltage disturbance	Mayordomo	[15]
Neural networks/Fuzzy logic		Technical comparison	Sadeghian	[18,19]
Chaos theory		Power quality	O'Neill	[10]

One important goal of EAF modeling is to improve the poor power quality it introduced to the power system. To take an immediate corrective action, it is necessary to forecast one or more cycles ahead accurately, taking account of the time used for data acquiring, calculation and control activity. Therefore, the model will be further generalized to a function space type, which will be more feasible for implementation and prediction over a short range in time. It should be able to characterize the dynamic features of the EAF current and voltage.

Sometimes people want to know the power quality indices directly from the model. This is the steady state characterization of the load. To meet this requirement, the models that have just been proposed will be used to generate a time series data and obtain the power quality indices from it without any knowledge of real-time EAF current and voltage, although some historic data is needed to build the model.

To summarize, the main objective of this work is to find an accurate model for a certain highly varying electric power systems load according to Markov chain concept from mathematics as well as advanced time series theory in statistics. It includes the following aspects:

- For steady-state studies, the model can be used to generate harmonic performance indices for power quality analysis and provide key information for harmonic mitigation and reactive power compensation.
- For dynamic studies, the model should support simulation for harmonic compensation with short time prediction, say, one cycle to several cycles ahead in time.
- For transient studies, the model can be embedded into other simulators, such as EMTP, with one or two steps prediction ahead in time.
- It should be feasible to apply such a model to other time series (such as birth and death chain) that represent similar nonlinear phenomena.

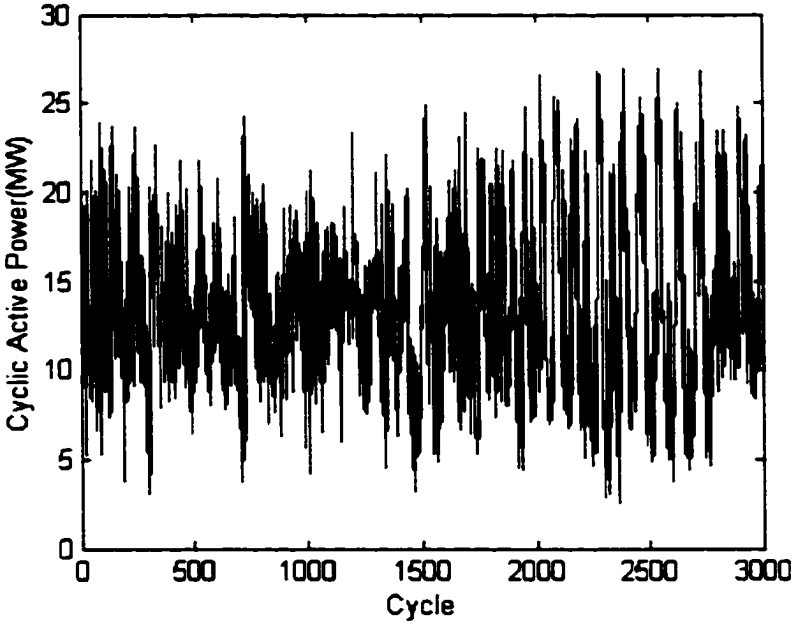

Figure 2.2 Cyclic active power of an EAF

3 BASIC MARKOV-LIKE MODELS

The approach proposed in this dissertation is to model the EAF system as a Markov-like sequence [39,40]. It will be shown that this approach makes it possible to simulate the EAF behavior accurately. The observed and recorded waveforms of an EAF system and other phenomena can be seen as nonlinear, dynamic time series, which may appear to behave chaotically. Developments in statistics and applied probability suggest that a suitable Markov-like model may fit a wide range of discrete-valued time series very well, in particular for dynamic data [39-42]. In the following sections, after a brief description of Markov theory, the procedures for developing a first order and second order Markov-like models from field data in time series format are described. Then, the two models are evaluated by comparing the modeling results with actual EAF current data derived from field. The dissertation also discusses the effectiveness of the one-step-ahead prediction approach using the results derived from the first and second order Markov modeling. The accuracy of the prediction is validated by a comparison of the results with the actual data. Simple statistical analysis of actual data and prediction results is also performed for evaluation. This method is used as the basis for a later generalization to the function space approach as discussed in Chapter 4.

3.1 Introduction to Markovian Theory

Consider a system that can be in any one of a finite or countably infinite number of states. Let S denote this set of states. We can assume that S is a subset of the integers. The set S is called the state space of the system. Let the system be observed at the discrete moments of time i = 0, 1, 2,... and let X_i denote the observation of the system at time i.

Since we are interested in non-deterministic systems, we think of X_i, $i \geq 0$, as random variables defined on a common probability space. Little can be said about such random variables unless some additional structure is imposed upon them. The simplest possible structure is that of independent random variables. This would be a good model for such

systems as repeated experiments in which future states of the system are independent of past and present states. In most systems that arise in practice, however, past and present states of the system influence the future states even if they do not uniquely determine them.

Many systems have the property that given the present state, the past states have no influence on the future. This property is called the Markov property, and systems having this property are called Markov chains. The Markov property is defined precisely by the requirement that, for every choice of the nonnegative integer i and the numbers $a_0, a_1, \ldots, k, l$, each in S [43]:

$$P\{X_{i+1} = l / X_i = k, X_{i-1} = a_{i-1}, \ldots\ldots, X_0 = a_0\} = P\{X_{i+1} = l / X_i = k\} \qquad (3.1)$$

where $k, l, a_{i-1} \ldots$, and a_0 are states in the state space S.

X is the successive observations on the variable.

Therefore, once the current state is known, prediction of future distribution cannot be improved by adding any knowledge of the past. But it should be noted, however, that this doesn't imply the past lacks information about the future behavior (although it is true for independent case). In fact, the past does affect the future through the present sate, as it can be seen from Figure 3.1. The figure depicts the situation where each oval reveals that two random variables are related through the Markov property. One can observe that the random variables $\{X_i, i = 1, 2, \ldots\}$ are connected by a chain [44].

Figure 3.1 Chain dependency in a Markov process

The conditional probabilities $P(X_{i+1}=l \mid X_i = k)$ are called the transition probabilities of the chain. Here we will only study Markov chains having stationary transition probabilities, i.e., those such that $P(X_{i+1}=l \mid X_i = k)$ is independent of i (For our study of EAF time series,

this property will be verified in Section 3.4). From now on, when we say that X_i, $i \geq 0$, forms a Markov chain, we mean that these random variables satisfy the Markov property and have stationary transition probabilities.

The study of such Markov chains is worthwhile from two viewpoints. First, they have a rich theory, much of which can be used at a fundamental level. Secondly, there are a large number of systems arising in practice that can be modeled by Markov chains, so the subject may have useful applications.

In order to introduce some basic concepts that will be used in developing the model with a discussion on results later, a small example considering Markov chains having only two states is given below:

This example considers a generator that at the start of any particular day is either broken down or in operating condition. Assume that if the generator is broken down at the start of the i^{th} day, the probability is p that it will be successfully repaired and in operating condition at the start of the $(i+1)^{th}$ day. Assume also that if the generator is in operating condition at the start of the i^{th} day, the probability is q that it will have a failure causing it to be broken down at the start of the $(i+1)^{th}$ day. Finally, let $\pi_0(0)$ denote the probability that the generator is broken down initially, i.e., at the start of the 0^{th} day. Let the state 0 correspond to the generator being broken down and let the state 1 correspond to the generator being in operating condition. Let X_i be the random variable denoting the state of the generator at time i. Figure 3.2 illustrated the state diagram of this example. According to the above description:

$$P(X_{i+1}=1 \mid X_i = 0)=p$$

$$P(X_{i+1}=0 \mid X_i = 1)=q$$

with the initial condition for state 0 to be:

$$P(X_0 = 0)= \pi_0(0)$$

Since there are only two states, 0 and 1, it follows immediately that

$$P(X_{i+1}=0 \mid X_i = 0)=1-p$$

$$P(X_{i+1}=1 \mid X_i = 1)=1-q$$

and that the probability $\pi_0(1)$ of being initially in state 1 is given by

$$\pi_0(1)=P(X_0 = 1)=1- \pi_0(0)$$

From this information, we can easily compute $P(X_i=0)$ and $P(X_i=1)$.

$$P(X_{i+1}=0) = P(X_i=0 \text{ and } X_{i+1}=0)+ P(X_i=1 \text{ and } X_{i+1}=0)$$

$$= P(X_i=0)P(X_{i+1}=0/ X_i=0)+ P(X_i=1)P(X_{i+1}=0/ X_i=1)$$

$$= (1-p)\, P(X_i=0)+q\, P(X_i=1)$$

$$= (1-p)\, P(X_i=0)+q\, (1-P(X_i=0))$$

$$= (1-p-q)\, P(X_i=0)+q \qquad (3.2)$$

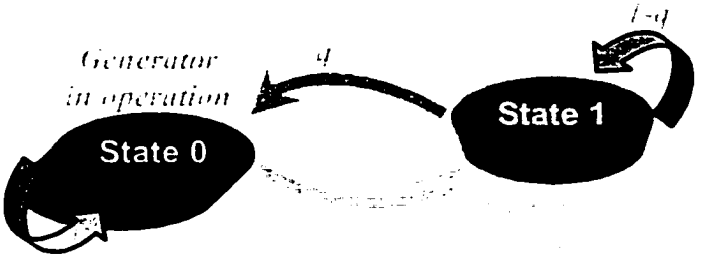

Figure 3.2 Illustration of states for a generator example

Now it is given $P(X_0 = 0)= \pi_0(0)$, so

$$P(X_1=0)= (1-p-q)\, \pi_0(0)+q$$

Similarly, from equation 3.2,

$$P(X_2=0)= (1-p-q)\, P(X_1=0)+q$$

$$= (1-p-q)^2\, \pi_0(0)+q[1+(1-p-q)]$$

The general form of $P(X_i=0)$ can be obtained by repeating this procedure i times,

$$P(X_i =0)=(1 - p - q)^i\, \pi_0(0)+ q \sum_{j=1}^{i-1} (1-p-q)^j \qquad (3.3)$$

Since $p+q>0$, then by the formula for the sum of such an infinite geometric progression,

$$\sum_{j=1}^{i-1}(1-p-q)^j = \frac{1-(1-p-q)^i}{p+q}$$

It can be concluded that

$$P(X_i=0) = \frac{q}{p+q} + (1-p-q)^i\,(\pi_0(0) - \frac{q}{p+q}) \tag{3.4}$$

and consequently $P(X_i=1)$ can be easily found as:

$$P(X_i=1) = \frac{p}{p+q} + (1-p-q)^i\,(\pi_0(1) - \frac{p}{p+q}) \tag{3.5}$$

Since p and q are neither both equal to zero nor both equal to 1, then $0<p+q<2$, which implies that $|1-p-q| < 1$. In this case we can let $i\to\infty$ in equations 3.4 and 3.5 to conclude that

$$\lim_{i\to\infty} P(X_i=0) = \frac{q}{p+q} \tag{3.6}$$

$$\lim_{i\to\infty} P(X_i=1) = \frac{p}{p+q} \tag{3.7}$$

The probabilities $q/(p+q)$ and $p/(p+q)$ in equations 3.6 and 3.7 can also be obtained in a different way. Suppose we want to choose $\pi_0(0)$ and $\pi_0(1)$ so that $P(X_i=0)$ and $P(X_i=1)$ are independent of i. It is clear from that to do this we should choose (a guess from common sense may be required)

$$\pi_0(0) = \frac{q}{p+q}$$

$$\pi_0(1) = \frac{p}{p+q}$$

Thus we see that if X_i, i >0, starts out with this initial distribution, then for all i

$$P(X_i=0) = \frac{q}{p+q}$$

$$P(X_i = 1) = \frac{p}{p+q}$$

On the other hand, the problem can be easily solved using transition function in its matrix format with the transition function being defined as:

$$P(k,l) = P\{X_{i+1} = l / X_i = k\} = p_{kl} \tag{3.8}$$

It means that if the Markov chain for the system is in state k at time i (and it doesn't matter how it got to k), it has the probability $P(k,l)$ of being in state l at the next step. Since only one transition is involved, it is called one-step transition probability. Similarly, one may be interested in finding the probability of k going to l in m steps. This m-step transition function is expressed as $P^m(k,l)$. It is defined by:

$$P^m(k,l) = \sum_{a_1} \sum_{a_2} \cdots \sum_{a_{m-1}} P(k,a_1)P(a_1,a_2)\cdots P(a_{m-2},a_{m-1})P(a_{m-1},l)$$

Suppose the state space S is finite and $S = \{0, 1, 2, \ldots n\}$, now a Markov chain can be easily expressed in matrix format $\boldsymbol{P}=(p_{kl})$, it is called transition matrix:

$$\boldsymbol{P} = \begin{array}{c} \\ 0 \\ 1 \\ \cdots \\ \cdot \\ n \end{array} \begin{array}{c} \begin{array}{cccc} 0 & 1 & \cdots & n \end{array} \\ \begin{bmatrix} p_{00} & p_{01} & \cdots & p_{0n} \\ p_{11} & p_{11} & \cdots & p_{1n} \\ \cdots & \cdots & \cdots & \cdots \\ p_{n0} & p_{n1} & \cdots & p_{nn} \end{bmatrix} \end{array} \tag{3.9}$$

Correspondingly, the m-step transition matrix $\boldsymbol{P}^m$ can be defined as the product of m one step transition matrices $\boldsymbol{P}$.

Besides the transition matrix, it is necessary to know the initial distribution π_0 if one wants to figure out what state the system is in over a specific time.

$$\pi_0 = (\pi_0(0), \pi_0(1), \ldots \pi_0(n))$$

The initial distribution, as well as the distribution of the system at any time, should sum up to 1. That is to say:

$$1 = \sum_{j=0}^{n} \pi(j) \tag{3.10}$$

Then the distribution at time step i is

$$\pi_i = \pi_0 P^i$$

To get the stationary distribution, one can make use of the equation

$$\pi(l) = \sum_{k=0}^{n} \pi(k) P(k,l) \tag{3.11}$$

For the above example:

$$\boldsymbol{P} = \begin{bmatrix} 1-p & p \\ q & 1-q \end{bmatrix} \tag{3.12}$$

Then

$$\pi(0) = \pi(0)*P(0,0) + \pi(1)*P(1,0) = \pi(0)*(1-p) + \pi(1)*q \tag{3.13}$$

$$\pi(1) = \pi(0)*P(0,1) + \pi(1)*P(1,1) = \pi(0)*p + \pi(1)*(1-q) \tag{3.14}$$

Considering that

$$\pi(0) + \pi(1) = 1 \tag{3.15}$$

Solve the three equations 3.13 to 3.15, the stationary distribution can be obtained.

$$\pi(0) = \frac{q}{p+q}$$

$$\pi(1) = \frac{p}{p+q}$$

The Markov property described in equation 3.1 is a simple and mathematical tractable relaxation of the assumption of independence [43]. Thus it is natural to consider discrete-time Markov chain on a finite state space as a possible model for time series taking values in that space. Combining that with equation 3.8, the first order Markov chain can be defined [42,45]:

$$P\{X_{i+1} = l / X_i = k, X_{i-1} = a_{i-1}, \ldots X_0 = a_0\} = P\{X_{i+1} = l / X_i = k\} = p_{kl} \tag{3.16}$$

again, p_{kl} is called the single-step transition probability of the variable from state k to l.

A second order Markov chain can also be defined as

$$\begin{aligned} &P\{X_{i+1} = l / X_i = k, X_{i-1} = h, X_{i-2} = a_{i-2}, \ldots X_0 = a_0\} \\ &= P\{X_{i+1} = l / X_i = k, X_{i-1} = h\} = p_{hkl} \end{aligned} \tag{3.17}$$

where k, l, h, a_{i-2} ..., and a_0 are states in the state space S.

p_{hkl} is called the two steps transition probability from state h to k to l.

This equation can be further simplified by defining $Y_i=(X_{i-1},X_i)$.

$$P\{Y_{i+1} = l / Y_i = k, Y_{i-1} = a_{i-1}, \ldots Y_0 = a_0\} = P\{Y_{i+1} = l / Y_i = k\} = p_{kl} \tag{3.18}$$

where k, l, a_{i-1} ..., and a_0 are states in the state space S×S.

p_{kl} is called the single-step transition probability from state k to l for the Y chain

One can accordingly generalize three (with the one-step transition probability denoted as p_{ghkl}) or higher order Markov chain in the same way. After calculating all the necessary transition probabilities, the time series under study can be examined to see if it is really a Markov chain. If $p_{hkl} = p_{kl}$ for all h, k, l, then it is a first order Markov chain; if not, one can further check if $p_{ghkl} = p_{hkl}$ for all g,h,k,l, if so, it is a second order Markov chain and so on.

Many systems in science and engineering fields have this Markovian property that given the present state, the past states have no influence on the future state. That is to say, the probability of current state depends only on the immediate past state, given the possibilities of all the past states. Many practical phenomena can be modeled as Markov processes and Markov theory has seen its successful applications in the areas of birth-death process of biological group, radiation and degradation of electronic articles, water level of reservoir and queuing chain of service desk in a supermarket, etc. [42]. In the field of power systems, Stankovic and Marengo [41] provided one case where the harmonics of a power system are treated as a superposition of a deterministic component and a stochastic component modeled

by Markov chain. Also, Charytoniuk et. al. [46] used it for probabilistic iterative harmonic analysis in power systems. The applications can also be found in a collection of papers on "Modeling and simulation of the propagation of harmonics in electrical power networks" by IEEE task force on harmonics modeling and simulation [47]. For the EAF under study, the arcing status is mainly determined by the length and position of the electrode, and the condition of the melting iron ingots or scrap. When the arc is working on some ingots at the surface, they change from solid state to liquid state gradually and sink down to the bottom of furnace. So the current state is only directly affected by the previous state and current random factors such as control operation. Accordingly this feature provides a possible physical background for Markov modeling of EAFs.

3.2 Essentials of Nonparametric Methods

This Markov-like model is a nonparametric model [48,49]. Nonparametric methods gain more and more attention now because they provide a practical application of statistical techniques. For instance, in power system area, W. Charytoniuk used a nonparametric regression model for short-time load forecast [46]. To identify if a method is nonparametric or not, at least one of the following criteria should be applied.

- The data are counted to represent the number of observation in each category (the proposed Markov-like model can be classified into this category since the transition matrix for the Markov-like model are estimated from observations).
- Nominal or ordinal scale of measurement of the data is utilized.
- The analysis does not deal with any parameter of a distribution.
- No specific information or assumptions can be imposed on the population (which consists all the possible data) while making an inference. Only general assumptions such as a continuous or symmetric population distribution may be used.

The nonparametric methods have many advantages over parametric methods. Some of them are:

- Only a basic knowledge of statistics is needed for an effective use of these methods.

- No hypothetical distribution functions are necessary (distribution-free) in nonparametric methods.
- They need much weaker assumptions than the parametric methods.

One benefit from nonparametric method is its applicability to a situation where there is insufficient theory or data to specify, or test compatibility with, highly specific statistical models such as normal, lognormal and weibull distributions. Based on the nature of EAF current and voltage, it is suitable to analyze it with the use of nonparametric method.

3.3 Basic Markov-like Model Construction

3.3.1 Problem of Modeling Highly Nonlinear System

The problem of modeling the EAF current evolution and other similar processes is as follows. Let $\{X(t): t\geq 0\}$ be a time evolving physical system where $X(t)$ denotes the state at time t. Suppose the system is observed at times $t=n\Delta$, $n=0,1,2\ldots$ where $\Delta>0$ is a convenient time span. Thus the observed and recorded waveforms of an EAF system and other phenomena can be seen as nonlinear, dynamic time series, which may behave chaotically. Given the data $X_j=X(j\Delta)$ for $0\leq j\leq n$ find a appropriate mathematical model to fit the data as well as make predictions of values of $X(t)$ for $t>n\Delta$ in the future. A deterministic approach involves finding a function $f(t)$ such as the solution of a differential equation and try to match $X_j=X(j\Delta)$ with $f(j\Delta)$ for $0\leq j\leq n$ and then use $f(t)$ for prediction of values for $t>n\Delta$. Often such a function is not easy to find and even when one has a reasonable candidate $f(t)$ it may turn out to be highly nonlinear involving a parameter θ that for certain threshold values makes the evolution chaotic. This renders prediction difficult. An alternative to this is to use stochastic model based on the idea of random dynamical system. In a deterministic discrete time dynamical system approach one looks for a function f on the state space such that for each $n\geq 0$, $X((n+1)\Delta)=f(X(n\Delta))$. This requires exact knowledge of $f(t)$ and exact computation. It is more realistic to postulate that at step n, $X((n+1)\Delta)=f_{n+1}(X(n\Delta))$ where f_{n+1} is an approximation to $f(t)$ that may also include computational errors. It is reasonable to propose

that for each n, f_n is one of many choices made according to some probability distribution. Thus the model describes a random dynamical system. In particular, if we assume that the $\{f_n,\ n=0,\ldots\ \infty\}$ are independent and identically distribution choices then the sequence $\{X_j=X(j\Delta): j\geq 0\}$ becomes a Markov chain with stationary transition probabilities. Thus, if the underlying dynamics of the process does not change with time but is subject to measurement and approximation errors and some random fluctuation then it is worthwhile to model the evolution as a Markov chain with stationary transition probabilities. In some cases, if $\{X_n\}$ itself is not approximately Markovian then a higher order chain that keeps some steps such as $X_{n,\tau}=(X_{n-j}: 0\leq j\leq \tau)$ could be approximately Markovian.

The implementation of the above program involves many steps that are data driven (ie. adapted to data) and dynamical in time. These are:

i. Identification of the range of values for the time series $\{X_j=X(j\Delta),\ 0\leq j\leq n\}$.

ii. A discretization of the range that is of appropriate level of refinement and computational feasibility.

iii. Postulating a transition probability matrix $P=((p_{ij}))$ and estimating p_{ij} by the empirical frequency of such (i,j) transaction from the data.

iv. Comparison of the estimate of one step transition probabilities of the first, second or higher order chains to decide the order of the Markovian approximation.

v. A continuous check for stationarity of the underlying dynamics through a comparison of the estimated transition probabilities by basing them on a moving window of a fixed length (which is fairly large over time)

3.3.2 Development of Basic Models

The development of the proposed basic models is based on ideas from Markov's theory [39-45]. The application of a first order Markov-like model is discussed at first in detail. Then these ideas are extended to a second order Markov-like model. The formulation of the model involves steps i) to ix) in the following in relation to Figure 3.3, which represents a typical arc current waveform.

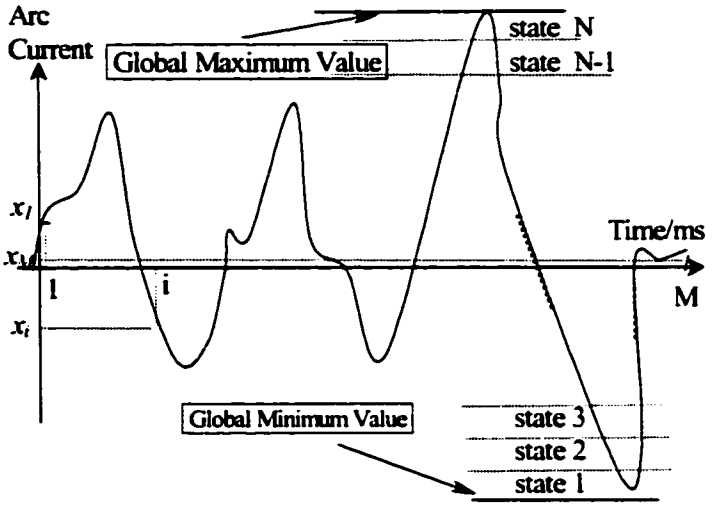

Figure 3.3 Illustration of states used in Markov-like model

Step i) The global minimum and maximum values of the variable (arc current or voltage, etc.) under study over the interval of observation are identified.

Step ii) All the values of the data from the global minimum to maximum are divided into a finite number (say N) of intervals to form N state: state 1, 2, ... N (see Figure 3.3).

Step iii) Given the time series $\{X_j: j=1, 2,\ldots M\}$ with its state space $S=\{1, 2, \ldots. N\}$, define

$$\begin{cases} \delta_{kj} = 1 \text{ if } X_j \in \text{ state } k \\ \delta_{kj} = 0 \text{ if } X_j \notin \text{ state } k \end{cases} \tag{3.19}$$

Then the frequency of visits to state k called Empirical Frequency Function (EFF) is

$$\pi_k = \frac{1}{M} \sum_{j=1}^{M} \delta_{kj} \tag{3.20}$$

Also define the Empirical Cumulative Distribution Function (ECDF)

$$F_k = \sum_{j=1}^{k} \pi_j \tag{3.21}$$

It equals proportion of visits to less than or equal to state k during the time period {1, 2, ... M}

Step iv) The frequency of one-step transition from state k to state l in relation to number of visits to state k is

$$\pi_{k/} = \sum_{j=1}^{M-1} \delta_{kj}\delta_{/(j+1)} / \sum_{j=1}^{M} \delta_{kj} \tag{3.22}$$

It is the ratio of the number of transitions from state k to /to the number of visits to state k in the data.

$\pi_{k/}$is an estimate of one step transition probability $P\{X_{i+1} \in state\ l / X_i \in state\ k\}$ for the first order chain $\{X\}$. Note that for each state k, $\{\pi_{k/}: /=1,2 \ldots.N\}$ estimates the transition probability distribution of the next state l given that the current state is k. This will be useful in making the prediction of the future state given the present state.

Step v) The frequency of two-step transitions from state h to state k and then to state l in relation to number of one-step transition (h,k) is

$$\pi_{hk/} = \sum_{j=1}^{M-2} \delta_{h\,j}\delta_{k(j+1)}\delta_{/(j+2)} / \sum_{j=1}^{M-1} \delta_{hj}\delta_{k(j+1)} \tag{3.23}$$

It is an estimate of one step transition probability $P\{X_{t+1} \in state\ l / X_t \in state\ k, X_{t-1} \in state\ h\}$ for the second order chain $\{Y_i=(X_i,X_{i+1})\}$,

Step vi) If $\pi_{k/} \simeq \pi_{hk/}$for all h, then the chain is approximately a first order Markov chain. Otherwise, find the third order transition frequency $\pi_{ghk/}$

$$\pi_{ghk/} = \sum_{j=1}^{M-3} \delta_{g\,j}\delta_{h(j+1)}\delta_{k(j+2)}\delta_{/(j+3)} / \sum_{j=1}^{M-2} \delta_{g\,j}\delta_{h(j+1)}\delta_{k(j+2)} \tag{3.24}$$

and check if $\pi_{ghk/} \simeq \pi_{hk/}$for all g. If so, it is approximately a second order Markov chain.

This statement is based on the basic theory as follows: If the sequence $\{X_j\}$ were a first order Markov chain, then the conditional probability that $X_{j+1} \in l$ given $X_j \in k$, $X_{j-1} \in h$ should be the same as the probability that $X_{j+1} \in l$ given only $X_j \in k$. An estimate of the two quantities is

respectively π_{hkl} and π_{hk}. Thus if π_{kl} is approximately equal to π_{hkl} for all h, k and l, then the time series $\{X_j\}$ resembles a realization of a Markov chain. For this reason, the time series $\{X_j\}$ will be referred to as a first order Markov like chain. Similar interpretation applies to second order, third order Markov like properties.

It will be illustrated in Section 3.4 that, for the EAF data, a second order Markov like chain was a good fit and one-step-ahead prediction was feasible and reasonably accurate.

Step vii) The second order chain Y is Markov-like but with state space $S \times S$, the Cartesian product of S with itself. This should make the estimate of conditional distribution of the future given the present sharper, thus reduce the level of uncertainty. If necessary one could go to a third or higher order Markov-like chain Z, where one records three or more consecutive X values instead of two consecutive values.

Step viii) For a first order Markov-like model, use equation 3.22 to estimate every transition probability π_{kl} for each state transition from actual EAF data. Correspondingly, a second order Markov-like model uses equation 3.23 to calculate π_{hkl} within its state space. Thus the transition matrix $P=(\pi_{kl})$ or $P=(\pi_{hkl})$ embodies the Markov-like model.

Step ix) In addition to the above Markov-like modeling, it is also useful to give simple statistical summaries of the data such as the mean, variance of EFFs from the arc current data and stationary distribution from the Markov-like model.

It is important to check continuously whether the underlying dynamics remains stationary or not. This could be accomplished by estimating the single and higher order transition probabilities using data on a moving window of the form $\{X_j: n-k \leq j \leq n\}$ of length K. If at some n this shows substantial deviation from the earlier estimates then the stationarity assumption should be re-examined.

Most systems that can be applied with Markov chains have obvious state spaces, but the EAF current bears no such clear states. So the novel part in this approach is identifying its state space and estimating the transition matrix. The application of the above to the practical EAF data is described in Section 3.4 and Section 3.5, whose performance is compared with an established ARMA/Kalman method in Section 3.6.

3.4 Validation of Basic Markov-Like Model for EAF Current

Actual EAF data for current/ voltage are used to form and test the models that have just been introduced in Section 3.3. This EAF is a 50 MVA, three-phase, device connected to a 34.5 kV bus behind a specially designed EAF transformer rated at 100 MVA. Twenty seconds of historical arc current and voltage data of phase A is utilized to build the model. A first order Markov-like model is proposed first for description of the concept in Section 3.4.2 after testing the Markovian property in Section 3.4.1. Then the second order Markov-like model for accurate modeling and prediction is discussed in Section 3.4.3 to Section 3.4.5.

3.4.1 Markovian Property Test

Before the application of Markov-like model, the collected field data (120 seconds long, with sample rate 10,000 samples/second) will be used to test the Markov property of EAF current. According to Section 3.3, for a second order Markov chain, the condition $\pi_{ghk,} \approx \pi_{hk,}$ for all g, h, k and $l$shou ld be verified, and for a first order Markov chain, $\pi_{hk,} \approx \pi_{k,}$ for all h, k and l is required. For the convenience of comparison, three overlapped data pieces were used: 70 seconds to 90 seconds, 30 seconds to 90 seconds and 20 seconds to 120 seconds, which is the largest sample. Table 3.1 and Table 3.2 illustrated the test result of fist order Markov property for EAF current when (k, l) is at states (79,79) and (3,4) respectively. Here the range of the data is divided into 90 states—N=90. The results for only two or three h's are listed in the tables because they are the only possible states for h for the given (k, l). Both of the tables show that the difference between $\pi_{k,}$ and $\pi_{hk,}$ becomes smaller when the sample size gets larger. One can extrapolate that $\pi_{hk,} \approx \pi_{k,}$ stands when the sample is large enough.

Table 3.1 First order Markovian property test for EAF current with k=79, l=79

Data Interval	π_{hkl}			π_{kl}
	h =78	h =79	h =80	
70s-90s	0.803922	0.679803	0.615385	0.692833
30s-90s	0.771654	0.619385	0.611650	0.647779
20s-120s	0.680269	0.630548	0.630058	0.659208

Table 3.3 and Table 3.4 are for second order Markov property test. The same conclusions for first order Markov chain case can be drawn here, while the accuracy is much better. When (h, k, l) is at state (9, 10, 11), the deviation between $\pi_{ghk,l}$ and $\pi_{hk,l}$ is even under 0.3%. One can infer from these indices that the EAF current behaves according a Markov-like chain.

The first order Markov property was also checked for EAF voltage and part of the result is shown in Table 3.5. It can be seen that the deviation between $\pi_{k,l}$ and $\pi_{hk,l}$ decreases and approaches zero for all h's with increased sample size. This implies that the behavior of EAF voltage is muck like a Markov chain.

Table 3.2 First order Markovian property test for EAF current with k=3, l=4

Data Interval	π_{hkl} h =2	h =3	π_{kl}
70s-90s	0.500000	0.250000	0.230769
30s-90s	0.200000	0.184211	0.166863
20s-120s	0.187563	0.172213	0.177541

Table 3.3 Second order Markovian property test for EAF current with h=42, k=42, l=42

Data Interval	π_{ghkl} g =41	g =42	g =43	π_{hkl}
70s-90s	0.757353	0.757208	0.640449	0.745475
30s-90s	0.750791	0.749625	0.672087	0.746085
20s-120s	0.7344386	0.732633	0.713166	0.727811

Table 3.4 Second order Markovian property test for EAF current with h=9, k=10, l=11

Data Interval	π_{ghkl} with g =9	π_{hkl}
70s-90s	0.090909	0.088435
30s-90s	0.051147	0.049896
20s-120s	0.042086	0.042208

Table 3.5 First order Markovian property test for EAF voltage with k=11, l=10

Data Interval	π_{hkl} h=11	h=12	π_{kl}
70s-90s	0.503226	0.546444	0.524342
30s-90s	0.463801	0.506815	0.483786
20s-120s	0.453863	0.449633	0.451263

3.4.2 First Order Markov-like Model

To illustrate this approach, the arc current data are divided into two independent sets (i.e. two samples) of 10 seconds duration. After computing the estimates of the transition probabilities from each sample, one can use the estimated transition matrix as the model to get the stationary distribution and compare it to the actual data to validate the model. The procedures for obtaining a first order Markov-like model for EAF current is illustrated in flow chart of Figure 3.4. Also, Figure 3.5 shows the flow chart computing the stationary distribution asymptotically.

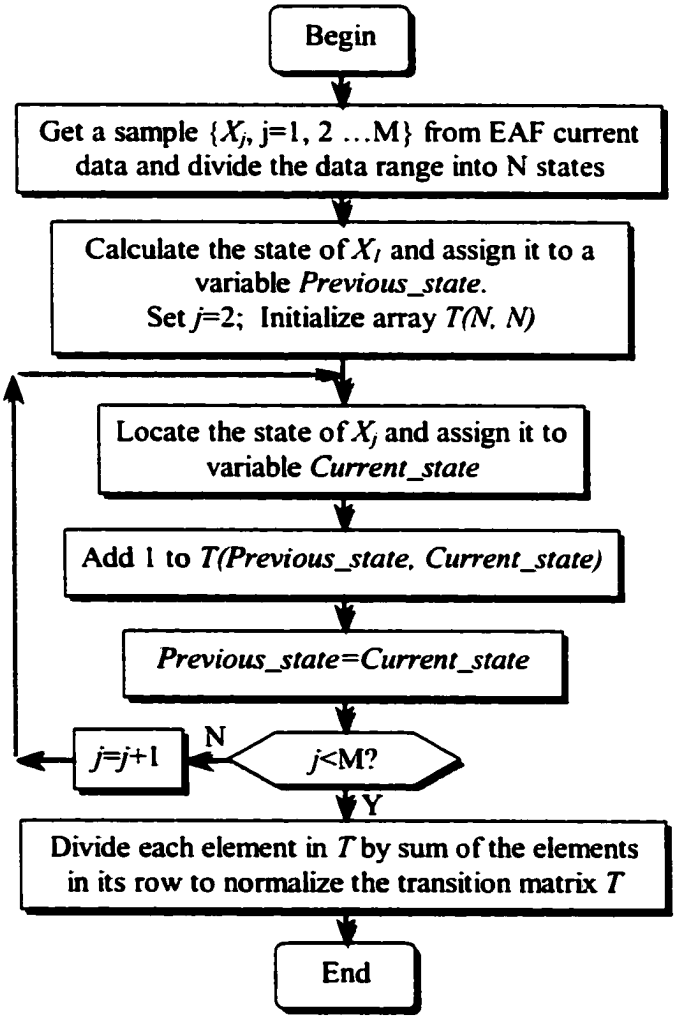

Figure 3.4 Flow chart of building a first order Markov-like model

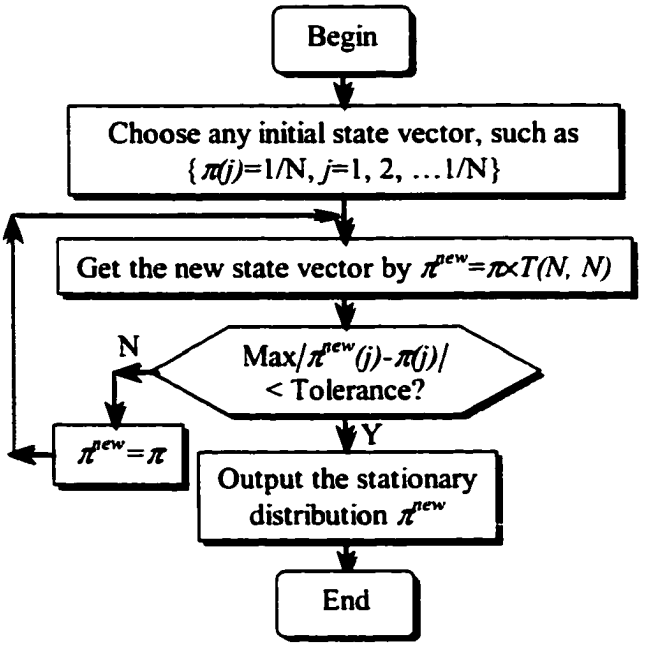

Figure 3.5 Computing stationary distribution for a first order Markov-like model

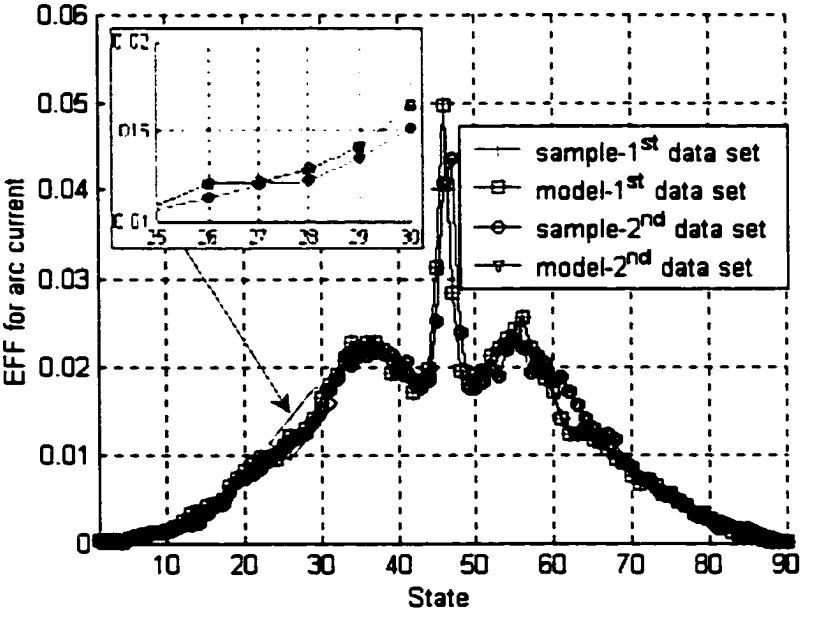

Figure 3.6 EFFs for actual arc current from a first order Markov-like model N=90

The results from the first order Markov-like model are shown in Figure 3.6, Figure 3.7 and Table 3.6. The main part of Figure 3.6 is the plots of the Empirical Frequency Function (EFF) π_k for the two samples and the stationary distribution from the related model. Since the

data are very close to each other, an expanded view within a small interval (states 25 to 30) for these EFFs is shown as a sub-window at the top-left part of Figure 3.6. Figure 3.7 shows the Empirical Cumulative Distribution Function (ECDF) F_k of the corresponding EFFs of Figure 3.6. Again, to make the figure clearer, within Figure 3.7 a sub-window gives an expanded view for states 25 to 30 at its top-left part. Table 3.6 indicates the mean and variance indices of EFFs from the EAF current sample and model.

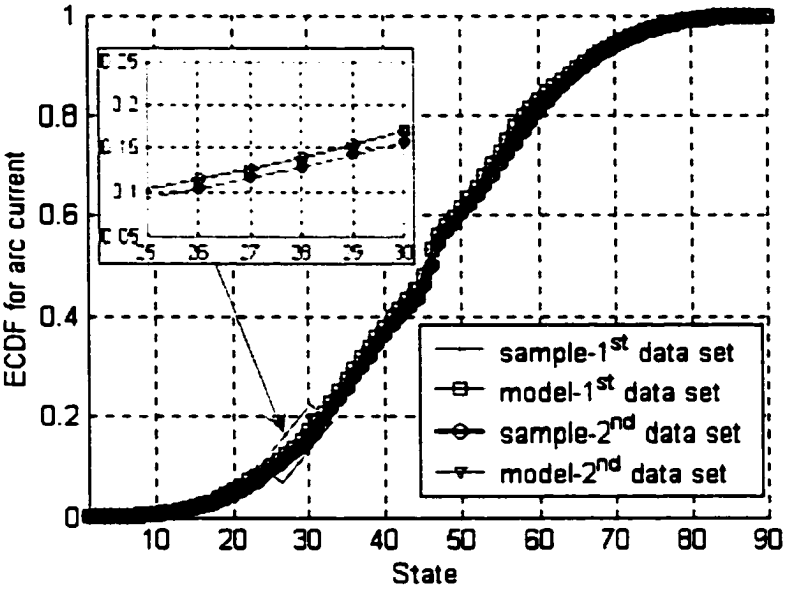

Figure 3.7 ECDFs for actual arc current from a first order Markov-like model N=90

Table 3.6 Statistical indices of EFFs for actual current samples and stationary distribution from a first order model

	Sample 1	Sample 2	Model 1	Model 2
Mean	0.011111	0.011111	0.011111	0.011111
Variance	0.0000865	0.0000849	0.0000855	0.0000851
RMS	0.014491	0.014435	0.014483	0.014442

It can be easily seen that the EFFs for the two actual data samples in Figure 3.6 are very much alike, and the ones from stationary distribution of the models are almost the same as the original actual data so that in the figure they are overlapped. In fact, during the computation of stationary distribution, even when the initial condition is changed, the results

did not have much variation. It can also be seen that, means are the same for the EFFs of the original data and modeling results. Their variances are also very close to each other. One may deduce from this comparison that the transition matrix is a natural parameter of this system. It appears as well that the statistical behaviors of the EAF current are stationary with respect to time from the similarities in characteristics for the two data samples. The statement can also be confirmed by observing the ECDFs of samples and stationary distribution from the models given in Figure 3.7. This suggested that a first order Markov chain is enough for characterizing the long-term statistical behavior of the EAF current.

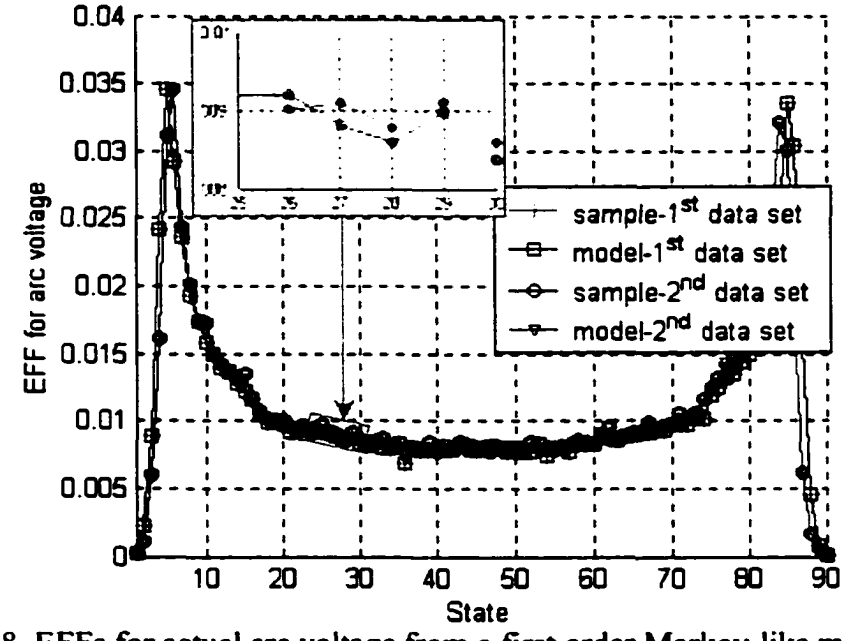

Figure 3.8 EFFs for actual arc voltage from a first order Markov-like model N=90

Table 3.7 Statistical indices of EFFs for actual voltage samples and models

	Sample 1	Sample 2	Model 1	Model 2
Mean	0.011111	0.011111	0.011111	0.011111
Variance	0.0000370	0.0000373	0.0000372	0.0000372
RMS	0.012682	0.012690	0.012687	0.012688

The same procedure is carried out on the EAF voltage and the corresponding EFFs are shown in Figure 3.8. An expanded view is shown for states 25 to 30 as a window at the top-

left part of this figure, just as in the case of processing EAF current. Since the EFFs are closer to each other than those from the EAF current, the model seems to be even more accurate for EAF voltage. This is to be expected, because the waveform of the EAF voltage is not so irregular as the EAF current. The statistical indices for the two data sets are almost the same, as it is shown in Table 3.7. Accordingly, specific attention of modeling is only paid to the EAF current in the subsequent sections.

3.4.3 Need for a Second Order Markov-like Model

The short-term and long-term predictions of the variable based on the present and past data are of practical interest and value to power engineers. Using the first order Markov-like model, the empirical frequencies of the states help in predicting future averages. Also, the estimated transition probability matrix helps prediction of the immediate future value given the present value. Some parts of the result file consisting of the elements from the transition matrix are shown in Table 3.8. Since the matrix is sparse, only nonzero elements are recorded in a format of $\{\pi_{kl}$: its value$\}$. For instance, the first line of data indicates that if the current state is 1, it has a high probability (π_{11}=0.9000) to stay in this state in the next step. This transition matrix is good for a long-term prediction from the earlier analysis, i.e., the characteristic of the model fits with the original data. However, it is found to be not good enough for short-term prediction. For example, in state 41, it has positive probability to enter each of the states 39, 40, 41, 42 and 43. While all of the probabilities are below 0.40, as it can be seen from Table 3.8. One cannot predict the next value with accuracy and confidence. The problem of finding a better model for an accurate prediction is now addressed.

Table 3.8 Some elements of transition matrix for a first order Markov-like model

π_{11} : 0.9000 π_{12} : 0.1000 ...
π_{21} : 0.1875 π_{22} : 0.6250 π_{23} : 0.1875 ...
.....
... $\pi_{41,39}$: 0.0095 $\pi_{41,40}$: 0.3091 $\pi_{41,41}$: 0.3944 ...
... $\pi_{41,42}$: 0.2417 $\pi_{41,43}$: 0.0453 ...
.....
... $\pi_{90,89}$: 0.1052 $\pi_{90,90}$: 0.8948 ...

3.4.4 Distinction Between the First and Second Order Models

For a short-term prediction, the transition probability estimates in the first order Markov-like model are not sharp (i.e., not very close to 1 or 0). This leads one to consider a second order Markov-like model, where a vector $Y_i=(X_{i-1}, X_i)$ is recorded for each time point. The first order Markov-like model, as it is shown in the part (a) of Figure 3.9, does not distinguish between increasing and decreasing trend. On the other hand, a second order Markov-like model does distinguish between increasing and decreasing trend, as shown in the part (b) of Figure 3.9. Also, most of the transition probabilities are close to 1 or 0, as shown in Table 3.9. This property makes it effective in short-term prediction, i.e., given current state value Y_i in Y chain, the value of Y_{i+1} can be estimated with higher accuracy.

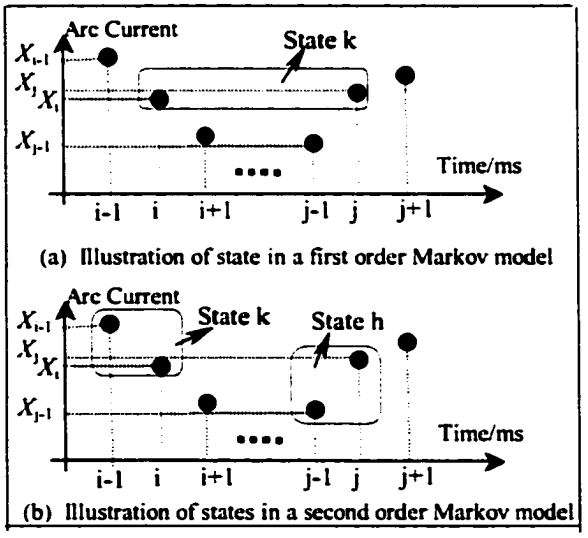

Figure 3.9 Comparison of states in first and second order Markov-like model

The transition matrix for the second chain $\{Y_i\}$ is similar to that of first order Markov-like model, although the dimension is double powered. That is to say, if the state number is set to be 50, for a first order Markov-like model the transition matrix is of the dimension (50×50), while for a corresponding second order Markov-like model, it is of the dimension (50×50)×(50×50)=(2,500×2,500). In Table 3.9, part of the matrix is also listed in the format

of $\{\pi_{hk/}$: its value$\}$, while the chain is defined as $Y_i=(X_{i-1}, X_i)$. Most of transition probabilities are larger than 0.9 or less than 0.1. In many states the probabilities are 1 or 0. So one can predict the arc current with a higher confidence level. For instance, when the present state is (1,2), one can estimate with reasonable certainty that it will enter state (2,2) according to the transition matrix (vide Table 3.9). As mentioned earlier, the fact that the estimates of the second order one-step transition probabilities are sharper than those of the first order one-step transition probabilities suggests that the underlying time series is not a strict first order Markov chain. Nevertheless, this methodology provides a somewhat accurate prediction of the seemingly chaotic time series.

Table 3.9 Some elements of transition matrix for a second order Markov-like model

π_{111} : 0.921053 π_{112} : 0.078947 ...
π_{122} : 1.000000 ...
.....
... $\pi_{27,28,28}$: 0.897181 $\pi_{27,28,29}$: 0.102819 ...
... $\pi_{28,26,26}$: 1.000000 ...
.....
... $\pi_{50,49,49}$: 1.000000 ...
... $\pi_{50,50,49}$: 0.076923 $\pi_{50,50,50}$: 0.923077 ...

3.4.5 Results From the Second Order Markov-like model

Only the EAF current is processed using a second Markov-like model since its waveform is more irregular. Such results are shown in Figure 3.10. It should be stressed that while the number N to divide the data range is 50, in a second order Markov-like model, there are 50*50 states, which are arranged in the sequence of (1,1), (1,2), ... (1,50), (2,1), (2,2),... (50,50). But for convenience, the states in the x-axis are lined up into one dimension from I to 2500. The data are still divided into two parts in this approach. In Figure 3.10, EFFs are plotted for the two samples together with the stationary distribution derived from a second order Markov-like model. In addition, an expanded view for states 500 to 600 is provided as a window at the top-left part of Figure 3.10.

It may be observed that the EFFs from the two actual data sets and the stationary distribution from the model are really similar. This suggests that EFFs and ECDFs from the actual data show the statistical characteristics when the sample data are large enough. It may not be the case if a small sample of data is selected. Statistical indices (mean and variance) are also listed in Table 3.10. The similarity of values verifies the effectiveness of this model.

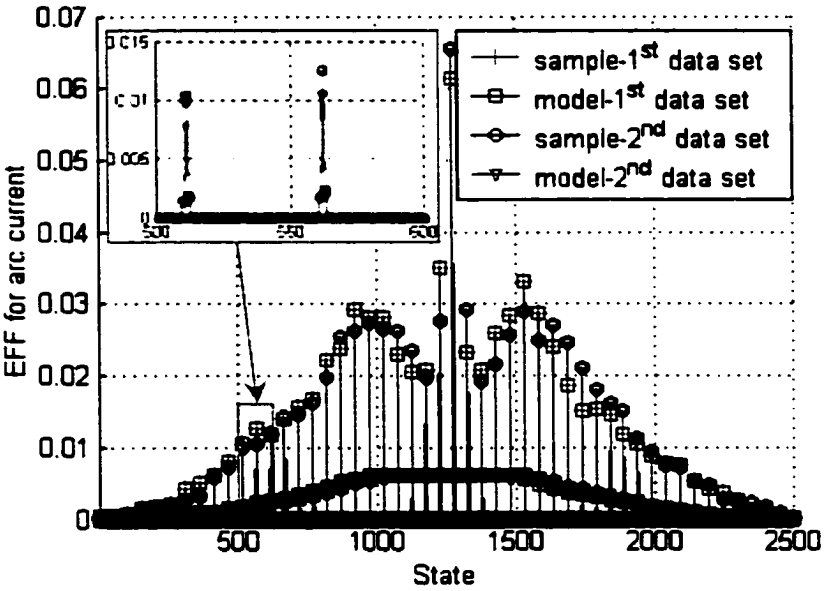

Figure 3.10 EFFs for actual arc current from a second order Markov-like model N=50

Table 3.10 Statistical indices of EFFs for actual current samples and stationary distribution from a second order model

	Sample 1	Sample 2	Model 1	Model 2
Mean	0.0004	0.0004	0.0004	0.0004
Variance	0.0000078	0.0000080	0.0000079	0.0000079
RMS	0.019510	0.019519	0.019515	0.019516

3.4.6 Stationary Test of the Time Series with a Classic Method

It seems that the EAF system shows statistical stationary features in the previous Markov-like models. To further verify if the model is robust, a traditional technique in time series is applied on the same EAF data set. According to time series theory, a time series $\{X_t,$

$t=0,1,2,...\}$ is said to be stationary if it has statistical properties similar to those of the time-shifted series $\{X_{t+h},\ t=0,1,2,...\}$ for each integer h. This definition is normally referred as strict stationary. But it bears a very strong assumption (sometimes even stronger than necessary for useful results) and is hard to verify in practice. So people care more about weakly stationary and regard $\{X_t,\ t=0,1,2,...\}$ to be (weakly) stationary when [50]:

- The Variance $Var(X_t) < \infty$ and is independent of t.
- The mean function $u_x(t)=E(X_t)$ is independent of t.
- The auto-covariance function $r_x(t+h,t)=Cov(X_{t+h}, X_t)=E[(X_{t+h}- u_x(t+h))(X_t - u_x(t))]$ is independent of t for each h.

For practical problems that do not have a specific model, but have observed data $\{X_1, X_2, ... X_n\}$, the mean function and auto-covariance function (ACF) cannot be computed directly. To assess the degree of dependence in the data or choose a suitable model for the data which reflects these properties, one can use sample mean (SM) and sample auto-correlation function (SACF) to estimate the mean and ACF. For a time series $\{X_1, X_2, ... X_{T+n}\}$ where T is the maximum value of the starting time set $\{t\}$. SM is calculated as follows:

$$\overline{X}_t = \frac{1}{n}\sum_{i=t}^{t+n} X_i \tag{3.25}$$

The SACF is:

$$\hat{r}_t(h)=\frac{1}{n}\sum_{i=t}^{t+n-h}(X_{i+h}-\overline{X}_t)(X_i-\overline{X}_t) \qquad 0\le h<n \tag{3.26}$$

Figure 3.11 and Figure 3.12 show the mean function and SACF for the EAF current data at different time-shift (or lag) h and starting time t. In the test, the time shift considered ranges from 0 to 500ms in time unit (when point was used as unit, it is 5000 points) and the points of lag are from 0 to 16.8ms (168 points, about one cycle). In addition, Table 3.11 and Table 3.12 list some numeric results for them. The variation of the mean for EAF current is less than 0.1A. Considering that the magnitude of the EAF current is over 2400A, one can just neglect the very small deviation and regard the mean as constant, which means it is not dependent on time t.

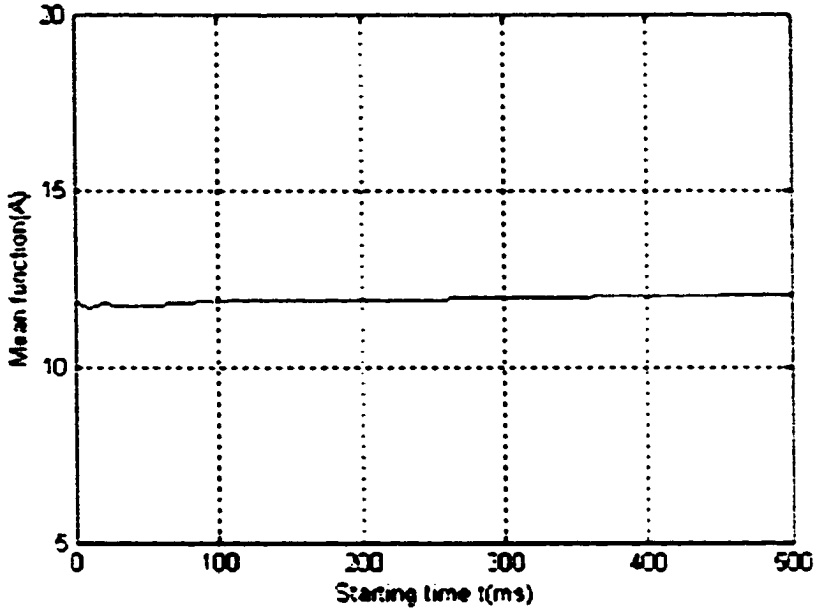

Figure 3.11 Mean of the data as function of starting point t

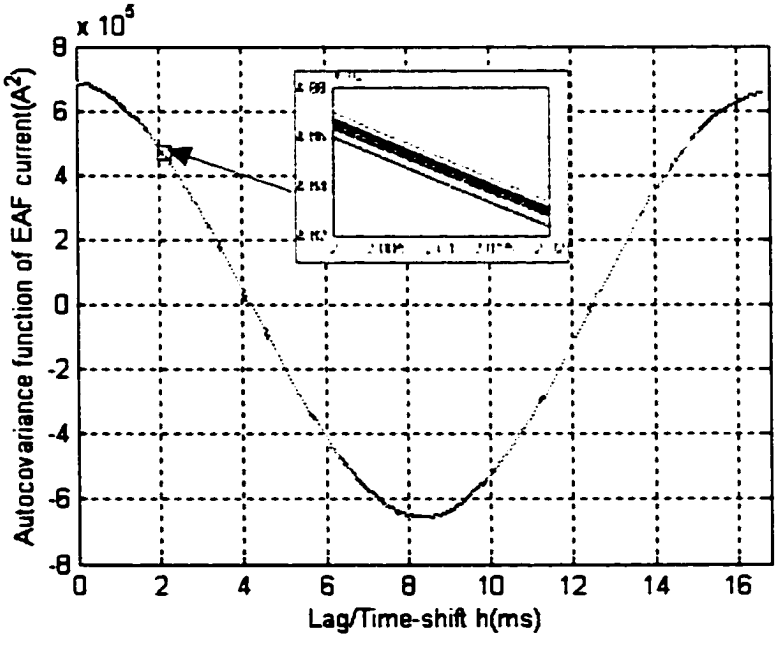

Figure 3.12 SACF of the data as function of time lag h for different starting times t

The curve in Figure 3.12, as a matter of fact, consists of thousands of such curves of the similar shape for different starting time t, as illustrated in the small window view. The SACF

changes with lag h. But for each h, it is almost the same for every starting time t (the maximum difference is less than 0.2% of the average SACF for every h). This means that the SACF is also independent of t for each h. Since the variance is also limited (the point at h=0) and is almost constant for all t, this EAF current time series is (weak) stationary, which demonstrated that the statement about stationarity from Markov modeling is justified.

Table 3.11 Mean function for some starting time

Starting point	Mean
1	11.7825
5	11.7843
10	11.7923
100	11.6380
1000	11.6960
5000	11.8612

Table 3.12 SACF function for some starting time and lag

	SACF			
	t=1	t =50	t =500	t =2500
h=1	683185.6656	683185.8179	683062.5219	683015.5254
h =5	673945.9764	673935.2205	673873.7175	673889.4789
h =10	638654.7313	638639.4729	638594.4139	638544.3084
h =100	-537771.1737	-537728.5239	-537652.8279	-537633.2078
h =150	508903.3961	508906.4861	508812.6851	508970.3660

3.5 One-step-ahead Prediction with Markov-Like Model

Ten seconds of additional actual data are selected for comparison with the results from one-step-ahead prediction by the second order Markov-like model. While predicting, given the state of $Y_i=(X_{i-1}, X_i)$, one can compute with the transition matrix and identify the state that most likely to happen in the next step (which will give the minimized mean squared error). Then the time domain value corresponding to that state is recorded as the estimate $\hat{X}_{i+1}$. The results can be achieved by following the same procedure for the next ten seconds.

3.5.1 Forecasting Techniques

There are many forecasting techniques in use for computing the estimate $\hat{X}_{i+1}$, such as, maximum probability, Monte Carlo and conditional expectation approaches. After getting the information on the current state, the maximum probability approach searches from the transition matrix for the maximum transition probability and locates the corresponding state as the estimate for the next step. While Monte Carlo approach generates a random value U between 0 and 1, which works as an index to find the state for next step. This state is the point at which the sum of transition probabilities for the states previous to it is less than U. But after some comparison, the conditional expectation seems to have an overall better performance of prediction than the other two techniques. In fact, according to principles of forecasting, the method based on conditional expectation method should be preferred. More such comparisons will be presented in Section 4.3. At first the concept will be presented [52], followed by its application to the prediction with Markov-like model.

Suppose we are interested in forecasting the value of a variable Y_{t+1} based on a set of variables X_t observed at time t. For example, we might want to forecast Y_{t+1} based on its m most recent values. In this case, X_t would consist of Y_t, Y_{t-1}, . . . , and Y_{t-m+1}.

Let $Y^*_{t+1/t}$ denote a forecast of Y_{t+1} based on X_t. To evaluate the usefulness of this forecast, we need to specify a loss function, or a summary of how concerned we are if our forecast is off by a particular amount. Very convenient results are obtained from assuming a quadratic loss function. A quadratic loss function means choosing the forecast $Y^*_{t+1/t}$ so as to minimize

$$E(Y_{t+1} - Y^*_{t+1/t})^2 \tag{3.27}$$

Expression 3.27 is known as the mean squared error (MSE) associated with the forecast $Y^*_{t+1/t}$, denoted

$$MSE(Y^*_{t+1/t}) = E(Y_{t+1} - Y^*_{t+1/t})^2 \tag{3.28}$$

The forecast with the smallest mean squared error turns out to be the expectation of Y_{t+1} conditional on X_t:

$$Y^{*}_{t+1|t} = E(Y_{t+1}|\, X_t) \tag{3.29}$$

To verify this claim, consider basing $Y^{*}_{t+1|t}$ on any function $g(X_t)$ other than the conditional expectation,

$$Y^{*}_{t+1|t} = g(X_t) \tag{3.30}$$

For this forecasting rule, the MSE would be

$$\begin{aligned} E[Y_{t+1} - g(X_t)]^2 &= E[Y_{t+1} - E(Y_{t+1}|\, X_t) + E(Y_{t+1}|\, X_t) - g(X_t)]^2 \\ &= E[(Y_{t+1} - E(Y_{t+1}|\, X_t)]^2 + 2E\{[Y_{t+1} - E(Y_{t+1}|\, X_t)]\,[E(Y_{t+1}|\, X_t) - g(X_t)]\} \\ &\quad + E\{[E(Y_{t+1}|\, X_t) - g(X_t)]^2\} \end{aligned} \tag{3.31}$$

Write the middle term on the right side of equation 3.31 as

$$2E[\eta_{t+1}]$$

where $\eta_{t+1} = \{[Y_{t+1} - E(Y_{t+1}|\, X_t)]\,[E(Y_{t+1}|\, X_t) - g(X_t)]\}$

Consider first the expectation of η_{t+1} conditional on X_t. Conditional on, X_t, the terms $E(Y_{t+1}|\, X_t)$ and $g(X_t)$ are known constants and can be factored out of this expectation (The conditional expectation $E(Y_{t+1}|\, X_t)$ represents the conditional population moment of the random variable Y_{t+1} and is not a function of the random variable Y_{t+1} itself. For example, if $Y_{t+1}|\, X_t \sim N(\alpha' X_t, \Omega)$, then $E(Y_{t+1}|\, X_t) = \alpha' X_t$, which does not depend on Y_{t+1}).

$$\begin{aligned} E[\eta_{t+1}|\, X_t] &= E\{[Y_{t+1} - E(Y_{t+1}|\, X_t)]|\, X_t\} * [E(Y_{t+1}|\, X_t) - g(X_t)] \\ &= 0 * [E(Y_{t+1}|\, X_t) - g(X_t)] \\ &= 0 \end{aligned} \tag{3.32}$$

By a straightforward application of the law of iterated expectations (see appendix A) , it follows that

$$E[\eta_{t+1}] = E_{X_t}[\eta_{t+1}|\, X_t] = 0 \tag{3.33}$$

Substituting this back into 3.31 gives

$$E[Y_{t+1} - g(X_t)]^2 = E[(Y_{t+1} - E(Y_{t+1}|\, X_t)]^2 + E\{[E(Y_{t+1}|\, X_t) - g(X_t)]^2\} \tag{3.34}$$

The second term on the right side of equation 3.34 cannot be made smaller than zero, and the first term does not depend on $g(X_t)$. The function $g(X_t)$ that makes the mean squared error in equation 3.34 as small as possible is the function that sets the second term in this equation to zero:

$$E(Y_{t+1}/ X_t) = g(X_t) \tag{3.35}$$

Thus the forecast $g(X_t)$ that minimizes the mean squared error is the conditional expectation $E(Y_{t+1}/ X_t)$, as claimed.

The MSE of this optimal forecast is

$$E[Y_{t+1} - g(X_t)]^2 = E[(Y_{t+1} - E(Y_{t+1}/ X_t)]^2 \tag{3.36}$$

3.5.2 Forecasting with Markov Chain

First, one needs to deduce the format of conditional expectation in the Markov-like model for prediction. In fact, it is very convenient to do so in this case. After building the model from historical data, one can get the Empirical Frequency Function (EFF). Let us denote the general form of EFF as $\pi_{k,}$, which is an estimate of one step transition probability from state k to state l $P\{X_{i+1} \in state\ l / X_i \in state\ k\}$ for the first order chain $\{X\}$. Now, let's assume that the current state is k with the actual value X_t, it has π_{k1} probability to jump to state 1, π_{k2} probability to jump to state 2, ..., π_{kl} probability to jump to state l.,..., π_{kN} probability to jump to state N. Since each state has a real value corresponding to it, say, D_1, D_2, ..., D_l, ...,D_N, the expected value for next step Y_{t+1} can be determined as follows:

$$\hat{Y}_{t+1} = E(Y_{t+1} / X_t) = \sum_{j=1}^{N} \pi_{kj} \times D_j \tag{3.37}$$

The detailed procedure for making predictions with a first order Markov-like model is shown in Figure 3.13.

When using a first order Markov-like model, the one-step-ahead prediction procedure is as follows, assuming that the system is currently at X_1 (i=1) and the number of states N=80:

i. Calculate the state of X_i.

ii. Suppose the state is k, locate the corresponding row of state $k$in the transition matrix to get π_{kl}, l=1,...,N.

iii. Use equation 3.37 to compute the prediction value for X_{i+1}, which is the conditional expectation of X_{i+1}.

iv. Get the next test data X_{i+1} for correction, assign i+1 to i and go back to step i) if the prediction process is not finished.

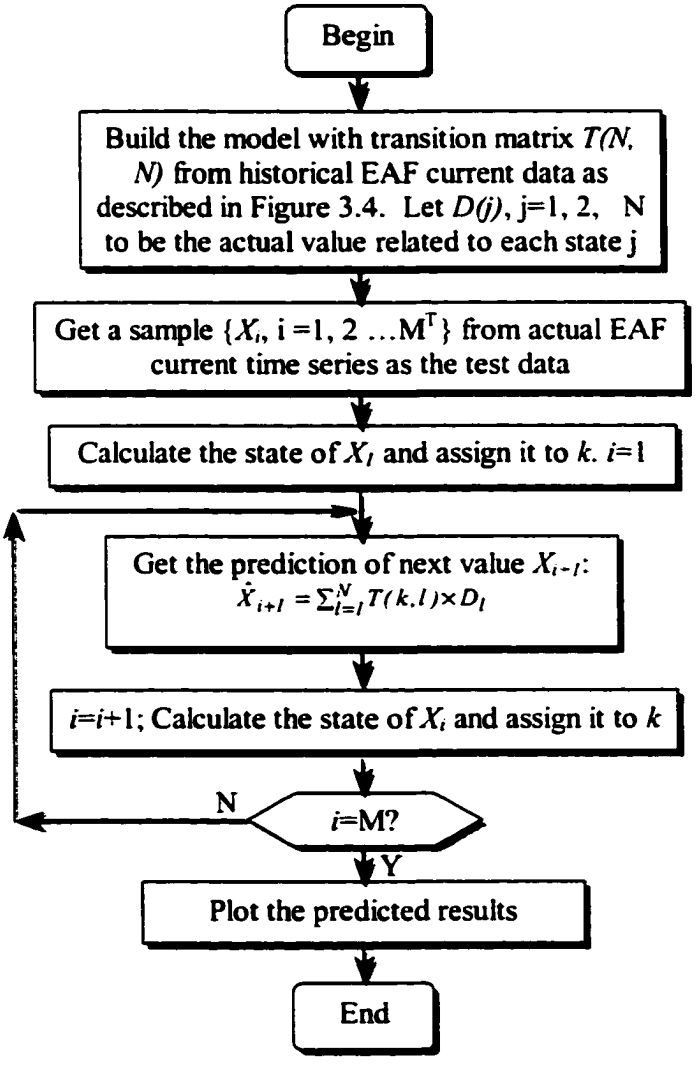

Figure 3.13 Flow chart of one-step-ahead prediction with a first order Markov-like model

The prediction procedure by a second order Markov-like model is similar but more complex since it use a second order chain $Y_i=(X_{i-1}, X_i)$ rather than X_i. The procedure is described below in reference to Figure 3.9(b) and the transition matrix in Figure 3.14.

i. Starting by getting two initial test data X_1, X_2; let i=1.

ii. Calculate the state of $Y_i=(X_{i-1}, X_i)$, again, N=80 here.

iii. Suppose the state is (a,b), locate the corresponding row of this state in the transition matrix π_{hkl}.

iv. Compute the prediction value for X_{i+1}, which is the conditional expectation of X_{i+1}:

$$\hat{X}_{i+1} = \sum_{l=1}^{N} \pi_{abl} \times D_l .$$

v. The state of prediction for X_{i+1} is c in Figure 3.14. Get the test data X_{i+1} to correct the prediction; let $i=i+1$ and go back to step ii) until 10 seconds of prediction is completed.

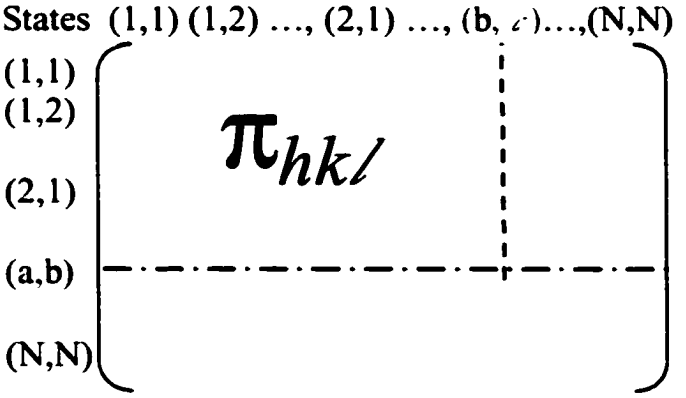

Figure 3.14 Prediction with transition matrix from a second order chain

3.6 One-step-ahead Prediction with ARMA/Kalman Approach

For the convenience of comparison, traditional time series approach will be used in this section for forecasting purpose. The main purpose of time series analysis is to draw inference

from the time series. To do this, first one needs to setup a proper model (stochastic, probabilistic, deterministic etc.) to represent the data. If the model is parametric, it becomes possible to estimate parameters and check for goodness of fit to the time series. If the model is nonparametric, which means it is distribution free—no distributions such as normal, weibull are assumed, then people can still use statistical indices to approach the data and make an inference. Both models can enhance the understanding of the mechanism generating the series. A model may be used simply to provide a compact description of the data, but a suitable model can also be used for testing hypothesis and making predictions. It is useful for simulation studies too. For example in a hydro-plant, the performance of a reservoir depends heavily on the daily inputs of the water to the system—which is random by nature—and the water discharged from the reservoir. Knowing the size and mode of operation of the reservoir, one can use the model to simulate a large number of independent sequences of input and discharge on a daily basis. The fraction of simulated sequence that cause the reservoir to run out of water is the estimate of the probability of emptiness of it during a period of time. Then the operator can schedule to do some pumped storage, if necessary.

Here an ARMA model with Kalman filtering was used for one-step-ahead prediction of the EAF current time series. A time series $\{X_t,\ t=0,1,2,\ldots\}$ is an ARMA(p,q) process if it is stationary and if for every t [50]

$$X_t - \phi_1 X_{t-1} - \ldots - \phi_p X_{t-p} = Z_t + \theta_1 Z_{t-1} + \ldots + \theta_q Z_{t-q} \qquad (3.38)$$

where Z_t is a white noise, $\{Z_t\} \sim WN(0, \sigma^2)$.

p and q are the orders for Auto-Regression (AR) part and Moving Average (MA) part of the ARMA process respectively.

To be concise, it is often expressed as:

$$\phi(B)\, X_t = \theta(B)\, Z_t \qquad (3.39)$$

$\phi(z) = 1 - \phi_1 z - \ldots - \phi_p z^p \quad \theta(z) = 1 + \theta_1 z + \ldots + \theta_q z^q$

Here B is an operator $B X_t = X_{t-1}$.

When using ARMA model to forecast time series taking account of Kalman filtering, the model needs to be represented in a state space format for the sake of Kalman recursions. The general state space representation of a system is:

$$Y_t = G X_t + W_t \tag{3.40}$$

$$X_{t+1} = F X_t + V_t \tag{3.41}$$

Equation 3.40 is observation equation, which expresses Y_t, the w-dimension observation, as a linear function of a v-dimension state variable X_t plus noise $\{W_t\} \sim WN(0, \{R_t\})$. Equation 3.41 is state equation. It updates the state variable X_{t+1} at time $t+1$ in terms of previous state X_t and a noise $\{V_t\} \sim WN(0, \{Q_t\})$.

For ARMA(p,q),

$G=[\theta_{r-1} \ \theta_{r-2} \ldots \theta_0]$; $\quad W_t=0$

$$F=\begin{bmatrix} 0 & 1 & 0 & \ldots & 0 \\ 0 & 0 & 1 & \ldots & 0 \\ \ldots & \ldots & \ldots & \ldots & \\ 0 & 0 & 0 & \ldots & 1 \\ \varphi_r & \varphi_{r-1} & \varphi_{r-2} & \cdots & \varphi_1 \end{bmatrix}; \qquad V_t=\begin{bmatrix} 0 \\ 0 \\ \ldots \\ 0 \\ 1 \end{bmatrix} Z_{t+1}$$

There are three steps involved in Kalman recursions: prediction, filtering and smoothing. In prediction step, the method does a one-step-ahead prediction for Y_t based on observations Y_0, Y_1 ..., Y_{t-1}. Here is the detailed formula. First, get the startup condition.

$$\hat{X}_1 = P\{X / Y_0\} = E(X_1)$$

$$\Omega_1 = E[(X - \hat{X}_1)(X - \hat{X}_1)']$$

where $\hat{X}_1$ is the prediction for X_1. Ω_1 is the error covariance matrix for this prediction. Then, to make use of Innovations algorithm, get the one-step prediction error (innovation) I_t and its mean squared error Δ_t as follows:

$$I_t = Y_t - G_t \hat{X}_t \tag{3.42}$$

$$\Delta_t = G_t \Omega_t G_t' + R_t \tag{3.43}$$

Prior to prediction, Kalman method corrects the state which is just predicted with the current observation and estimate its error covariance $\Omega_{t/t}$. This step is called Kalman filtering:

$$X_{t/t} = \hat{X}_t + \Omega_t G_t' \Delta_t^{-1} I_t \tag{3.44}$$

$$\Omega_{t/t} = \Omega_t - \Omega_t G_t' \Delta_t^{-1} G_t \Omega_t \tag{3.45}$$

Now, it is time to make one-step-ahead prediction for X_{t+1}. Ω_{t+1} is the error covariance matrix for the prediction.

$$\hat{X}_{t+1} = F_t X_{t/t} \tag{3.46}$$

$$\Omega_{t+1} = F_t \Omega_{t/t} F_t' + Q_t \tag{3.47}$$

The previous three steps—innovation, filtering and prediction—will be performed recursively until $t=n$. After this, one can do smoothing based on the n observations. Normally people use fixed interval smoothing, where n is fixed, $1<t<n$. With the n observations, work backward for $t=n-1, n-2, \ldots, 1$. This procedure will estimate X_t again and give its error covariance matrix Ω_t.

$$\Omega_t^* = \Omega_{t/t} F_t' \Omega_{t+1}^{-1} \tag{3.48}$$

$$X_{t/n} = X_{t/t} + \Omega^*_t (X_{t+1/n} - \hat{X}_{t+1}) \tag{3.49}$$

$$\Omega_{t/n} = \Omega_{t/t} + \Omega_t^* (\Omega_{t+1/n} - \Omega_{t+1}) \Omega_t^{*\prime} \tag{3.50}$$

There are some general strategies in such time series modeling:

- Plot the data and check the main features of the graph profile to see if there are trend, seasonality, outlier (widely points, may due to record error).
- Remove the trend, seasonal components etc. to get weak stationary residuals by preliminary transformation (difference, estimate and subtract) to the data.
- Fit the residuals with weak stationary model using some statistical tools like autocorrelation function.

- Put the pieces such as trend and seasonal components back for prediction and explanation.

Now A professional software for time series analysis, PEST (version ITSM2000 [51]), will be used as a tool to analyze the EAF current *X(t)* following the above strategies. First, assume

$$X(t) = m(t) + A(t) \tag{3.51}$$

where *m(t)* is the estimated trend and seasonality function.

A(t) is the ARMA model to be estimated

From the plot of this time series such as in Figure 1.4, harmonic regression maybe a better choice for fitting the EAF current. Taking into account that the current has some kind of seasonality—the fundamental and 2^{nd} to 8^{th} harmonic components are significant, Generalized Least Squares (GLS) method is used to estimate them (the *m(t)* part) and take them away. The regression fit can be seen in Figure 3.15 with the original data.

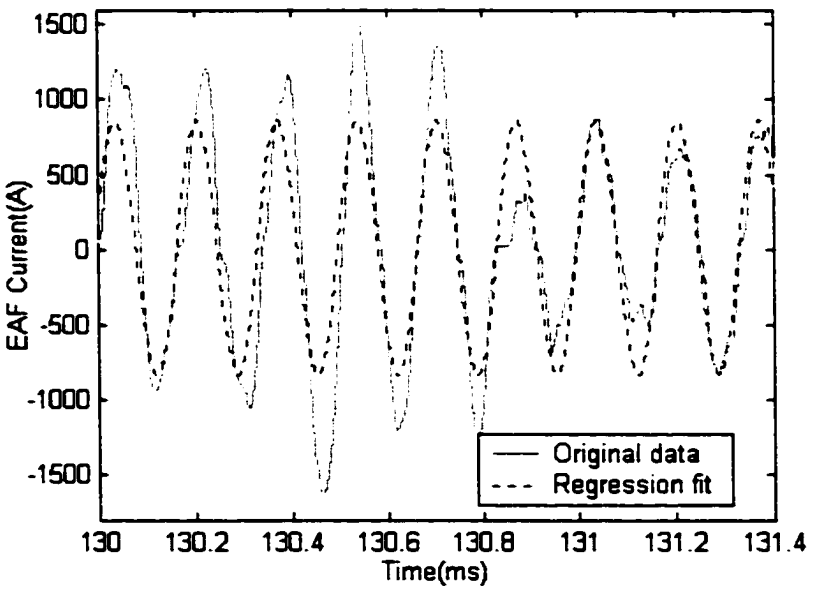

Figure 3.15 Regression fit of EAF current

To find the best ARMA model for A(t), the ACF/PACF (Partial AutoCorrelation Function) for the sample was plotted to check which order of ARMA process is suitable, based on the statistical judgement. PACF (denoted as $\alpha(i),\ i=1,2,\ldots h$) can be calculated as follows from components of ACF $r(i),\ i=1,2,\ldots h$.

$$\alpha(0)=1$$

$$\alpha(h)=\phi_{hh},\ h\geq 1 \tag{3.52}$$

where ϕ_{hh} is the last component of matrix ϕ_h:

$$\phi_h=\Gamma_h^{-1} r_h \tag{3.53}$$

where the square matrix $\Gamma_h=(r(i-j)),\ i,j=1,2,\ldots h$.

the vector $r_h=[r(1), r(2), \ldots, r(h)]$.

The ACF/PACF plot is illustrated in Figure 3.16. But it is somewhat difficult to justify visually since the bound $\pm 1.96/\sqrt{n}$ is very small and can hardly be seen because n is large here. So a preliminary estimate will be used to find a best AR order for it based on minimum AICC (Akaike's Information Criterion, bais-Corrected version) method with Innovation approach. Then use the Maximum Likelihood (ML) technique to optimize the ARMA model. The final step in model construction is to test the whiteness of the residuals to see if model is accurate enough, if not one needs to go back to change model parameters and reestimate it.

After geting the ARMA model, one can use it for one-step-ahead prediction. To make use of the Kalman filtering technique, one should take a new measurement into account and follow the innovation, filtering, prediction procedures as described in equations 3.42 to 3.47 after every predition.

3.7 Case Study of One-step-ahead Prediction

In this case study, a first order Markov chain, a second Markov chain as well as the ARMA/Kalman method were used to make one-step-ahead prediction. The historical data for building the models and the test data for evaluating the prediction performance are all the

same for these three methods. Two hundred points of such prediction results were given in Figure 3.17 along with the actual test data. It shows that the difference between the actual and predicted data at every time step is very small. To measure the accuracy of the prediction, a strict but effective index is the Root Mean Squared value of prediction Error $e_i = |X_i - \hat{X}_i|$ [53], which is called RMSE in the following. This will yield the absolute value. One can also obtain the relative RMSE of *Np* points of predictions as a fraction of the peak value in the data (EAF current in this case) as a percentage, which is expressed as %RMSE:

$$\%RMSE = RMSE \div (peak\ of\ data) \times 100 \tag{3.54}$$

$$\text{where } RMSE = \sqrt{\frac{1}{Np}\sum_{i=1}^{Np}(\hat{x}_i - x_i)^2} \tag{3.55}$$

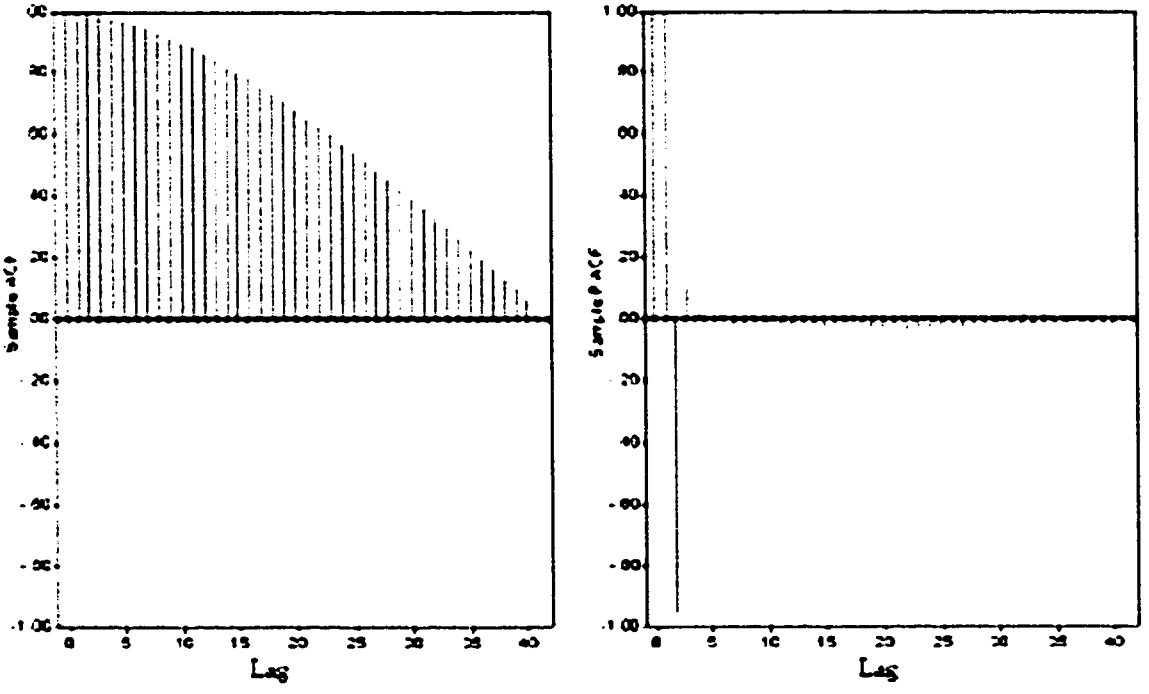

Figure 3.16 Sample ACF/PACF for the regression residual of EAF current

In Table 3.13 one compares the predicted values according to a first order Markov chain, a second order Markov chain and ARMA/Kalman method. All these methods seem to

be efficient when performing one-step-ahead prediction with their %RMSE indices less than 0.8%. But comparatively, the second order Markov chain offers higher accuracy than the other two methods. What's more, the first order Markov chain works slightly better than the ARMA/Kalman method. This can be easily seen from prediction errors plot in Figure 3.18.

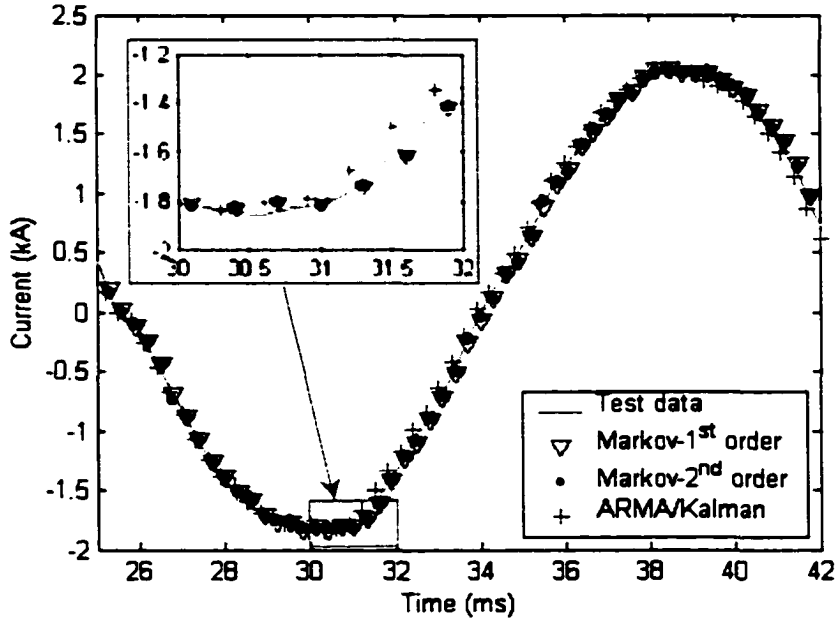

Figure 3.17 Comparison of predicted current from various approaches with actual data

Table 3.13 Comparison of various prediction approaches

	RMSE (A)	%RMSE
Second order Markov chain	31.925614	0.590297
First order Markov chain	38.685712	0.715289
ARMA/Kalman	39.635698	0.732854

So one can conclude that, although the ARMA model and the Markov-like models applied to the same data and the same length of predictions are made, the Markov chain model is more accurate than modified traditional ARMA process for EAF current, especially the one with a second order Markov chain. Kalman Filtering technique is powerful for prediction and application in control. For time series, the ARMA model is also popular. But every method has its limitations. ARMA assumes that the time series is a linear process, as it

can be seen from equation 3.39. But the EAF current is very difficult to be expressed in a structure of finite linear items. This fact may be easily found from Figure 3.19, which shows the ACF and PACF for both sample and model of *A(t)*—EAF current after being taken away the trend and seasonality by regression. The light shaded area depicts the sample ACF/PACF and the heavy shaded area is for the model ACF/PACF. The model can characterize the sample ACF/PACF for the first 50 lags, but not the ones that after. If one tries to build an accurate model, he may need infinite sequence of $\phi(B)$ and $\theta(B)$ in equation 3.39, which is not realistic in practice.

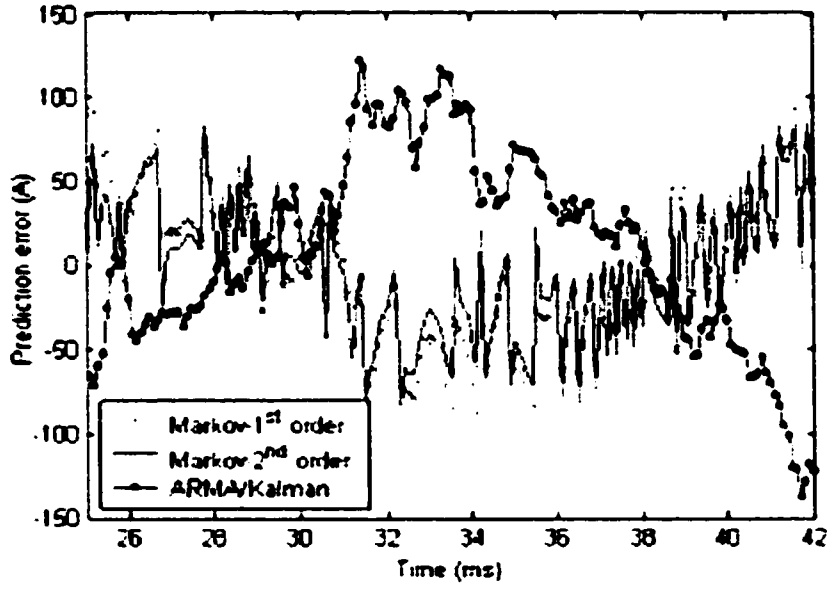

Figure 3.18 Waveforms for one-step-ahead prediction error

Some statistical indices such as EFF and ECDF are computed in the same way to the predicted data as to the actual data in the second order Markov chain framework. The EFFs from the result are shown in Figure 3.20. They are close to those in Figure 3.10 (the EFF for "post-model" is the stationary distribution from the second order Markov-like model on the predicted data). It is also the case in Table 3.14, where for predicted data the statistical indices of mean and variance are compared with those derived from the actual data. This suggests that the model is very effective for short and long term predictions.

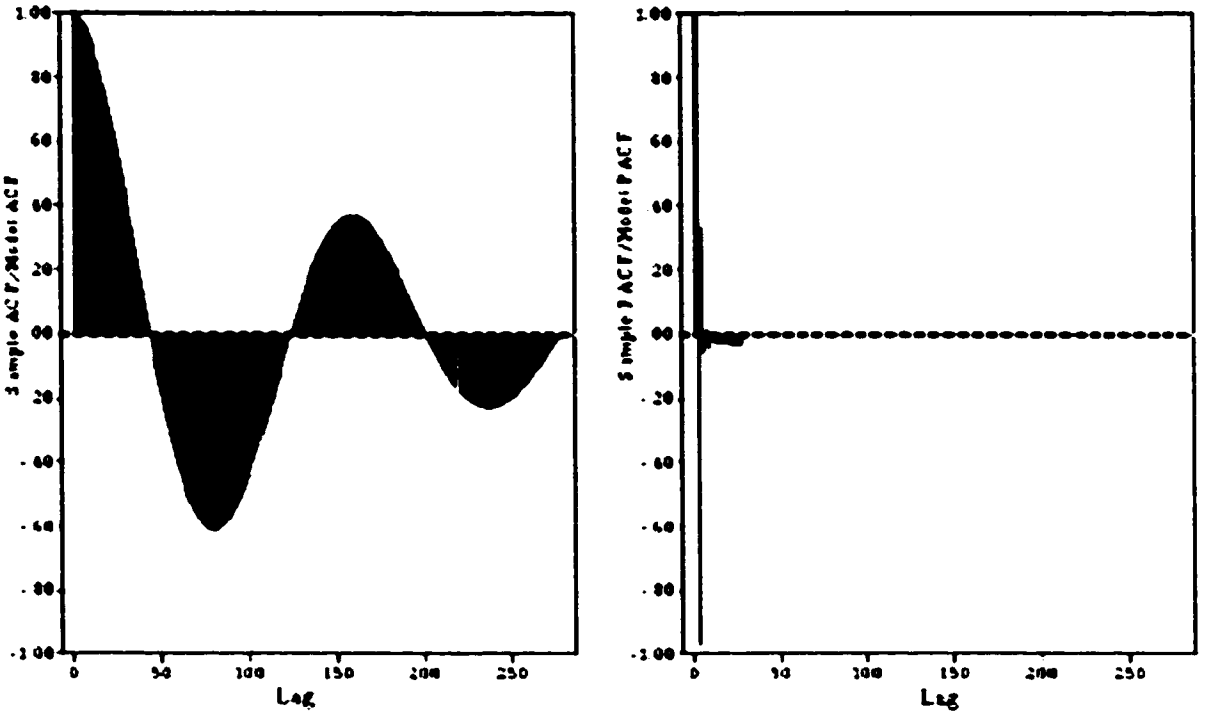

Figure 3.19 Sample and model ACF/PACF for EAF current

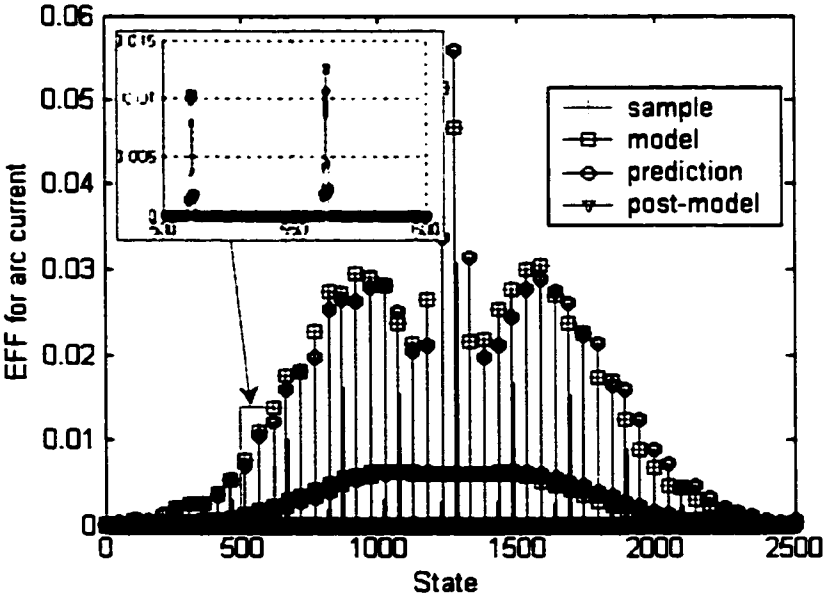

Figure 3.20 EFFs for the predicted current from a second order Markov-like model N=50

Table 3.14 Statistical indices of EFFs for current test sample and predicted data

	Predicted data	Actual data
Mean	0.0004	0.0004
Variance	0.0000079	0.0000080

Based on these results, it is suggested that the transition matrix should be a key parameter of the model for the following reasons:

- The transition matrix reflects the dynamic characteristics of the system, and it is flexible for prediction.
- The prediction using the model is proved to be effective.

3.8 Summary

Based on the Markov-like Modeling of the EAF current/voltage data as detailed in Section 3.4 to Section 3.6, as well as the comparison with ARMA/Kalman method in Section 3.7, one is able to draw the following conclusions.

- From a deterministic point of view, the EAF current time series $\{X_i: i=1, 2, \ldots M\}$ look quite chaotic and nonlinear. However, from the Markov-like modeling point of view and classic time series theory, there is a remarkable regularity. This property was further tested according to classic time series theory.
- The Empirical Frequency Function, Empirical Transition Frequencies and other time averages exhibit consistency over time. Thus observing the first part of the data set it is possible to make prediction about various time averages for the following data sets. For a long-term time average prediction of this kind, the first order Markov-like model for $\{X\}$ is quite adequate.
- In short-term prediction, the second order Markov-like chain Y is better. It is found that the calculated probabilities based on $\{Y_i=(X_i, X_{i+1})\}$ are sharper, i.e., very close to I or 0. Hence it is better for accurate prediction than the first order ones. This suggests that the first order time series $\{X\}$ is not strictly Markovian and yet the methodology provides a relatively accurate prediction scheme. Thus the procedure

is statistically robust. In some cases, it maybe necessary to use a third or higher order Markov-like model, but at the expense of increased computation.

- The Markov-like models reveal a better performance than the ARMA/Kalman method in forecasting. This is mainly due to their effectiveness in portraying the dynamics of the EAF current in a statistical sense.

In all, it appears that the Markov-like modeling is a very effective alternative to analyze the dynamics of an EAF system and other kinds of discrete-valued time series with similar behaviors. However, in power system operation, people care more about on-line corrections and power quality improvement, which requires longer length of accurate prediction for adaptive adjustments. This will be discussed in the next chapter.

4 FUNCTION SPACE VALUED MARKOV-LIKE MODEL

In Chapter 3, a first and second order Markov chain was used to model the EAF data. In the extension of this modeling problem, a novel approach of function space valued Markov-like model is proposed to make it more convenient and powerful for an effective prediction. The approach uses the fundamental idea of Markov-like modeling but generalizes the point case to the concept of a cycle-vector function. This makes it possible to predict the EAF variables over one or more cycles ahead.

4.1 Introduction to Function Space Approach

In the model proposed earlier [11], only states illustrated in Figure 3.3 were considered to build the basic Markov-like models (first order and second order) for the EAF current. Based on these models, one can generate appropriate power quality indices. It is also useful for prediction. However, the prediction is only one point/state ahead in time. Although the accuracy of prediction was quite remarkable with a second order Markov like model, it is not so practical since data measurements and communications in power system may not be fast enough for fast, adaptive and accurate compensation. The function space approach proposed in this chapter generalizes the point case idea to the cycle-vector (vector consists of points over a cycle) case. The explanation to the concepts of point, state case and cycle case is illustrated in Figure 4.1. They differ from each other by the way of treating the object under study. In the point case, the characteristics of the individual time series data are the major concern. It indulges into the detail and may loose the sense of an overall trend. The state case has been used in Chapter 3. By dividing the data range into several suitable states, powerful mathematical tools can be applied to get good results. The cycle case goes somewhat further. In order to grasp the development of the whole phenomenon, it considers each cycle as an analytical element. This concept will be demonstrated further in this chapter.

Since a cycle-vector, as it is defined in Section 4.2.2, is a function over a random length of time domain involving several random variables from the original time series, it is called function space valued Markov-like model. Also, the original cycle-vector function is too

complex and cumbersome to describe and process. Several simplified functions are brought in to approximate this function. Among these approximations are FFT frequency decomposition, polynomial fit, function of maxima, minima and their positions—f(Max, Min, Positions), and function of maxima, minima, length and shape of a cycle—f(Max; Min; Cycle Length; Shape). These approximations are studied in detail in Section 4.2.3. The results and analysis are presented in Section 4.3 through extensive applications.

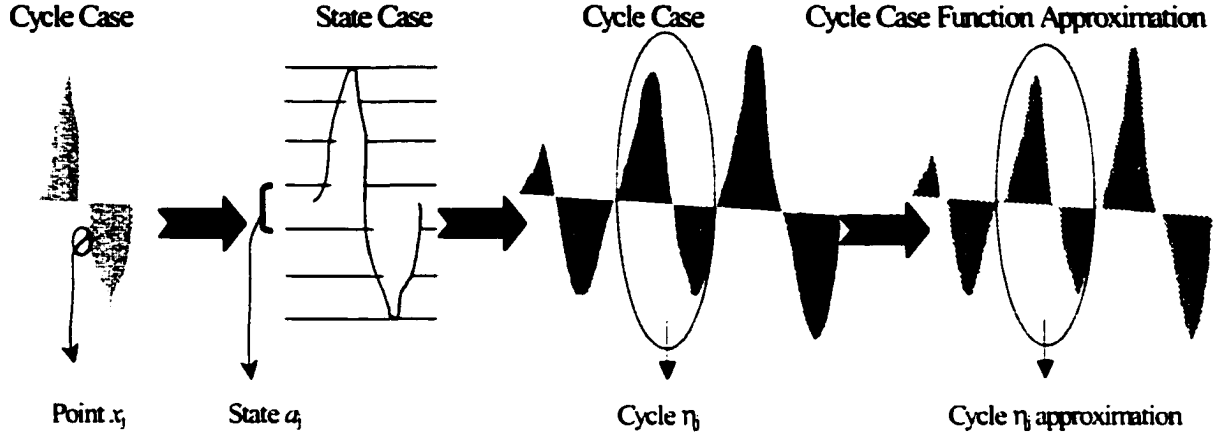

Figure 4.1 Illustration of cycle case, state case and function approximation of a cycle case

4.2 Model Development

To develop the Markov-like model in function space, it is a good practice to check the Markovian property for the EAF current, as it is for the basic models. The general method for this purpose is addressed first. Then the cycle-vector representation of the original time series is discussed. To simplify the problem and make its prediction efficient and practical, several functions are proposed to approximate a cycle and Markov method is applied to the parameters of such functions, as illustrated in Figure 4.2. For each parameter $k(i)$ there is a transition matrix $\boldsymbol{P}^i$ corresponding to it, where $\boldsymbol{P}^i$ is estimated from the time series $k_1(i)$, $k_2(i)$, ... The detailed formulation of the model is discussed in Section 4.2.1 to Section 4.2.3.

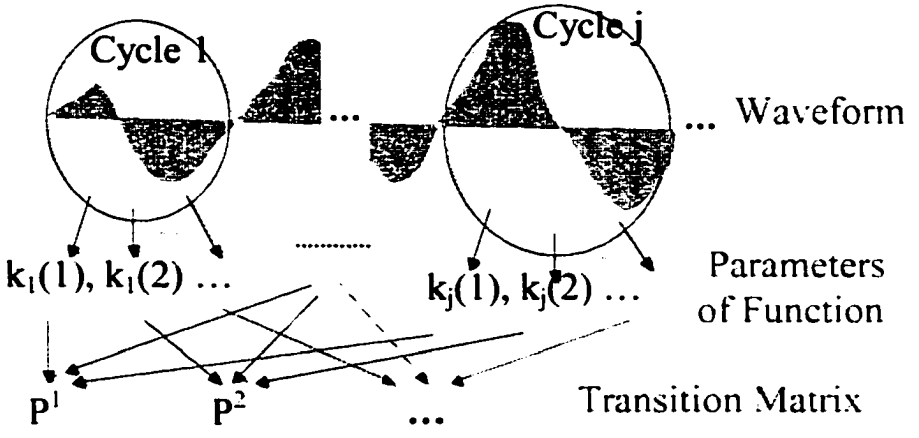

Figure 4.2 Illustration of function approximation using Markov-like modeling

4.2.1 Verify the Markov Property of the EAF Current

As detailed in Section 3.3, given the time series X_j with a continuous state space, break up the range of the global minimum to global maximum into a finite number (say N) of intervals and discretize state space into $\{1,2,\ldots. N\}$ with $X_j \in$ State k if X_j falls in the k^{th} interval. Now consider a time series $\{X_j, j=1,2,\ldots M\}$ with its state space $S=\{1,2,\ldots. N\}$ as illustrated in Figure 3.3. Follow the same terminology about the empirical transition probabilities such as π_{kl} , π_{hkl} and π_{ghkl}, the Markov property of the time series of EAF current/voltage can be tested as follows.

- Check whether $\pi_{kl} \approx \pi_{hkl}$ for all h, if so, the time series is a first order Markov chain based on the non-memory property of Markov chain as defined in equation 4.1.
- If it is not a first order Markov chain, test if $\pi_{ghkl} \approx \pi_{hkl}$ for all g, if so, it is a second order Markov-like chain and so on.

4.2.2 Generalization to a Function Space Approach

Before the generalization from state case Markov chain to function space valued Markov chain, specific definition of a cycle will be addressed here. The EAF current or

voltage waveform is not periodic. To make the expression of the approach and prediction convenient, two kinds of cycle concepts are applied in the following models. One of them is to, taking account of the system frequency (60hz), set time period 1/60s as the fixed cycle interval. Another is to define the cycle as the interval between two consecutive positive crossing points. The latter one is done by first fixing a level that is identified as zero level. A cycle begins when the time series has a positive crossing. It goes from below zero to above zero and ends when the next positive crossing takes place. In between, it increases to maximum followed by a decrease to a minimum with a negative or down crossing of zero level and then increase to a positive or up crossing of zero level, as illustrated in Figure 4.3. In this case, the intervals are varying from cycle to cycle. The range of frequencies of the EAF for the p-cycle is generally between 51Hz to 71Hz.

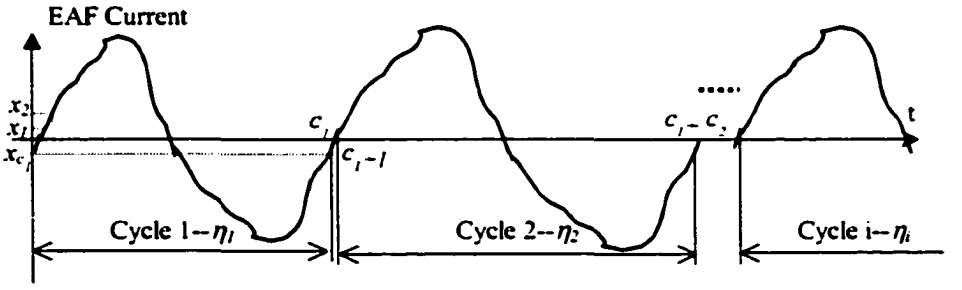

Figure 4.3 Definition of a cycle

Now, it is time to generalize from the state case to cycle case.

Let η_1, η_2, η_3, ..., $\eta_{M'}$ (here M' is the number of cycles) be consecutive cycles as defined below:

$$\begin{aligned}
\eta_1 &= X_1, X_2, X_3, \ldots\ldots, X_{c_1} \\
\eta_2 &= X_{c_1+1}, X_{c_1+2}, X_{c_1+3}, \ldots\ldots, X_{c_1+c_2} \\
\eta_3 &= X_{c_1+c_2+1}, X_{c_1+c_2+2}, X_{c_1+c_2+3}, \ldots\ldots, X_{c_1+c_2+c_3} \\
&\ldots\ldots
\end{aligned} \qquad (4.1)$$

where c_1, c_2, c_3...are the number of time points in cycles 1, 2, 3..., respectively

Now $\{\eta_j, j=1,2,...M'\}$ is a new time series and the Markov-like theory described in 3.3.2 can be applied. In particular, if $\{\eta_j\}$ is a first order Markov chain in cycle case, then for two consecutive cycles η_i, η_{i+1} with the number of points c_i and c_{i-1}, the following is true.

$$\begin{aligned}
&P\{X_{L+c_i+c_{i+1}} \in \hat{a}_{L+c_{i+1}+c_i}, X_{L+c_i+c_{i+1}-1} \in \hat{a}_{L+c_{i+1}+c_i-1}, \ldots X_{L+c_i+1} \in \hat{a}_{L+c_i+1} / \\
&\quad X_{L+c_i} \in \hat{a}_{L+c_i}, X_{L+c_i-1} \in \hat{a}_{L+c_i-1}, \ldots X_{L+1} \in \hat{a}_{L+1}, X_L \in a_L, X_{L-1} \in \hat{a}_{L-1}, \ldots\} \\
&= P\{X_{L+c_i+c_{i+1}} \in \hat{a}_{L+c_{i+1}+c_i}, X_{L+c_i+c_{i+1}-1} \in \hat{a}_{L+c_{i+1}+c_i-1}, \ldots X_{L+c_i+1} \in \hat{a}_{L+c_i+1} / \\
&\quad X_{L+c_i} \in \hat{a}_{L+c_i}, X_{L+c_i-1} \in \hat{a}_{L+c_i-1}, \ldots X_{L+1} \in \hat{a}_{L+1}\} \\
&= P\{\eta_{i+1} \in (\hat{a}_{c_i+c_{i+1}}, \hat{a}_{c_i+c_{i+1}-1}, \ldots \hat{a}_{c_i+1}) / \eta_i \in (\hat{a}_{c_i}, \hat{a}_{c_i-1}, \ldots \hat{a}_1)\}
\end{aligned} \tag{4.2}$$

where L is the number of points from the start to the beginning of the present cycle i.

$$\hat{a} \in S = \{1,2,\ldots N\}$$

To be simple, Equation 4.2 can be written as

$$\begin{aligned}
&P\{\eta_{i+1} \in s_{i+1} / \eta_i \in s_i, \eta_{i-1} \in s_{i-1}, \ldots, \eta_1 \in s_1\} \\
&= P\{\eta_{i+1} \in s_{i+1} / \eta_i \in s_i\}
\end{aligned} \tag{4.3}$$

where $s_1, s_2, \ldots s_i, s_{i-1}$, are state sequence sets for cycles $\eta_1, \eta_2, \ldots, \eta_i, \eta_{i+1}$ respectively.

That is to say, the conditional distribution of η_{i+1} giving η_i is the same as that of η_{i+1} giving $\eta_i, \eta_{i-1}, \ldots\ldots \eta_1$. The procedure of building the model is similar to that in Section 3.3. The difference is that in 3.3.2, the time series is $\{X_j, j=1,2,...M\}$ with state space {1, 2, ..., N}; while in the cycle-case, the time series is $\{\eta_j, j=1,2,...M'\}$ with state vectors $\{s_j\}$ whose components are from S={1, 2, ..., N}. But this approach needs much more data to get satisfactory accuracy. Thus it is necessary to find out if any cycle η_i can be represented using several decoupled parameters so that one is able to apply Markov-like chain on the parameter series for all the cycles just like on individual measurements.

4.2.3 Function Approximations to a Cycle-vector

In reality, the direct use of cycle case Markov-like chain maybe not feasible. For example, if only 10 states are used, and one cycle is divided into 10 intervals, the state space

for the cycle chain $\{\eta_j, j=1,2,...M'\}$ would be 10^{10}=10 billion—that is too huge. So it is not practical—since memory requirement of the computer is high, computational work is heavy and no commercial PC can ever handle it. For applicability each cycle needs to be approximated by a fewer number of parameters. Several approaches for this approximation are tried for a comparison between them as described below.

4.2.3.1 FFT Frequency Decomposition

4.2.3.1.1 Random Cycle length case

Considering the Fourier transformation, for the data of i[th] cycle $\eta_i = \{X_j; j=L+1, L+2, \ldots L+c_i\}$. We can get the FFT components [54-56]

$$F_i(k) = \frac{1}{C^m} \sum_{n=0}^{C^m-1} (X(L+n+1)\cos(2\pi kn/C^m) - jX(L+n+1)\sin(2\pi kn/C^m)) \qquad (4.4)$$

Then the vector $(F_i(1)\ F_i(2)\ldots\ldots\ F_i(C^m))$ can represent cycle η_i. Since the length of each cycle varies, a constant value C^m, which is not less than the maximum value of $\{c_1, c_2, \ldots c_{M'}\}$, will be used to make sure the frequency components of each cycle are for the same sequence of frequencies. For cycles whose lengths are less than C^m, zero-padding them to $C^m = max\{c_i, i=1,\ldots,M'\}$ numbers (Assign 0 to $\{x_j; j=c_{i-1}, c_{i-2}, \ldots C^m\}$) and then apply FFT on the new time series of each cycle.

In practice, truncated number of frequencies can be used, such as $k=1,2,\ldots.Tr$ $(Tr<<c_i)$, because the magnitudes of some later frequencies are close to zero for EAF current. Therefore $\eta^*_i = \{F_i(k), k=1,2,\ldots..,Tr\}$, $i=1,2,\ldots M'$ will be the new time series under study. The cycle by cycle Fourier series are illustrated in Table 4.1.

Here an important assumption about the underlying system will be made to simplify the problem, namely that signal of different frequencies are independent of each other (i.e. not coupled). This implies that for different frequency numbers $k=1,2,\ldots..,Tr$, the time series $\{F_i(k), i=1,2,3\ldots M'\}$ are independent of each other, which is true for most electric systems.

With this assumption, Markov method can be applied to the time series $\{F_i(k), i=1,2,\ldots.M'\}$ separately for each $k=1, 2, \ldots Tr$ (i.e. a column in Table 4.1) with a first or a

second order Markov chain just like the procedure for basic models in Section 3.3.2 [11]. As a result, transition matrices P^1, P^2, ..., P^{Tr} are estimated for each frequency component $k=1, 2, \ldots$ and Tr respectively.

Table 4.1 Fourier components of frequency numbers up to Tr for each cycle

Cycle	Fourier frequency components					
	1	*2*	...	*k*	...	*Tr*
1	$F_1(1)$	$F_1(2)$	...	$F_1(k)$	...	$F_1(Tr)$
2	$F_2(1)$	$F_2(2)$	...	$F_2(k)$	...	$F_2(Tr)$
...	...	...	...	...	...	...
i	$F_i(1)$	$F_i(2)$	...	$F_i(k)$	...	$F_i(Tr)$
...	...	...	...	...	...	...
M'	$F_{M'}(1)$	$F_{M'}(2)$	...	$F_{M'}(k)$	...	$F_{M'}(Tr)$

For prediction with a first order Markov chain, assuming the system is now at cycle i and the cycle is truncated up to $Tr<<c_i$ harmonics with the frequency parameters being $F_i(1)$, $F_i(2)$, ..., $F_i(Tr)$, each of which has its transition matrix P^1, P^2, ..., P^{Tr}. The jth frequency component of the (i+1)th cycle is then obtained by conditional expectation as presented in Section 3.5.1: $\hat{F}_{i+1}(j) = E(F_{i+1}(j)) = \sum_{l=1}^{N} p_{hl} \times D_l$ where $\hat{F}_{i+1}(j)$ is the value to be predicted, h is the current state for $F_i(j)$ and D_l is the real value corresponds to each state $l=1, 2,\ldots, N$. Here N is the number of states. This gives a minimized mean squared error $E(F_{i-1}(j)-\hat{F}_{i+1}(j))^2$. It can also be estimated as the one with the highest empirical frequency giving the values of jth frequency component of the ith cycle if a first order Markov chain is used.

$$F_{i+1}(j) = \{m_j : P^j((F_i(j), m_j)) = max(P^j(F_i(j), k), k = 1,2,\ldots,N\} \quad (4.5)$$

Or one can use Monte Carlo concept on the cumulative distribution frequency (CDF) of the transition probability from the current state to the immediate future state:

$$F_{i+1}(j) = \{m_j = max(k), (cdf(P^j(F_i(j), k), k = 1,2,\ldots,N) < U\} \quad (4.6)$$

where U is a generated random value in (0,1).

Once getting all the Fourier components for cycle i+1: $F_{i-1}(1)$, $F_{i-1}(2)$, ..., $F_{i-1}(Tr)$, perform re-convolution (reverse FFT) to achieve data for cycle i+1:

$$\hat{X}(n) = \sum_{k=0}^{Tr-1} (real(F_{i+1}(k)\cos(2\pi\ kn/C^m) - imag(F_{i+1}(k))\sin(2\pi kn/C^m)) \qquad (4.7)$$

$$n=1,2, \ldots .c_{i+1}$$

After correcting forecasted data $\hat{X}(n)$, n=1, 2, $\ldots c_{i+1}$ of the $(i+1)^{th}$ cycle with actual data, one can continue to predict more cycles ahead following the same procedure described here.

4.2.3.1.2 Fixed Cycle length case

However, the cycle length is really random (as illustrated in Figure 4.4), one may have difficulty to apply FFT. Although zero-padding is possible to make the Fourier components of each cycle relate to the same frequencies, more errors may be introduced. Here one can choose a fixed number of points for each cycle, that is to say, $c_1 = c_2 = \ldots = c_i = \ldots = C$. Since the fundamental frequency of the system is 60HZ, it will be more convenient to set $C=166$ *or* 167 (with the sample rate—10,000 points per second). When taking account of the mechanism of FFT algorithm, selecting a close number $C=167$ with zero padding to 256=2^8 will increase the computational speed.

Figure 4.5 depicts the main structure of such a model. First, the nonparametric model—transition matrices are constructed from the historical data. Only a necessary truncated number (Tr) of parameters are used for the sake of computation resources in this function approximation. Then at the beginning of every current cycle, use FFT transfer to get the FFT series of the previous one or two cycles. According to the features of the FFT series, one can get predictions of FFT series for the next one cycle or several cycles with the prediction techniques of either conditional expectation or maximum probability, or Monte Carlo. Prediction data thus can be obtained by applying FFT re-convolution (inverse FFT) on the new FFT series. This structure is also applicable to other function approximations for the Markov-like model.

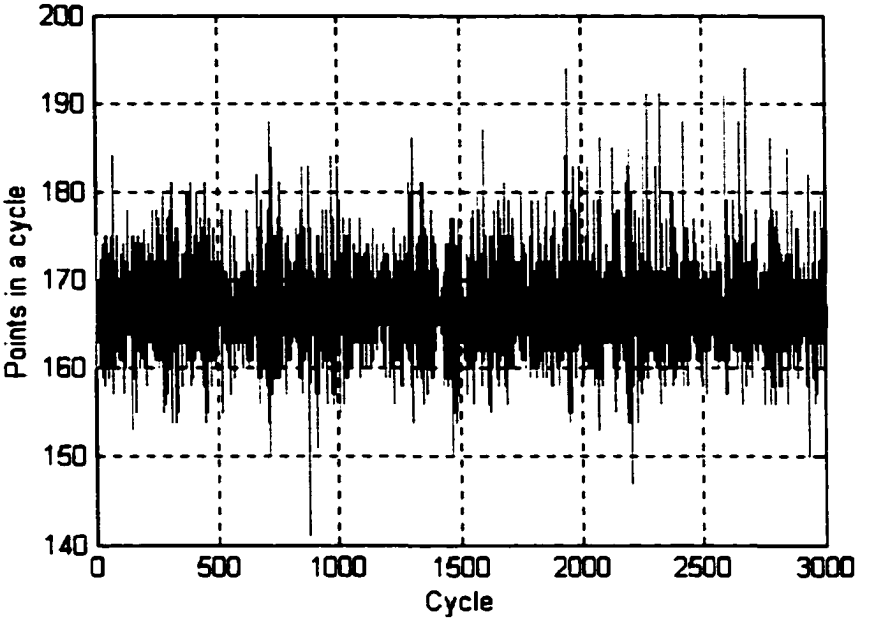

Figure 4.4 Illustration of change of cycle length (in points)

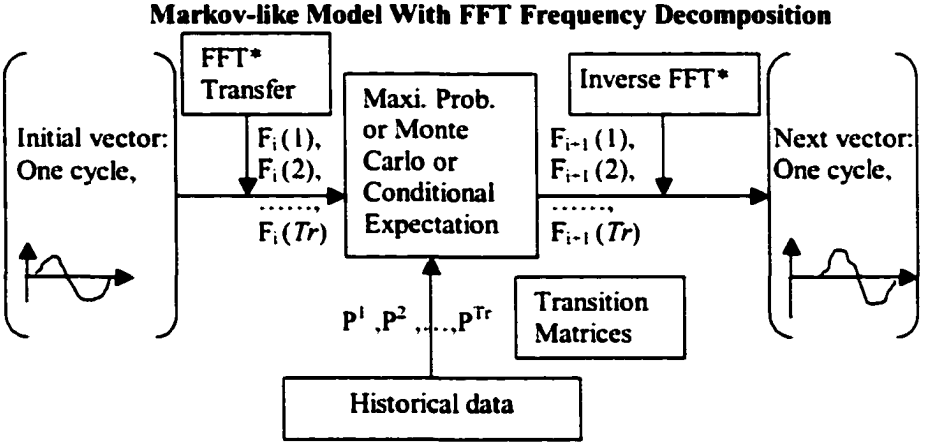

Figure 4.5 EAF prediction model using FFT frequency decomposition

4.2.3.2 Polynomial Fit

In this approach, the i^{th} cycle $\eta_i = \{X_{L+1}, X_{L+2}, \ldots, X_{L+c_i}\}$ is approximated using a polynomial function:

$$X_i(t) = b_i(1) + b_i(2)*t + b_i(3)*t^2 + \ldots b_i(s+1)*t^s \qquad (4.8)$$

where t=1, 2..., c_i

s=the highest order of the polynomial function.

Generally, for the sinusoid like waveforms, s=3 is enough (the higher order coefficients are zero in this case).

Then transition matrices can be built for $\{b_i(k),\ i=1,2,...M'\}$ corresponding to $k=1,2,...,s+1$ separately, just like in the FFT frequency decomposition method. Also, these transition matrices will be used in prediction with test data in a similar way.

If the random cycle length is used, transition matrix for the length (or frequency) of the cycles should also be constructed and included in the prediction procedure. The structure of prediction using this model is shown in Figure 4.6. It is not much different from Figure 4.5 except the function approximation related parts.

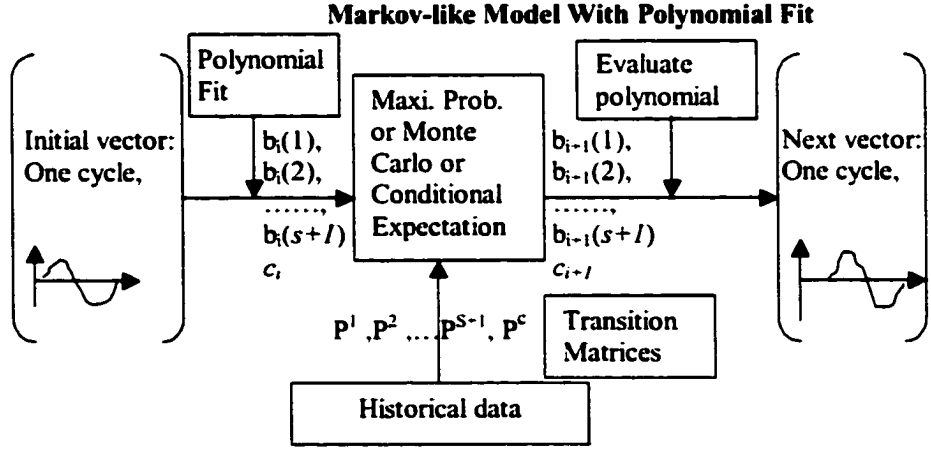

Figure 4.6 EAF prediction model using polynomial fit

But the above suggestion is based on the assumption that $\{b(k),\ k=1,2,...,s+1\}$ are independent of each other. In fact, this assumption doesn't hold here, thus the prediction results should be very bad, as it will be shown later.

To solve the problem of dependence, a new series called pattern index sequence, is generated in the following way:

i). Arbitrarily mark the coefficients vector $\{b_1(k),\ k=1,2,\ldots,s\}$ of the first cycle with pattern index one.

ii). For the following consecutive cycles, compare the coefficients vector $\{b_i(k),\ k=1,2,\ldots,s\}$ to the coefficients vector recorded as patterns. If the error is within accuracy tolerance for a specific pattern, Mark this cycle with the same pattern index as this pattern. Otherwise, create a new record by increasing the pattern index by 1. This procedure is illustrated in Table 4.2

Table 4.2 Procedures of pattern index approach for polynomial fit

cycle no.	cycle coefficients	pattern index
1	$b_1(1), b_1(2),\ldots, b_1(s),$	1
2	$b_2(1), b_2(2),\ldots, b_2(s),$	1 (if $\lvert b_2(k)-b_1(k)\rvert<\varepsilon$) or else 2
i	$b_i(1), b_i(2),\ldots, b_i(s),$	1 (if $\lvert b_i(k)-b_1(k)\rvert<\varepsilon$) or 2 (if $\lvert b_i(k)-b_2(k)\rvert<\varepsilon$) or ...even i

Then one can build transition matrix on the pattern index and apply Markov-like method to it as the previous methods. Also, the coefficients corresponding to the pattern indices are recorded and will be used in prediction.

4.2.3.3 Function of Maximum, Minimum and Positions

In this approach the vector $(M_i, m_i, T_i(1), T_i(2), T_i(3), T_i(4))$ is used to capture the i^{th} cycle $\eta_i = \{X_j,\ j=L+1,\ L+2,\ldots,\ L+c_i\}$. For the EAF current, the maximum and minimum values of each cycle are also stochastic, as illustrated in Figure 4.7. According to Figure 4.8, for cycle η_i, M_i is the maximum value, m_i is the minimum value, $T_i(1)$ is the time period from the beginning to the maximum, $T_i(2)$ is the time period from the maximum to negative cross, $T_i(3)$ is the time period from the negative cross to the minimum and $T_i(4)$ is the time period from the minimum to the end.

Apply Markov method on M_i, m_i, $T_i(1)$, $T_i(2)$, $T_i(3)$ and $T_i(4)$ or M_i, m_i, $T_i(1)$, $T_i(1)+T_i(2)$, $T_i(1)+T_i(2)+T_i(3)$ and $T_i(1)+T_i(2)+T_i(3)+T_i(4)$ separately with the assumption

that these random variables are independent. If the results show that the assumption is not reasonable, make pattern indices for $\{M_i, m_i\}$ and $\{T_i(1), T_i(2), T_i(3), T_i(4)\}$ as in the polynomial fit approach above. The structure for one-cycle ahead prediction using this method is similar to those for FFT frequency decomposition (Figure 4.5) and polynomial fit (Figure 4.6). Only the function approximation parts need to be changed accordingly.

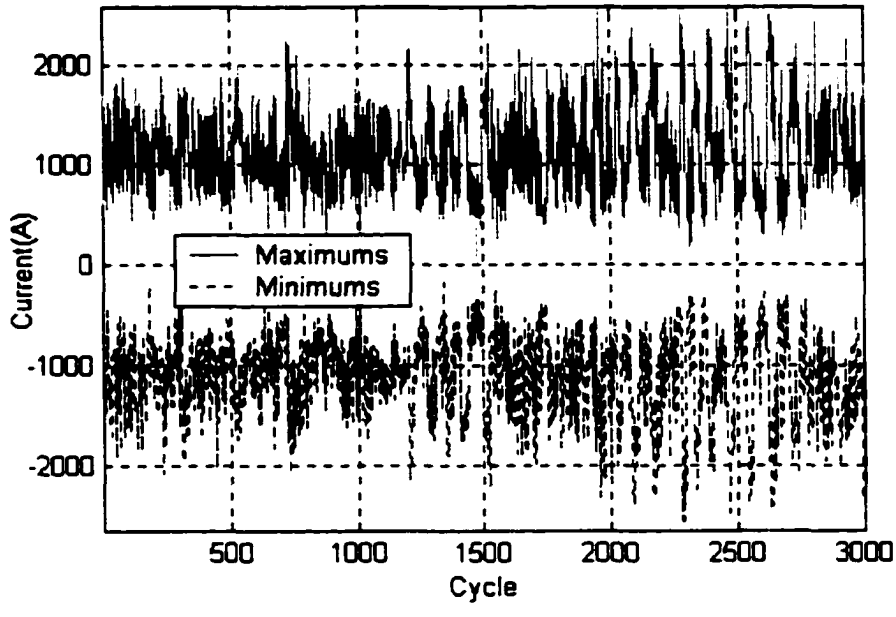

Figure 4.7 Minimum, Maximum of each cycle for EAF current

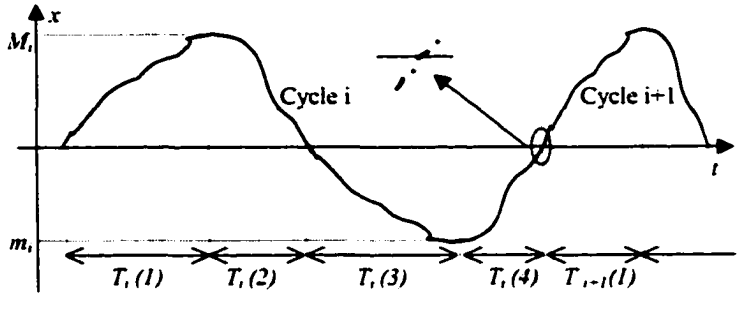

Figure 4.8 Illustration of M, m, T(1), T(2), T(3) and T(4)

4.2.3.4 Function of Maximum, Minimum, Frequency (Cycle Length) and Shape

Since the waveform of the EAF variables, especially current, varies from time to time, a sinusoid function may not be sufficient to describe it. So a shape (S) concept is introduced. It is created through pattern index in the same way as the above approaches. First, cycle i with $\eta_i = \{ X_j, j=L+1, L+2,..., L+c_i\}$ is divided into R intervals, pattern index is applied on the averaging values of each interval. Table 4.3 gives an illustration of these steps.

Table 4.3 Procedures of pattern index approach for obtaining the Shape

cycle no.	discrete data	Interval averages	pattern index
1	$X_1(1), X_1(2),...,X_1(c_1)$,	$v_1(1),v_1(2),...,v_1(R)$	1
2	$X_2(1), X_2(2),...,X_2(c_2)$,	$v_2(1),v_2(2),...,v_2(R)$	1 (if $\|v_2(k)-v_1(k)\|<\varepsilon$) or else 2
.....	.....		
i	$X_i(1), X_i(2),..., X_i(c_i)$,	$v_i(1),v_i(2),...,v_i(R)$	1 (if $\|v_i(k)-v_1(k)\|<\varepsilon$) or 2 (if $\|v_i(k)-v_2(k)\|<\varepsilon$) or ...i
.....	.....		

Corresponding to the maximum (M), minimum (m) and frequency or cycle length (L), there are several options for the prediction methods with selections from direct Markov chain or pattern indices. Here are some:

- Apply the direct Markov method on M, m, L and S separately, thus the function can be expressed as $f(M; m; L; S)$
- Process {M, m} with pattern index and L with direct Markov chain respectively, therefore the function becomes $f(\{M, m\}; L; S)$
- Make pattern index for {M, m, L} and get the function $f(\{M, m, L\}; S)$

The structures for one-cycle ahead prediction as illustrated in Figure 4.5 and Figure 4.6 also fit this model after modifying the function approximation method to the ones listed above and changing the parameters to *M; m; L;* and *S*.

4.3 Predictions and Accuracy Comparisons

All of the function approximations for the proposed function space valued Markov-like model presented above are studied with the same current data sets that have been used in the basic Markov-like modeling in Section 3.4. Fifty seconds (30s~80s) of historical arc current of phase A is utilized to build the model and three other data sets, each of 10 seconds (90s~100s~110s~120s), are used for prediction test. Since a first order Markov chain is applied in these models, the first cycle of each data sample will be processed in the beginning to give the initial conditions.

Two kinds of prediction approaches are tried when making forecasting. One is "uncorrected course of prediction", which predict several future cycles based only on the information of one initial cycles (without measurements corrections). Another is "prediction based on the corrected course of action", which predicts every next one cycle assuming that the information of one immediate past cycles is known. The former mode allows more time for power system operations or measurements while the later one gives higher accuracy.

4.3.1 Prediction Based on the Corrected Course of Action

The Markov property of EAF data is checked before using the Markov theory [39-45]. The result shows that both first order and second order Markov-like chains are suitable, but the first order chain is enough (it contains the information of one whole cycle) in most cases for the EAF data available and will be mainly used in the following. Figure 4.9 shows the first 0.25 seconds of prediction results, compared with the actual EAF current data, from FFT frequency decomposition approach. The truncated harmonic number used here is 7. It is reasonable to do this since the spectrum magnitude after 300Hz is very small (less than 5% of the fundamental frequency magnitude), as shown in Figure 4.10.

Some other function approximation methods are also examined. They are FFT frequency decomposition with 25 harmonics, polynomial fit with direct Markov method, polynomial fit with pattern index, f(Max, Min, Positions) with direct Markov method, f(Max, Min, Positions) with pattern index, f(Max; Min; Length; Shape), f({Max, Min}; Length;

Shape) and f({Max, Min, Length}; Shape). The result from classic ARMA/Kalman method is also recorded here. The prediction summary and comparisons for the first data set are shown in Table 4.4. The accuracy is based on the RMSE and %RMSE indices as described in equation 3.55. In addition, three forecasting techniques—conditional expectation, maximum probability and Monte Carlo method—are compared for their effectiveness. As for the order of Markov chain, different methods have different structures, depending on the nature of the information to be used. Most of the time a first order Markov chain is enough and shows good performance. Therefore, in Table 4.4 the results from applications of this order of Markov chain are listed, except for polynomial fit method, which has a better accuracy with a second Markov chain.

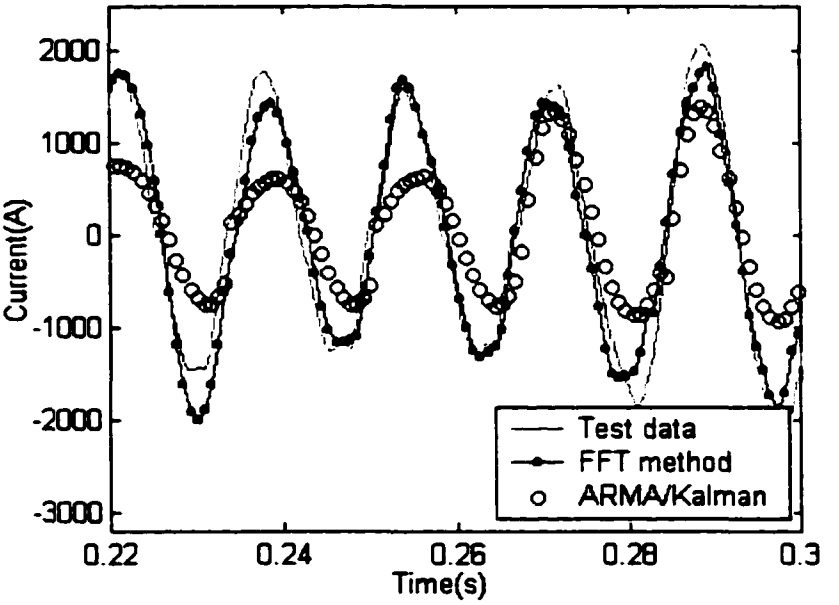

Figure 4.9 Illustration of corrected course of prediction by FFT frequency decomposition

It appears that FFT frequency decomposition approach works well for this EAF model. The accuracy is much higher than other approaches. The accuracy of polynomial fit with direct Markov method is not high because of the dependence between the polynomial coefficients. In fact, when checking Figure 4.11, which is done by this approach, one can see that both the cycle periods and prediction values lose their synchronization to the test data.

But after the pattern index was generated, the method improved a lot, as illustrated in Figure 4.11. Its accuracy cannot be increased much further because the waveform shape cannot be fitted into a third-order polynomial efficiently. The ARMA/Kalman method used is just as the one introduced in Section 3.6. The only difference in application is that here it predicts a whole cycle, rather than one point at one time. The accuracy of this method is only better than polynomial fit method in Table 4.4. It did not show the good performance as in point case. The main reason for that is the accumulation of error when predicting one point by one point for a cycle. So the larger the offset from the starting point (known measurement), the smaller the accuracy because of uncertainty.

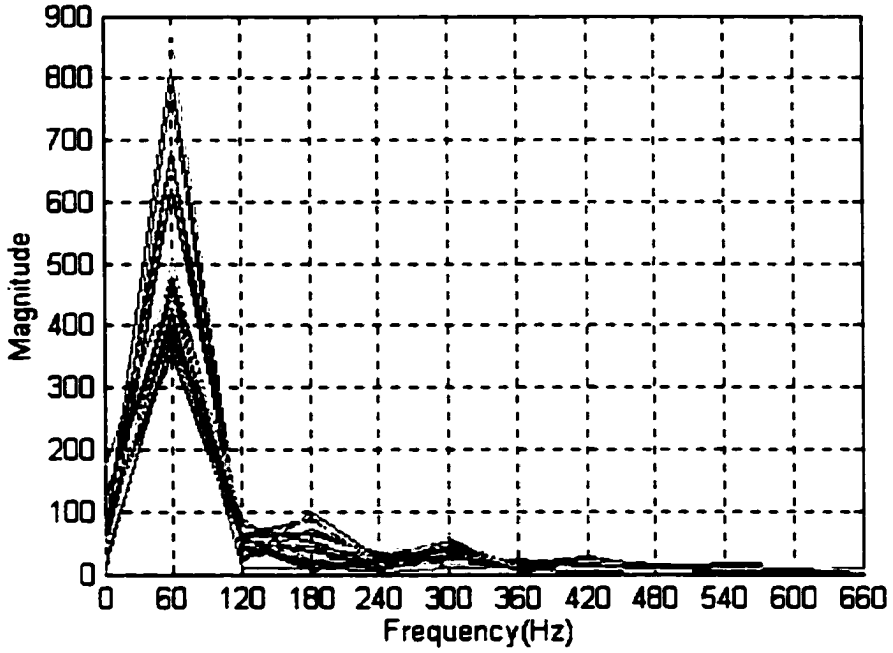

Figure 4.10 Illustration of FFT frequency spectrum for the EAF data

Another point of interest is the computational burden for each of these approaches. An approach is not realistic if its accuracy is high but the computational burden is too much. Also, if the accuracy is very poor, the approach is of no use, no matter how fast it is during the prediction. Table 4.5 shows what computer resources are used according to the first 5 approaches. This information cannot be directly obtained for ARMA/Kalman, but it is

estimated to be about 100 seconds for the results to come out. It is interesting to see that the computer burden decreases a lot in FFT frequency decomposition approach when it uses 7 harmonics rather than 25 harmonics, without significant loss of its accuracy. It seems that the FFT frequency decomposition approach with 7 harmonics approach is a good option for the EAF model.

Table 4.4 Comparisons of prediction accuracy for the first test data set

Approximations \ Prediction Techniques		Conditional Expectation	Maximum Probability	Monte Carlo method
FFT frequency decomposition (25 harmonics)	RMSE(A)	214.039	248.8836	304.4532
	%RMSE	3.9820	4.6303	5.6641
FFT frequency decomposition (7 harmonics)	RMSE(A)	216.161	252.5128	308.8512
	%RMSE	3.9901	4.6978	5.7459
Polynomial fit (direct Markov method)	RMSE(A)	3038.765	3532.2852	3611.6352
	%RMSE	56.5334	65.7149	67.1912
Polynomial fit (pattern Index)	RMSE(A)	422.207	490.9384	500.89
	%RMSE	7.8548	9.1335	9.3186
f(Max, Min, Positions) (direct Markov method)	RMSE(A)	269.744	313.656	330.436
	%RMSE	5.0183	5.8353	6.1475
f(Max, Min, Positions) (pattern Index)	RMSE(A)	269.084	312.8884	349.886
	%RMSE	5.0061	5.8210	6.5093
f(Max; Min; Length; Shape)	RMSE(A)	252.083	293.12	317.3528
	%RMSE	4.6898	5.4532	5.9041
f({Max, min}; Length; Shape)	RMSE(A)	220.761	256.6996	256.7204
	%RMSE	4.1071	4.7757	4.7760
f({Max, min, Length}; Shape)	RMSE(A)	238.351	277.1524	278.382
	%RMSE	4.4343	5.1562	5.1790
ARMA/Kalman	RMSE(A)	334.552		
	%RMSE	6.223		

To make certain of the ranking, five approaches with higher prediction accuracy are applied for two other data sets. Table 4.6 lists the results. It proves that the ranking is fair. Also, it can be found that the averaging RMS values for errors in these two data sets are a little higher than those of the first set. It is mainly due to the uncertainty of the data. This uncertainty even makes the accuracy of FFT frequency decomposition approach with 7 harmonics better than the one with 25 harmonics. The time period of these two data sets are farther from the historical data, which are used to build the model. So the performance of the

model on those data will be a little poorer. When the size of historical data used becomes larger, this difference will get smaller.

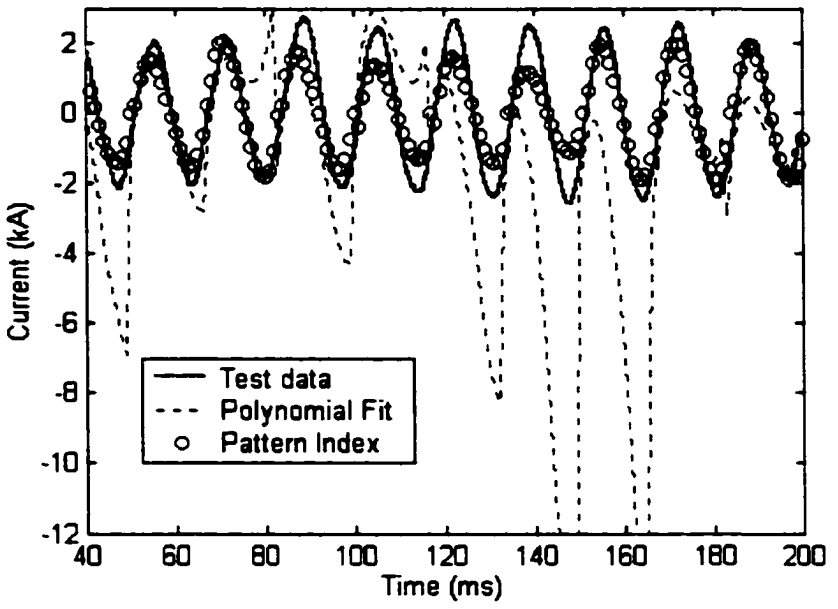

Figure 4.11 Illustration of prediction by polynomial fit method

Table 4.5 Comparison of computational resources used

	Time(s)	Memory(byte)
FFT frequency decomposition (with 25 harmonics)	692.189	40500000
FFT frequency decomposition (with 7 harmonics)	3.628	11340000
Polynomial fit (pattern Index)	5.342	19059057
f({Max, min}; Length; Shape)	7.321	11841205
f({Max, min, Length}; Shape)	7.848	3991153

Table 4.6 Comparison of prediction accuracy –the second and third test data sets

	%RMSE	
	the second data set	the third data set
FFT frequency decomposition (with 25 harmonics)	5.0444	5.6337
FFT frequency decomposition (with 7 harmonics)	5.0304	5.6196
Polynomial fit (pattern Index)	7.6413	9.1334
f({Max, min}; Length; Shape)	5.9876	5.6207
f({Max, min, Length}; Shape)	6.2524	5.7458
ARMA with Kalman filtering	7.7078	8.6419

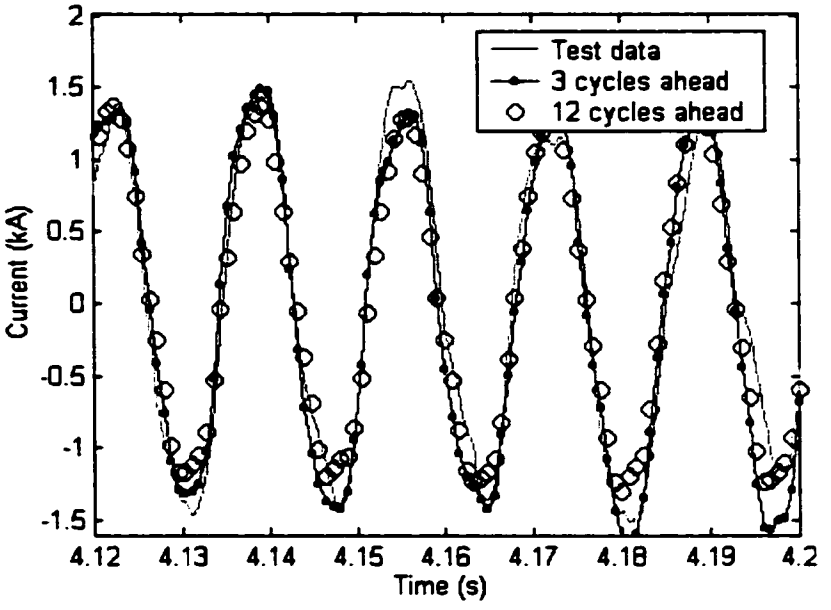

Figure 4.12 Illustration of uncorrected course prediction by FFT frequency decomposition

4.3.2 Uncorrected course of prediction

Sometimes power system engineers hope that the model can predict somewhat further into future in order to allow more time for control or data acquiring operations. To satisfy this demand, prediction of three or more cycles ahead is evaluated. Figure 4.12 illustrated the waveforms of predictions for 3 cycles ahead, using FFT frequency decomposition with 7 harmonics method. Also, Table 4.7 exhibits the performance of the four selected approaches and ARMA/Kalman method in predicting 3 cycles ahead through uncorrected course of prediction mode. The quality of the first three approaches in the table is not bad, and the prediction results are also very close to the test data. In addition, the comparison still shows that the FFT frequency decomposition with 7 harmonics method is the best of approximations purpose. The polynomial fit approach and ARMA/Kalman is not so effective in prediction, which indicates that they didn't characterize the EAF current very well. To find out how the method performs for prediction of somewhat longer period, it is further applied on the test data for 12 cycles prediction. Figure 4.12 and Table 4.8 shows the results. The magnitude, phase and shape of the waveform for prediction data are still close to those for

the test data, which demonstrates that this Markov-like model is effective. In addition, the ranking confirms that the FFT frequency decomposition with 7 harmonics method is the best.

Table 4.7 Comparison of prediction accuracy—3 cycles ahead

	%RMSE		
	the first data set	the second data set	the third data set
FFT Frequency decomposition (with 7 harmonics)	4.8660	5.9713	6.7434
Polynomial fit (pattern Index)	5.2785	6.7776	6.7543
f({Max, min}; Length; Shape)	5.5085	6.9667	6.9286
f({Max, min, Length}; Shape)	8.2511	8.1089	9.8776
ARMA with Kalman filtering	8.8692	8.9724	9.5361

Table 4.8 Comparison of prediction accuracy—12 cycles ahead

	%RMSE		
	the first data set	the second data set	the third data set
FFT frequency decomposition (with 7 harmonics)	6.2352	7.2006	8.6528
Polynomial fit (pattern Index)	6.8922	7.9173	9.0272
F({Max, min}; Length; Shape)	6.9984	7.2702	8.6606
F({Max, min, Length}; Shape)	9.6857	8.6564	11.4093
ARMA with Kalman filtering	10.8023	10.9628	12.1511

Generally, the accuracy of corrected course of prediction is somewhat better than that of uncorrected course of prediction. It is pretty reasonable since the prompt measurements will correct the errors that have been introduced in the prediction and reduce the effect of data uncertainty.

4.3.3 Comparison of Power Quality Indices

To determine how well the function space valued Markov-like model represents the load in a given system, several standard indices of the data and simulation results from the model are compared to quantitatively validate the model. These indices are Total Harmonic Distortion (THD), K-factor, zero-peak flicker factor and crest factor, with the definitions as follows:

$$THD = \sqrt{\sum_{i=2}^{\infty} I_i^2} \,/\, I_1 \qquad (4.9)$$

$$K - factor = \sum_{i=1}^{\infty} (i \cdot I_i)^2 \,/\, \sum_{i=1}^{\infty} (I_i)^2 \qquad (4.10)$$

$$Zero - peak \;\; flicker \; factor \;\; = | I_{peak} - I_{1.0-pk} | \,/\, I_{1.0-pk} \qquad (4.11)$$

$$Crest \; factor \;\; = I_{peak} \,/\, I_{rms}, \qquad (4.12)$$

where: I_i —rms value of the i^{th} harmonic current component of $i(t)$.

I_1 — rms value of the fundamental current component of $i(t)$.

$I_{1.0\text{-}pk}$ —the zero to peak value of the 60 Hz current component.

I_{peak} —the peak value of $i(t)$.

$$I_{rms} — I_{rms} = \lim_{T \to \infty} \sqrt{\frac{1}{T} \int_0^T i^2(t) dt} \qquad (4.13)$$

Table 4.9 shows the comparison of power quality indices between ten seconds of actual EAF current data and simulation results from function space valued Markov model. In this model FFT frequency decomposition with 7 harmonics method is used for cycle approximation. It is found that the difference of each index for the two data sets is within reasonable accuracy, which demonstrated that the proposed model can characterize the EAF system in terms of power quality properties. One may note that the power quality indices for simulation results are a little bit higher than those for actual data. The difference comes from the computation resolution of FFT method. During the transformation, since limited data (one cycle) are used for limited point FFT process, the spectrum tends to spread due to leakage effect. This effect makes I_1, the fundamental current component, a little smaller and accounts for the slight over-estimation of the power quality indices. But it is not significant.

Table 4.9 Comparison of power quality indices

Power Quality Indices	Actual data	Simulation results
THD (%)	4.427	4.430
K-factor	1.034	1.035
Zero-peak flicker factor	2.521	2.524
Crest factor	3.107	3.109

4.3.4 Search for the Best Conditions for Prediction

So far, many different methods including FFT frequency decomposition and ARMA/Kalman are compared for prediction accuracy and efficiency. One would have a preferred method in mind. Moreover, after selecting the most favorable method, one may be interested in finding out the optimal conditions that would give the best performance for the method. For this purpose, it is necessary to consider some major factors that have influence on prediction performance:

- Modeling methods (such as FFT frequency decomposition, Polynomial fit, ARAM)
- Forecasting techniques (such as Maximum Probability, Conditional Expectation and Monte Carlo Method)
- Detail implementation of the technique, using FFT frequency decomposition as an example, the following issues need to be considered.
  - How many states to be chosen (what is the number **N**, as shown in Figure 3.3)?
  - First order or second order Markov chain?
  - Which truncated frequency set is the most suitable, accurate and efficient?
  - How large should processing unit be in order to get a better result?
  - Is the methods time independent? That is to say, if the starting point for a prediction varies, will the result change much?

i). Selection of Modeling methods

This topic has been discussed a lot in the previous sections. For EAF current, FFT frequency decomposition is demonstrated to be strong in accuracy and efficiency. In the following, it will focus on this method.

ii). Forecasting techniques

Maximum probability, conditional expectation and Monte Carlo forecasting techniques are compared before. The Monte Carlo technique cannot magnify its effect until a somewhat

long time has been processed. Also, the accuracy is only in the distribution of states aspect. So the maximum probability and conditional probability is the main concern.

The best result using conditional expectation for FFT frequency decomposition we can get is 216 of the RMSE (which is 3.98% of the peak value), as listed in Table 4.4. While the smallest RMSE we can get from maximum probability is 269 (which is above 5% of the peak value), which is not as good as the conditional expectation technique. It is the case for most methods discussed in Section 4.3.1. This demonstrated that conditional expectation forecasting is more effective when predicting a little longer range of data. Figure 4.13 shows a part of prediction with maximum and conditional expectation techniques.

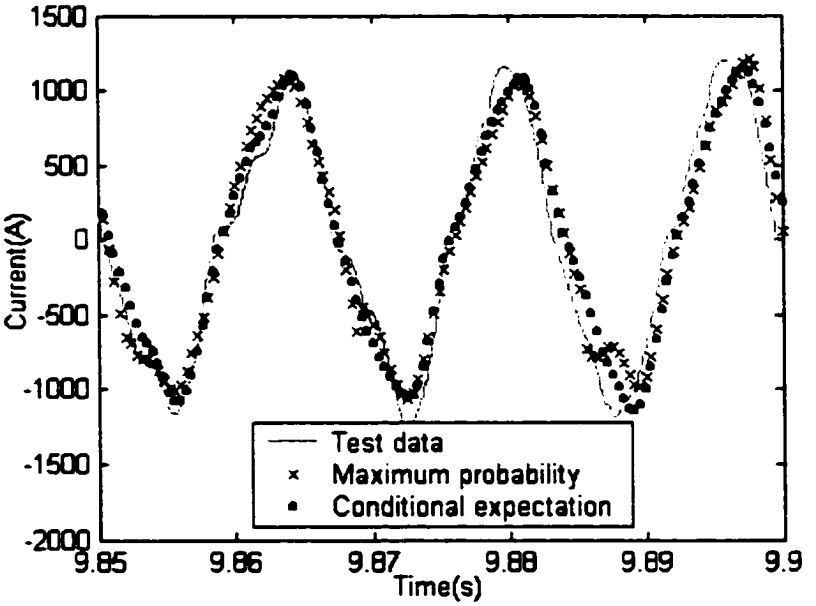

Figure 4.13 Prediction with Conditional Expectation technique

iii). Number of intervals to divide the data range

It is also useful to decide the number of intervals that the data range should be divided. If the number is large, the interval is small and data will be sensitive to the change of time series values. Especially in the EAF current case, the change of one cycle sometimes is far different from the previous ones. So the model built will meet annoying uncertainty when

practicing prediction. But a small number of intervals may also result in less accuracy. Since the interval is kind of larger, it is difficult to get a more precise value although the state maybe correct.

N was tested from 28 to 60 and it is found that 36 is an appropriate figure. When all the other factors are at their optimal values, the best RMSE (choose N=36) is 216, the worst is 222 (N=29). It can be seen that there is some difference, but not much.

iv). Choose the proper order of Markov chain

With FFT frequency decomposition, a first order Markov chain and a second order Markov chain have been compared. It shows that their performance is not much different for the test data close to the historical data that has been used for building model. But for test data a little far from the historical data, the first order Markov chain shows even better accuracy (for test data 10 seconds from the historical data, the RMSE for it is 216 while the second order Markov chain gives 250). This doesn't mean that a first order Markov chain is absolutely better. In fact, if the historical data is large enough, second order Markov chain should be sharper. For some methods of function approaches such as polynomial fit, second order Markov chain is demonstrated to be a little better than the first order one. As a first order Markov chain saves more memory and runs much faster, we will still select it for prediction.

v). Select an optimal truncated frequency set

Apparently, we need choose the truncated frequency set that has the largest power in spectrum plot and the larger the set the better. This is not necessarily true. From our previous work on frequency analysis of EAF current, most of the frequency components are shifting vibrantly with time going on. This will increase the difficulty of prediction. If one loses synchronization of one frequency, it will reduce the accuracy by predicting in an opposite direction. But we have to face the harmonics with high power and try to get rid of them.

Truncated numbers from 4 to 20 were tested for FFT frequency decomposition method. It is found that the best one (RMSE=216 with truncated number 8) and the worst one (RMSE=219 with truncated number 4) didn't have significant difference. The main reason

for this is that 60Hz component is very large so that the influence of harmonics can't attribute a lot to the accuracy of the whole prediction.

Another thing that should be mentioned is about the low frequency (less than 60Hz) components. Most of them have higher power than the harmonics and distribute almost all the low frequency range from 0Hz to 60Hz, as shown in Figure 4.14. The worst thing is that their magnitude and phase are also shifting from time to time. Taking account of them into prediction cannot improve the accuracy, but may degrade the accuracy of prediction.

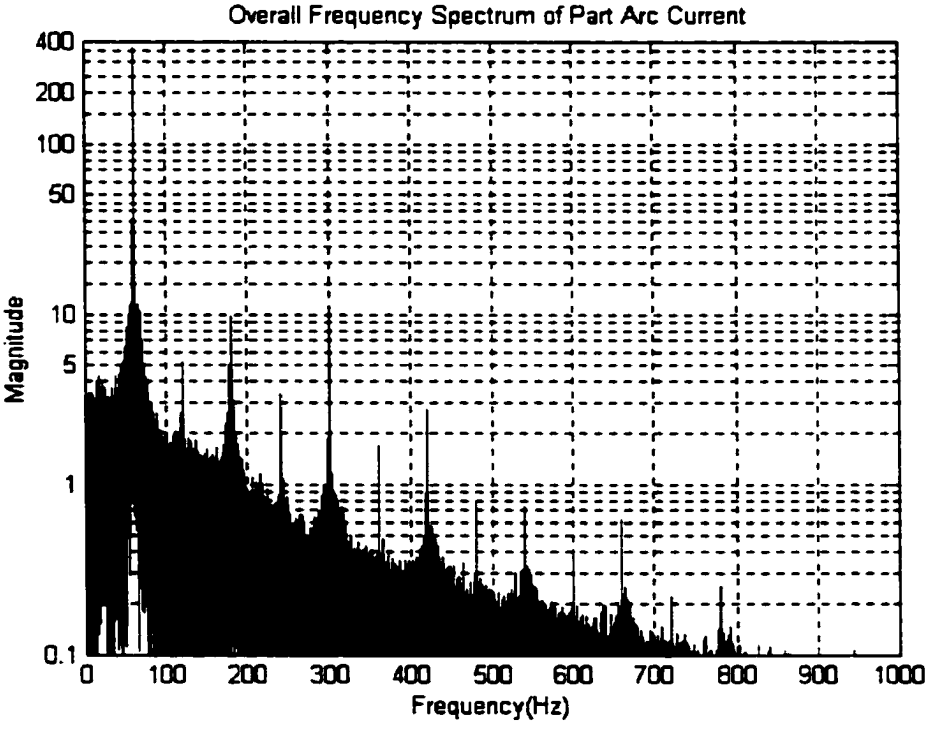

Figure 4.14 Overall spectrum of EAF current

vi). Decide the size of processing unit

The size of processing unit is very important to prediction, especially for the FFT frequency decomposition method. Let us use pure sinusoid waveform as an example. If one cycle has 100 points, then one will not meet any problem during prediction if he chooses 100 points, 200 points, or other multiple of 100 points as a processing unit. But if he chooses 80

points, 90 points or 95 points as a processing unit, synchronization problem may creep in. The magnitude of the fundamental frequency of every processing unit may be the same, while the phases are different and moving regularly. Prediction accuracy may be damaged if one doesn't take account of the change. In our EAF current case, it is more complex. Most of the frequency components shift irregularly except the fundamental one, which shows some kind of trend. Since the power of fundamental frequency is much larger than others, the size of processing unit should concentrate on it.

Many kinds of situations for processing unit are tested. Since the sampling frequency is 10,000 points/second and fundamental frequency is 60 Hz, so there will be 500 points for 3 cycles and 166.7 points for one cycle. Thus the test cases include 80 points to 200 points, 500 points, 1000 points and many multiples of 500 points. The RMSE ranges from 216 (167 points) to 1000 (129 points), which indicates that this factor significantly affects the prediction quality.

vii). Should initial point be concerned?

For some methods, initial point has a big effect on the outcome of prediction. But for the Markov-like model used, the effect is not so significant, because the model is basically built in a statistical sense and has characterized the change or shift of the frequency components. The seemingly irregularity of the EAF current cancels some of the influence of starting point. This statement can be verified by some tests. The start points are set from 1 to 180 points (1 cycle contains about 167 points) off the beginning of the test data sets to check the result. RMSE index shows that the smallest one is 216 (start at point 44), the largest one is 224 (start at point 35).

4.4 Summary

In this section, the basic Markov-like model of the EAF current data was advanced to function space valued Markov-like model. After the generalization from point-case of EAF time series $\{X_i: i=1, 2, \ldots M\}$ to cycle-case time series $\{\eta_j, j=1, 2, \ldots M'\}$ with η_j composed of a cycle of data from the original time series, it is possible to predict one or more cycles

ahead accurately. Several methods to approximate the cycle vector are proposed since it is not computationally practical to apply Markov-like method directly on the cycle chain. Compared to the other functions or methods such as polynomial fit with pattern index, f({Max, min}; Length; Shape) and f({Max, min, Length}; Shape), ARMA/Kalman Filtering etc., FFT frequency decomposition with 7 harmonics seems to perform better in both corrected course of prediction and uncorrected course of prediction for a few cycles. Although the accuracy may increase a little if the number of considered harmonics increases, it is at the expense of much larger computation.

5 MARKOV-LIKE MODEL FOR RELATED EAF CURRENT AND VOLTAGE

The Markov models discussed so far are mainly for EAFs connecting to light buses, the terminal voltage of which is not significantly different from its source voltage. They are very suitable since the collected field data is from that kind of situation. To make the Markov-like model more applicable to general cases including heavy buses, where EAF current may lead to considerably voltage drop, both current and voltage values should be taken into account. The basic framework of related current and voltage modeling will be introduced first in point case study. Since function space valued Markov chain approach with FFT frequency decomposition approximation has demonstrated to be effective for EAF current in Section 4.3, it will also be extended to model EAF current and voltage together in this chapter and described in a little more detail.

5.1 Related Current and Voltage in a Point Case

Let the individual EAF current time series be $\{ I_j , j=1, 2,\ldots M \}$ with state space $S_I = \{a_1, a_2, \ldots, a_{N_I}\}$ and the individual voltage time series be $\{V_j , j=1, 2,\ldots M\}$ with state space $S_V=\{b_1, b_2, \ldots, b_{N_V}\}$. Then the state space for the related current and voltage Markov-like model is $S_I \times S_V$. One of the transition matrix structures may look like the following,

$$\boldsymbol{P} = \begin{bmatrix} P(a_1b_1, a_1b_1) & P(a_1b_1, a_1b_2) & \cdots & P(a_1b_1, a_1b_{N_V}) & P(a_1b_1, a_2b_1) & \cdots & P(a_1b_1, a_{N_I}b_{N_V}) \\ P(a_1b_2, a_1b_1) & P(a_1b_2, a_1b_2) & \cdots & P(a_1b_2, a_1b_{N_V}) & P(a_1b_2, a_2b_1) & \cdots & P(a_1b_2, a_{N_I}b_{N_V}) \\ \cdots & \cdots & & \cdots & \cdots & & \cdots \\ P(a_1b_{N_V}, a_1b_1) & P(a_1b_{N_V}, a_1b_2) & \cdots & P(a_1b_{N_V}, a_1b_{N_V}) & P(a_1b_{N_V}, a_2b_1) & \cdots & P(a_1b_{N_V}, a_{N_I}b_{N_V}) \\ \cdots & \cdots & & \cdots & \cdots & & \cdots \\ P(a_{N_I}b_{N_V}, a_1b_1) & P(a_{N_I}b_{N_V}, a_1b_2) & \cdots & P(a_{N_I}b_{N_V}, a_1b_{N_V}) & P(a_{N_I}b_{N_V}, a_2b_1) & \cdots & P(a_{N_I}b_{N_V}, a_{N_I}b_{N_V}) \end{bmatrix}$$

where the order of the states are listed in sequence as $\{a_1b_1, a_1b_2,\ldots, a_1b_{Nv}, a_2b_1, \ldots, a_2b_{Nv},\ldots, a_{N_I}b_{Nv}\}$. But any other convenient sequence is acceptable. The current and voltage time series should be processed synchronously to get the estimate of transition probability to build

the Markov model. The detail procedure is similar to the one described in Section 3.3. One need only pay attention to the change of state space. Here it composes of the information from both variables while the previous one is only from one variable (current).

After building the model, one can now use it to get the EFF and ECDF after calculating stationary point of the system and get its state distribution. The results are much like Figure 3.6 and Figure 3.7 for EAF current and Figure 3.8 for EAF voltage.

To make predictions, the procedure as described in Section 3.5.2 is followed. The only additional step is to discompose the predicted state into two sub-states for current and voltage correspondingly after identifying it. Figure 5.1 and Figure 5.2 show the plots for current and voltage by one-step-ahead prediction. The prediction follows the actual test data closely, which demonstrates that it has a sound accuracy. But the %RMSE (0.75% for current) is not as good as that from Markov-like model on EAF current or voltage only. This is strange, while it reasonably explains that the EAF current and voltage are not strongly correlated so that the information from another variable is not very helpful.

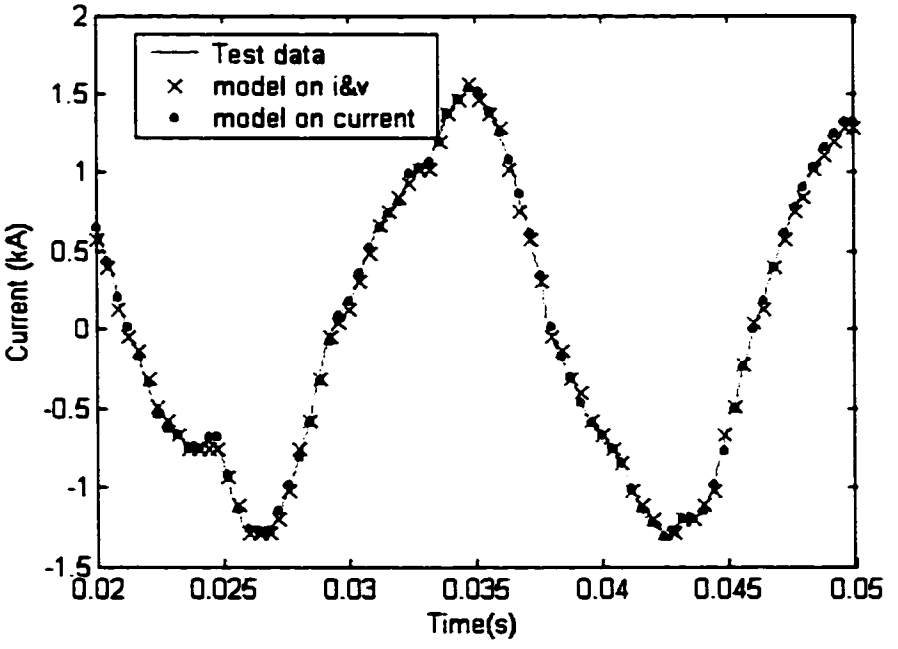

Figure 5.1 Current prediction with related i-v model in point case

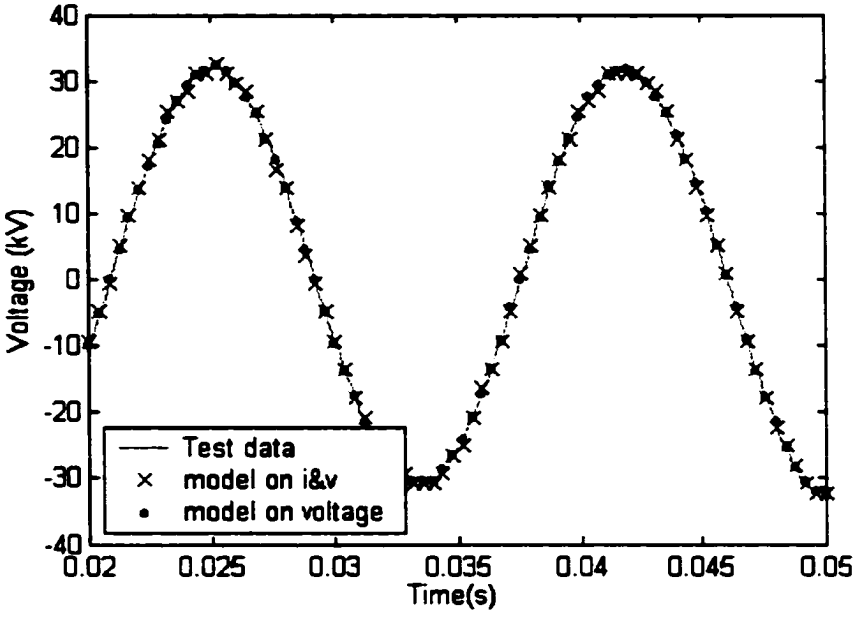

Figure 5.2 Voltage prediction with related i-v model in point case

5.2 Related Current and Voltage in Function Space

The concept of Markov modeling on related current and voltage in function space is the same as that for point case. In the sections to follow, the efficient and practical method discussed in section 4.2.3.1—FFT frequency decomposition—shall be used for realizing the model and making predictions.

5.2.1 Building Transition Matrices

Fifty of 128 seconds of field data was used to build the transition matrices for function space valued Markov model. Figure 5.3 shows a simple structure for such a process. A fixed cycle length of 167 is used as the processing unit (C=167). From the historical data, one can get its FFT series by applying FFT transfer on each cycle of data. Let M' to be the number of total cycles for the historical data. For the ith cycle EAF current $\eta'_i = \{X_{Li-1}, X_{Li-2}, \ldots, X_{Li-C}\}$, the FFT components are:

$$F_i^I(k)=\frac{1}{C}\sum_{n=0}^{C-1}(X(L_i+n+1)\cos(2\pi kn/C)-jX(L_i+n+1)\sin(2\pi kn/C)) \quad (5.1)$$

$$k=1, 2, \ldots, c_i, \qquad i=1, 2, \ldots, M'$$

where C is the number of data measurements in cycle i, here it is 167,

L_i is the number of data measurements from the beginning of the present cycle i,

$F^I_i(k)$ is the kth FFT component of ith cycle of current data $\{X_{Li-1}, X_{Li-2}, \ldots, X_{Li-ci}\}$, it is a complex number which can be expressed as $F^I_i(k)= R^I_i(k)+ j\, I^I_i(k)$. $R^I_i(k)$ is its real part and $I^I_i(k)$ is its imaginary part.

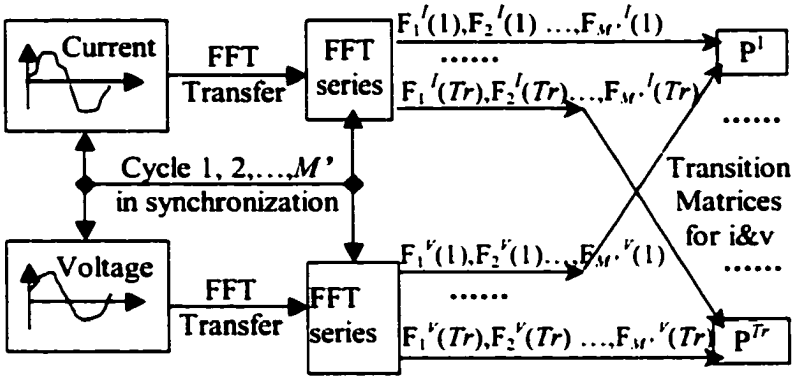

Figure 5.3 Structure of building transition matrices from EAF data

In a similar way, the FFT components can also be obtained for the ith cycle of voltage η^V_i = $\{V_{Li-1}, V_{Li-2}, \ldots, V_{Li-C}\}$

$$F_i^V(k)=\frac{1}{C}\sum_{n=0}^{C-1}(V(L_i+n+1)\cos(2\pi kn/C)-jV(L_i+n+1)\sin(2\pi kn/C)) \quad (5.2)$$

where $F^V_i(k)$ is the kth FFT component of ith cycle of voltage data $\{V_{Li-1}, V_{Li-2}, \ldots, V_{Li-C}\}$, it is a complex number which can be expressed as $F^V_i(k)= R^V_i(k)+ j\, I^V_i(k)$. $R^V_i(k)$ is its real part and $I^V_i(k)$ is its imaginary part.

Then the vector $(F^I_i(1)\ F^I_i(2)\ldots\ldots\ F^I_i(C))$ can represent the ith cycle of current η^I_i, and the vector $(F^V_i(1)\ F^V_i(2)\ldots\ldots\ F^V_i(C))$ can represent the ith cycle of voltage η^V_i. For the same reason discussed in Section 4.2.3.1—the magnitudes of the higher frequencies are close to

zeros, truncated number of frequencies can be used so that vector ($F^I_i(1)\ F^I_i(2)\ldots\ldots\ F^I_i(Tr)$) is enough to characterize η^I_i, and vector ($F^V_i(1)\ F^V_i(2)\ldots\ldots\ F^V_i(Tr)$) is enough for η^V_i. Here Tr is much less than C.

Under the assumption that different frequencies are independent of each other, Markov-like approach that has been discussed in Section 3.3 can be applied separately on the FFT series of different frequencies,

$F^I_1(1), F^I_2(1) \ldots, F^I_{M'}(1)$ together with $F^V_1(1), F^V_2(1) \ldots, F^V_{M'}(1)$

$F^I_1(2), F^I_2(2) \ldots, F^I_{M'}(2)$ together with $F^V_1(2), F^V_2(2) \ldots, F^V_{M'}(2)$

.....

$F^I_1(Tr), F^I_2(Tr) \ldots, F^I_{M'}(Tr)$ together with $F^V_1(Tr), F^V_2(Tr) \ldots, F^V_{M'}(Tr)$

The transition matrices for the coupled current and voltage are P_R^1, P_R^2, ..., P_R^{Tr} respectively for real parts and P_I^1, P_I^2, ..., P_I^{Tr} for imaginary parts. These matrices are the models needed for prediction application. One thing should be mentioned is about the states for transition matrices. They are different from transition matrix for single variable such as EAF current. If the EAF current is divided into N_I states, and EAF voltage, N_V states, then the total states for related current and voltage is $N_I \times N_V$. In particular, they can be listed in sequence like (a^1,b^1), (a^1,b^2), ...,(a^1, b^{N_V}), (a^2,b^1), (a^2,b^2), ...,(a^2, b^{N_V}),..., (a^{N_I},b^1), (a^{N_I},b^2), ...,(a^{N_I}, b^{N_V}). The dependence between current and voltage are totally reflected in this way.

5.2.2 Real-Time Prediction by Function Space Models

Having setup all the transition matrices, one is ready to do real-time prediction. At one point, assume information is known about the previous cycle (for instance, the i^{th} cycle), and one or several cycles need to be forecasted. Figure 5.4 illustrated the main procedure for such an implementation. The first several steps before "Markov model" box are similar to those described in Section 5.2. The only difference is that a whole period of historical data was used in building transition matrices at one time, but only one cycle of data is used here for each prediction.

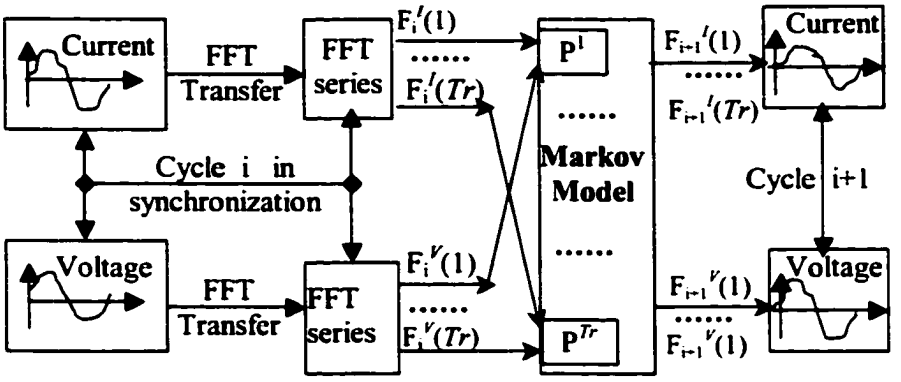

Figure 5.4 Procedure of predicting one cycle ahead with EAF data

To get the time series of current and voltage for the $(i+1)^{th}$ cycle, every frequency component, $F^I_{i-1}(1)$, ...$F^I_{i-1}(k)$, ..., $F^I_{i-1}(Tr)$ and $F^V_{i-1}(1)$, ...$F^V_{i-1}(k)$, ..., $F^V_{i-1}(Tr)$ of this coming cycle should be estimated. In practice, the k^{th} frequency component of the $(i+1)^{th}$ cycle is estimated to be the conditional expectation with the associated empirical frequency given the values of k^{th} frequency component of the i^{th} cycle. One can also use maximum probability or simple Monte Carlo approach to get these components using the information on FFT components of the i^{th} cycle (it is pretty useful for generating power quality indices), while the former method is much shaper in short term prediction. After getting all the Fourier components for cycle i+1, one can do re-convolution (inverse FFT) to achieve EAF current and voltage data for this cycle respectively,

$$X(n)=\sum_{k=0}^{Tr-1}(real(F^I_{i+1}(k)cos(2\pi\, kn/C)-imag(F^I_{i+1}(k))sin(2\pi kn/C)) \qquad (5.3)$$

$$V(n)=\sum_{k=0}^{Tr-1}(real(F^V_{i+1}(k)cos(2\pi\, kn/C)-imag(F^V_{i+1}(k))sin(2\pi kn/C)) \qquad (5.4)$$

$$n=1, 2, ...C$$

where $real(F^I_{i+1}(k))$, $real(F^V_{i+1}(k))$ are the real parts of the complex FFT components for EAF current and voltage at cycle i+1 respectively.

$imag(F^I_{i+1}(k))$, $imag(F^V_{i+1}(k))$ are the imaginary parts of the complex FFT components for EAF current and voltage at cycle i+1 respectively.

Figure 5.5 and Figure 5.6 show the prediction performance of related current and voltage Markov-like model that has just been presented. The effect is satisfactory, for the current, the predicted data sequences are in synchronization to the test data and their magnitudes of each cycle are very close. One can even notice that their shapes of waveforms are also alike. Since the voltage itself is quite regular, its prediction in this case fits well. There is almost no deviation from the test data.

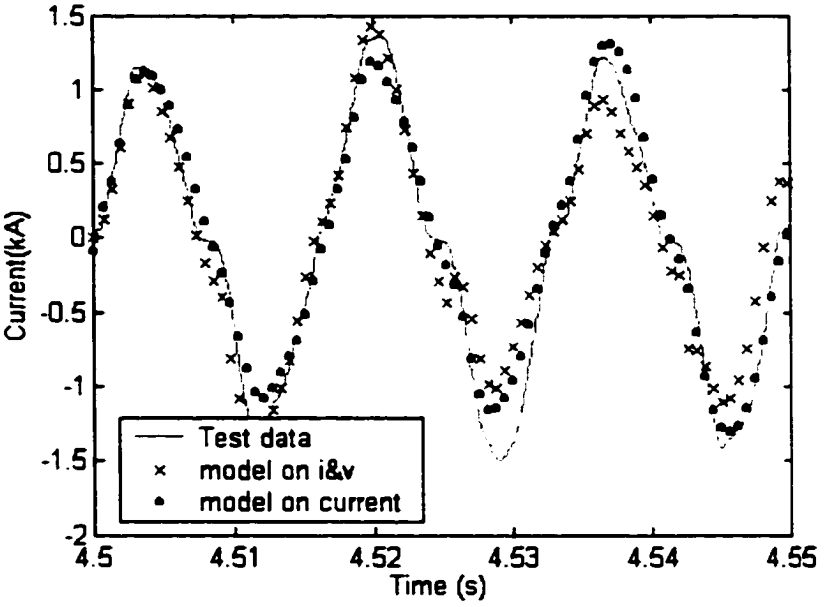

Figure 5.5 Illustration of one cycle ahead prediction for EAF current

In addition to the qualitative checkout from the figures, the quantitative indices can be found in Table 5.1. As expected, the %RMSE index for error between test data of EAF voltage and its prediction is as low as 1.16%. When compared to the results listed in Table 4.4 and Table 4.6, the %RMSE values for the error between current test data and its prediction values is somewhat higher. This phenomenon can be largely explained from observation of the waveform of EAF current and voltage in Figure 1.4. The current changes abruptly during some period of time but the voltage seems still "normal". This means that the relationship between current and voltage is very weak. On one hand, the Markov-like model has to increase its dimension when processing the related multi-variable time series. At the

same time, the precision of dividing the state (N in Figure 3.2 will be smaller) needs to be decreased to relieve the computational burden. This should contribute to a larger prediction error. On the other hand, bringing two weakly related time series together is not beneficial, if not harmful, for modeling and prediction. Since the historical data are limited, the multi-variable model may record some state combinations that do not characterize the dependence of the variables. If this information is used in prediction, the degree of error will most probably rise.

For the first data set, the accuracy for current from related Markov-like model is significantly less than that of Markov models for EAF current variable itself. Due to the less erratic pattern of EAF voltage, the accuracy for it doesn't degrade so much. One of the prediction results from Markov modeling only on voltage is also given in Figure 5.6. The %RMSE value is 1.15, which is not significantly different from the correlated model. But the errors from the related current and voltage approach improved substantially for the second and third data sets. Although it is only first order Markov chain, the information from the voltage bridges some gap to the second order Markov models.

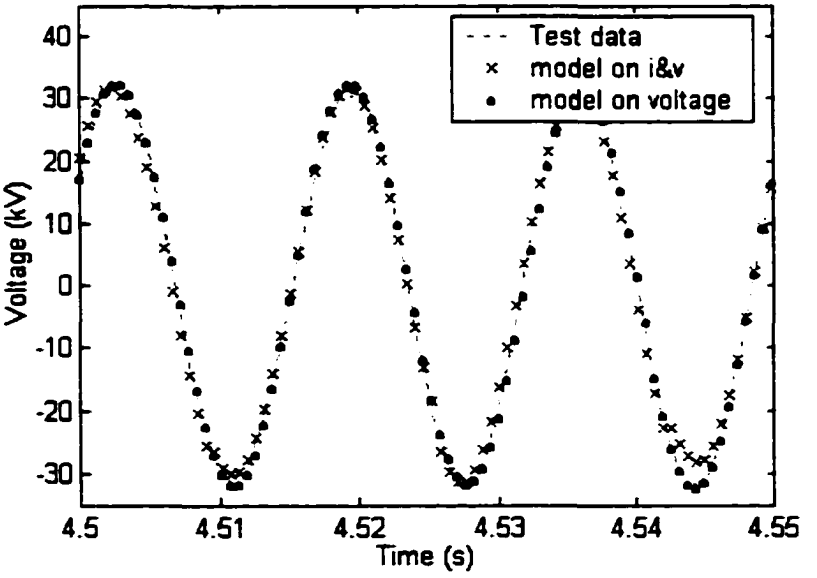

Figure 5.6 Illustration of one cycle ahead prediction for EAF voltage

Table 5.1 Statistical indices for one cycle ahead prediction with related current and voltage Markov-like model

	%RMSE		
	first data set	second data set	third data set
Current	4.5033	5.2050	5.6080
Voltage	1.1623	1.1954	1.2066

5.3 Test of Independence

Before modeling on the multi-variable system, it is better to know if their time series are closely related or not. If not, the series can be modeled separately, which would simplify the procedure and save some computational resources. To determine the dependence, one may first plot the waveform of these time series and observe whether the change of one time series has some influence on the other ones. Then carry out quantitative analysis to find out the degree of dependence. Assume there are m interrelated time series to consider: X_t^1, X_t^2, ...,X_t^m. Represent them in a vector

$$\mathbf{X}_t = \begin{bmatrix} X_t^1 \\ X_t^2 \\ \cdots \\ X_t^m \end{bmatrix} \tag{5.5}$$

Then the mean vector of these time series is

$$\mu = E\mathbf{X}_t = \begin{bmatrix} EX_t^1 \\ EX_t^2 \\ \cdots \\ EX_t^m \end{bmatrix} \tag{5.6}$$

and the associated covariance matrix at a time shift h is

$$\Gamma(h) = E[(\mathbf{X}_{t+h} - \mu)(\mathbf{X}_t - \mu)'] = \begin{bmatrix} \gamma^{11}(h) & \gamma^{12}(h) & \cdots & \gamma^{1m}(h) \\ \gamma^{21}(h) & \gamma^{21}(h) & \cdots & \gamma^{2m}(h) \\ \cdots & \cdots & & \cdots \\ \gamma^{m1}(h) & \gamma^{m2}(h) & \cdots & \gamma^{mm}(h) \end{bmatrix} \tag{5.7}$$

The components of the mean vector and covariance matrix can be estimated from the real time series $\{X_t^j; t=1, 2, \ldots n\}$ where $j=1, 2, \ldots m$.

$$\overline{X}^j = \frac{1}{n}\sum_{t=1}^{n} X_t^j \tag{5.8}$$

$$\hat{r}^{ij}(h) = \frac{1}{n}\sum_{t=1}^{n-h}(X_{t+h}^i - \overline{X}^i)(X_t^j - \overline{X}^j) \qquad 0 \le h < n \tag{5.9}$$

and the correlation between X_{t+h}^i and X_t^j is

$$\hat{\rho}^{ij}(h) = \hat{\gamma}^{ij}(h)/\sqrt{\hat{\gamma}^{ii}(0)\hat{\gamma}^{jj}(0)} \tag{5.10}$$

$\hat{\rho}^{ij}(h)$, $i \neq j$ is the index whose value is between 0 and 1. It can be used to justify the dependence of the time series under study. If the values of the index are small enough and close to 0 for all i and j, the dependence between the time series is weak. Otherwise, if they are kind of large and close to 1, the dependence is strong.

If the original current and voltage time series were used to test their dependence, the correlation coefficients should not be small since both of them have dominant 60 Hz components. To avoid this problem and stress the influence of each other, the fundamental frequency components of the two time series are filtered and the residuals are analyzed. It is found from $\hat{\rho}^{ij}(h)$ up to 167 time shift (h=0, 1, ...167) for i, j=1 or 2 that over 95% of the index values are less than 0.1, with the largest value being around 0.3. Thus one can conclude that the dependence between the EAF current and voltage from the system where the data were recorded is weak. This further confirms the study by Markov modeling on both of the variables.

5.4 Summary

This chapter shows how to model EAF current and voltage with Markov chain in case that these two variables are closely related. Markov models are built in point case and function space case with FFT frequency decomposition for the EAF current and voltage data. It appears that their performance is not as good as the models for separate current or voltage variable. This means the variations of current and voltage from the data under study do not

have much dependence between each other (the coupling is weak since the EAF is installed at a stiff bus). Nevertheless, the proposed Markov models provide practical methodology for modeling of related variables, for example, the current and voltage from an EAF installed at a weak bus.

6 IMPLEMENTATION FOR HARMONIC COMPENSATION

One of the important techniques to improve power quality in a power system is to compensate for reactive power and/or harmonic currents. However, in a power network that is polluted by high capacity EAFs, the system unbalance, current fluctuation and voltage flicker is so serious that momentary real power compensation is also necessary. Traditional methods that use passive filters may be helpful to appease the situation but cannot solve the problem totally. Thanks to the development of semiconductors, it is possible to build large, force-commutated, voltage-source inverter with power rating up to hundreds of MVA. They can be coordinated with passive components to achieve better results for compensation. STATCOM is a popular device of in this area. In this chapter, it will be used to test the proposed Markov models (especially the one in function space) with Simulink simulation.

6.1 Introduction to STATCOM

STATCOM stands for STATic COMpensator [57]. Its operation is fundamentally different from SVC, which is the abbreviation of Static Var Compensator. SVC operates by selectively connecting passive components such as capacitors or inductors to the power line. While STATCOM is essentially a controlled ac voltage source connected to the power line through a suitable tie reactance. Any desired current can be forced to flow through the tie reactance by appropriately controlling the STATCOM voltage source [58].

The basic behavior of a STATCOM is very similar to that of a synchronous compensator. So it may be helpful to describe the synchronous compensator, which is referred to in Figure 6.1.

The dynamic behavior of a synchronous compensator depends on the voltage which is developed in its ac winding by the dc excitation of the field winding. The reactive current flowing into or out of a synchronous compensator depends on the difference between the voltage of the supply system and the excitation voltage of the machine. This is illustrated in Figure 6.2. The synchronous compensator has an excitation voltage V_t. It is connected to the

system busbar, with a voltage V_s through an equivalent inductive reactance X. When V_t is smaller than V_s, the machine is "under-excited' and the current flowing into the synchronous compensator lags behind the system voltage; the machine then acts as a inductive impedance, absorbing Mvar from the system as shown in Figure 6.2 (a). When V_t exceeds V_s, then it is "over-excited" and acts as a shunt capacitor, generating Mvar, as illustrated in Figure 6.2 (b).

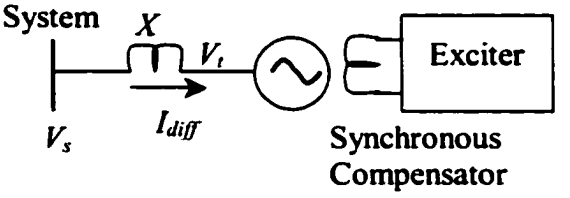

Figure 6.1 Simplified representation of a synchronous compensator

(a) Inductive operation (b) Capacitive operation

Figure 6.2 Reactive converter operation of a synchronous compensator

STATCOM is based on dc to ac converter in which a real alternating voltage (or current) can be produced from a direct voltage (or current) by the process of inversion in a solid-state dc to ac converter, as exemplified in Figure 6.3. The converter can be controlled to behave as if it were an idealized synchronous compensator.

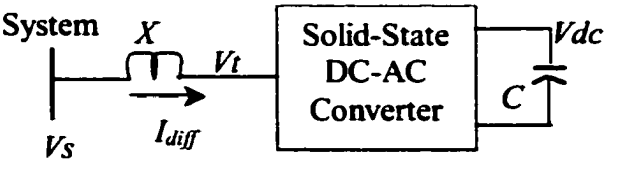

Figure 6.3 Simplified representation of a STATCOM

If the voltage generated by the STATCOM is less than the voltage of the system busbar to which it is connected, the STATCOM will act as an inductive load, drawing lagging Mvar from the supply system. On the contrary, it will act as a shunt capacitor generating Mvar into the supply system when its generated voltage is higher than the system voltage.

There are various types of inverter circuit and source for the STATCOM. The dc voltage-sourced converter (VSC) is the type that has received most attention in the practical realization of the STATCOM. A very simple inverter (Figure 6.4) produces a square voltage waveform as it switches the direct voltage source on and off. Clearly this waveform has a large content of low order harmonic components. The direct voltage source can be a battery, whose output voltage is effectively constant, or it may be a capacitor, whose terminal voltage can be raised or lowered by controlling the inverter in such a way that its stored energy is either increased or decreased.

The inverter uses either conventional thyristors with forced commutation, or devices which can be turned off as well as turned on, such as gate turn-off (GTO) thyristors, which have been used for many years in drives for traction and industrial applications. A new generation of devices that require less energy for the switching process includes Integrated Gate Bipolar Transistor (IGBT), Integrated Gate Commutated Thyristors (IGCT) and MOS-Controlled Thyristors (MCT). These devices are becoming available with ratings that can be used for STATCOMs. Devices with a higher voltage rating, using silicon carbide (SiC), are expected to become commercially available within the next few years.

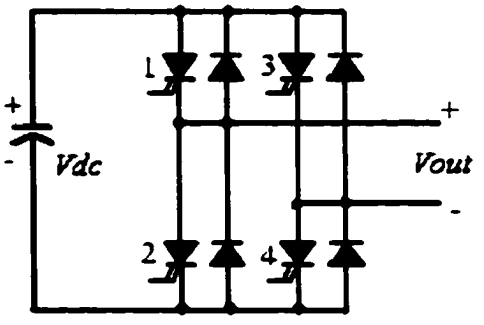

Figure 6.4 Single-phase voltage-sourced converter

The switching pattern of the semi-conductor devices in the single-phase converter of Figure 6.4 depends on whether the current leads or lags the voltage. Normally the negative terminal of V_{out} is connected to ground and V_{dc} is selected to be greater than the peak of system voltage V_s. Thus, if during the interval t_0 to t_1, V_{out} equals to V_{dc} (see Figure 6.5). It is in phase with and greater than the system voltage, the converter will act as a capacitor (as seen from the system) and the current flowing into the converter through the conducted poles 1 and 4 will lead the voltage by 90°.

In contrast, when V_{out} is in phase with but less than the ac system voltage, the converter will act as an inductor (as seen from the system) and the current into the converter at the output terminal will lag the voltage by 90°. In this case, from time t_2 to t_3, GTO poles 2 and 3 is deblocked, the output voltage will be - V_{dc} and current flow will transfer (at its peak value) to poles 2 and 3 and pass the dc source in an opposite direction.

From time t_1 to t_2 GTO poles 1 and 3 are forced to turn off by control action, at the same time, poles 2 and 4 turns on in order to ensure continuation of the current. The GTO is blocked and the output voltage V_{out} becomes zero. The current through pole 1 ceases to flow. However, the line current itself is not interrupted because it now finds a low impedance path through poles 2 and 4 and back into the system. During this time, the GTO works in either capacitive or inductive mode, depending on the system voltage. If V_s is less than zero, it is like a capacitor, otherwise, it is like an inductor. Since in this case the current though the inductor link X changes much slower than the cases when the voltage output is V_{dc} or $-V_{dc}$, it is useful when the output current is already in a desire range.

The STATCOM switches at an appropriate high frequency to alter the output voltage V_{out} [59]. But the current I_{diff} will not change as suddenly as V_{out}, but increases or decreases gradually since the inductor has an inertia to the change of current.

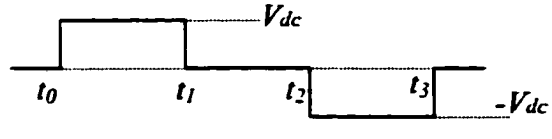

Figure 6.5 Voltage output from STATCOM operation

6.2 *Simulation Structure for Harmonic Compensation*

Figure 6.6 illustrated a simplified diagram for compensation with STATCOM. The place of great interest is Point of Common Coupling (PCC), where the STATCOM feeds compensation current i_{diff} to improve the EAF current (i_{uncom} in the figure) and make the current close to system side (i_{com} in the figure) cleaner. The controller for the STATCOM measures the current and voltage of the EAF and the output current of the STATCOM through the inductor link X. Then it sends the triggering signal generated by the Markov-like model discussed in Chapter 4 to the STATCOM. Figure 6.7 is the realization block diagram for simulation using Power System Blockset (PSB) from Mathworks. Since PSB is inherited from Simulink, many features bear similarity to simulation tools for control or communication system, which is not so familiar to people who are used to power simulator. In the figure, the measurement components and accessory elements are placed in the same way as for power system devices. In order to distinguish them the power system network is shown in the bold lines. The components connected by bold lines are from PSB library. The rest are from Simulink library. Also, one can just neglect the arrows for the signals and treat them as bare lines. The components and their individual functions will be described below.

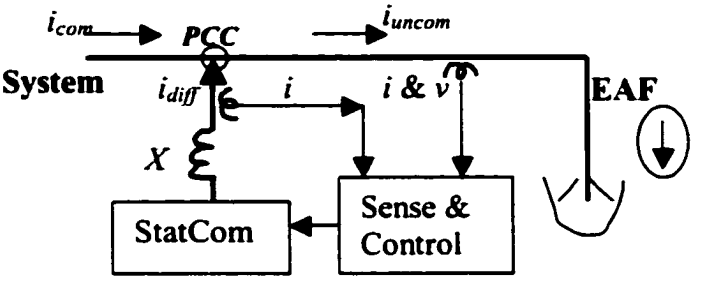

Figure 6.6 Simplified diagram of EAF load with STATCOM compensation

➢ *EAF Current Data, EAF Voltage Data—From File blocks*:

In the diagram, the *Voltage Data and Uncompensated Test Data* are "From File" blocks, which read data from a file and output it. The block icon displays the pathname of the

file supplying the data. The file must contain a matrix of two or more rows. The first row must contain monotonically increasing time points. Other rows contain data points that correspond to the time point in that column.

In this case, the block is used to input test data of EAF voltage into the simulator. The output is a Simulink signal that has a waveform whose values at each time step are defined by the data file according to the .mat format.

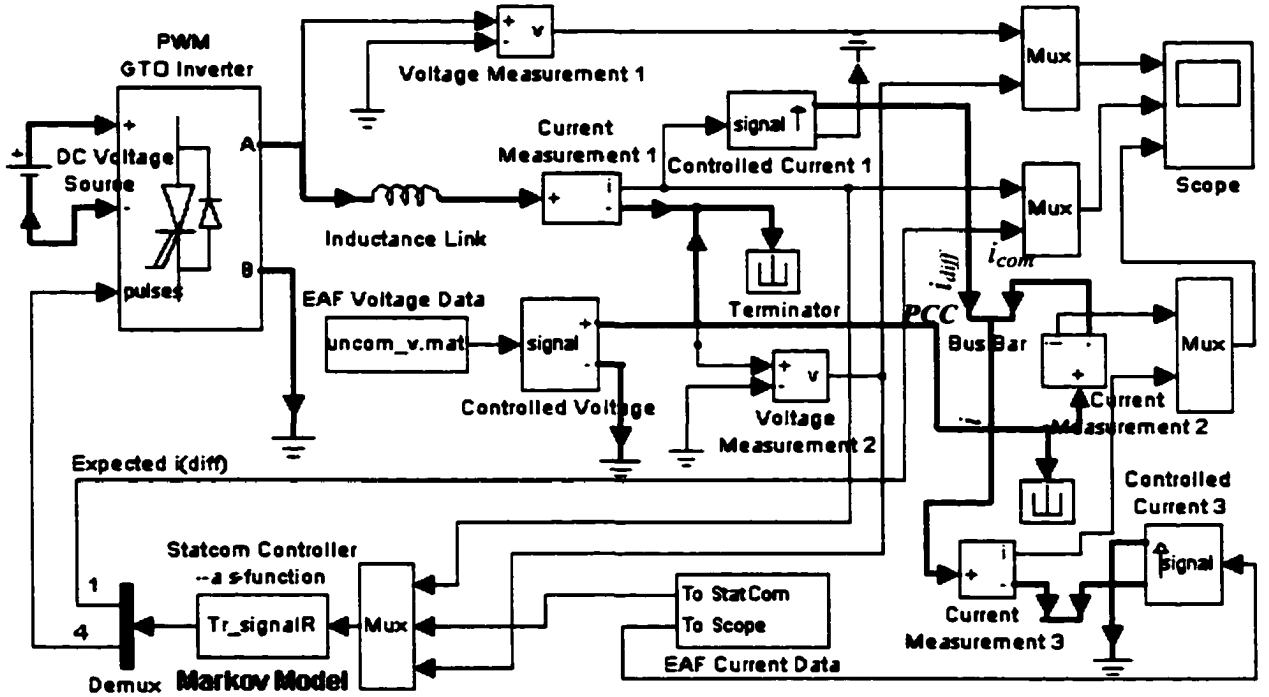

Figure 6.7 Simulink based block diagram of STATCOM compensation for phase A

➢ *STATCOM Controller—a S-function:*

A S-function is a computer language description of a Simulink block. S-functions can be written in MATLAB, C, C++, Ada, or Fortran. The C, C++, Ada, and Fortran S-functions are compiled as MEX-files using the mex utility. As with other MEX-files, these are dynamically linked into MATLAB when needed.

S-functions use a special calling syntax that enables it to interact with Simulink's equation solvers. This interaction is very similar to the interaction that takes place between the solvers and built-in Simulink blocks. The form of an S-function is very general and can accommodate continuous, discrete, and hybrid systems.

The S-function here is embedded with the Markov model. It reads the input signals from actual test data (EAF current and voltage) and the output current of STATCOM. Then runs the Markov-like model as described in Section 4.3 to predict EAF current for next cycle and determines the reference values. Following that, the S-function calculates the current needed for compensation, which is denoted *Expected i(diff)* in the block diagram. Finally, it generates an appropriate triggering signal for the STATCOM based on the difference of the compensation current and the existing current flow at the STATCOM terminal. To avoid sharp spikes during STATCOM operation, the triggering signal sometimes makes the output voltage to be zero (ground) if the expected compensation current is close to the existing current at the terminal of the STATCOM. One can do that only if the terminal (PCC) voltage is closer to zero than to the dc source voltage value. Figure 6.8 illustrates the flow chart for implementation of this controller to go with the STATCOM using function space valued Markov-like model according to FFT frequency decomposition.

➢ *Controlled Current 1/3—a Controlled Current Source*

The Controlled Current Source block provides a current source controlled by a Simulink signal. The positive current direction is as shown by the arrow in the block icon. One can initialize the Controlled Current Source block with a specific ac or dc current.

Since the Simulink signals cannot be connected to power system in PSB, the controlled current source block here works as an interface between these two simulation modules. It is configured so as to draw the EAF current from the PCC to the EAF.

➢ *Controlled Voltage—a Controlled Voltage Source*

The Controlled Voltage Source block provides a voltage source controlled by a Simulink signal. The first and second outputs of the block are respectively the positive and the negative terminals of the voltage source. One can initialize the Controlled Voltage Source block with a specific ac or dc voltage by double clicking the icon and input the values.

Just like the Controlled Current Source, Controlled Voltage Source is especially useful as an interface between PSB and Simulink. The PSB uses the Simulink as its platform but simulink signal cannot be treated as power system signal. So this block makes the voltage signal from the file acceptable to PSB.

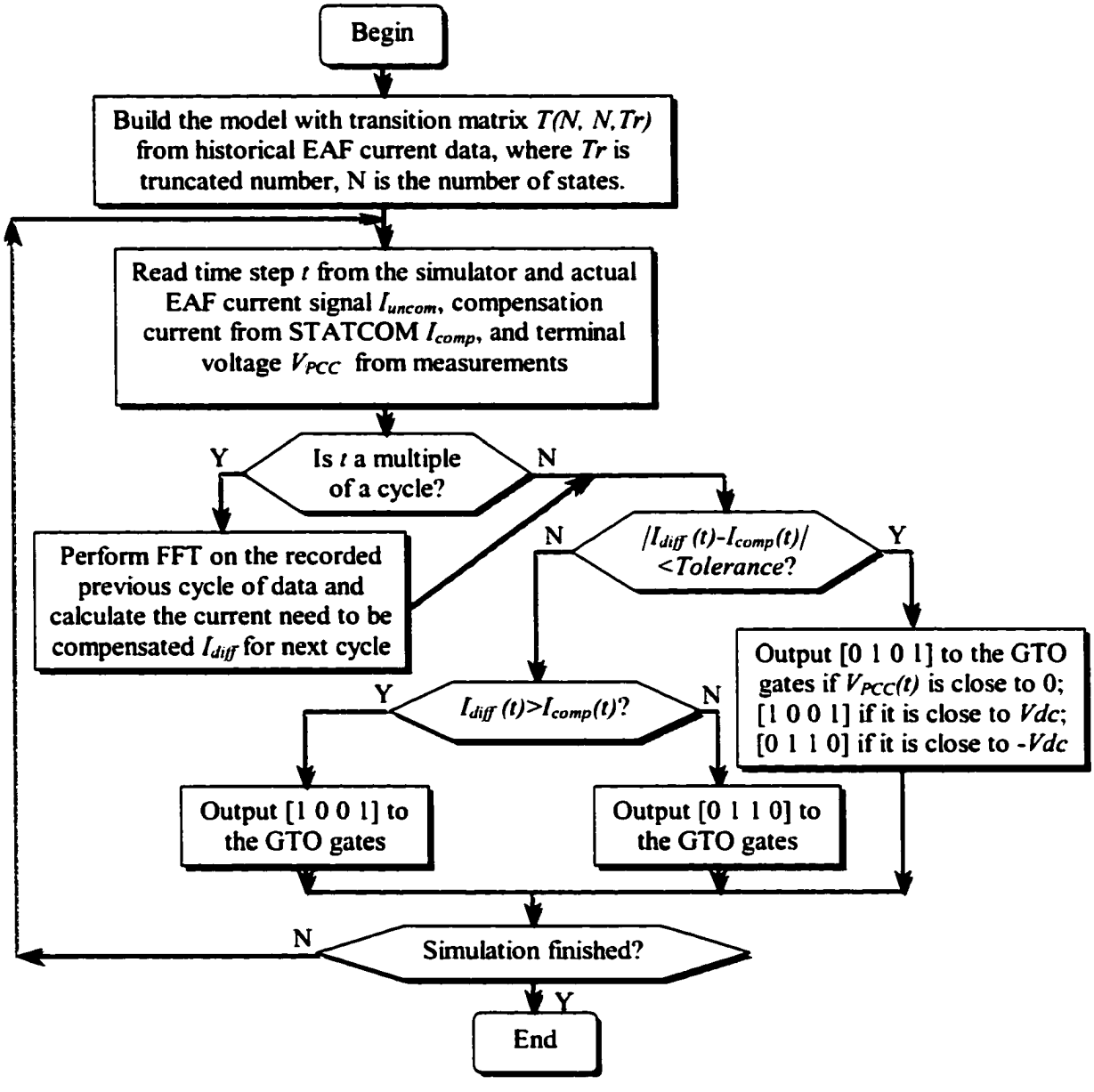

Figure 6.8 Flow chart of STATCOM controller making use of the function space Markov-like model

➢ *PWM GTO Inverter*

The prototype of GTO Inverter is a Universal Bridge block, which implements a universal three-phase power converter that consists of six power switches along with anti-parallel diodes connected as a bridge, as shown in Figure 6.9. The types of power switch and converter configuration are selectable from the dialog box. One can specify it to be Inverter or Converter, three phases (6-arm bridge) or single-phase (4-arm bridge).

The GTO Inverter here is chosen as a single-phase inverter, as shown in Figure 6.4 with poles 5, 6 and terminal C ignored of Figure 6.9. The switching frequency is set to be 10 kHz.

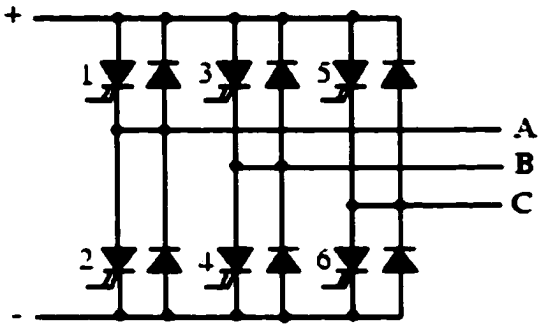

Figure 6.9 Structure of GTO Inverter—full bridge

➢ *Mux:*

The Mux block combines its inputs signals into a single output signal. An input can be a scalar, vector, or matrix signal. Depending on its inputs, the output of a Mux block is a vector or a composite signal, i.e., a signal containing both matrix and vector elements. If all of a Mux block's inputs are vectors or vector-like, the block's output is a vector. A vector-like signal is any signal that is a scalar (one-element vector), a vector, or a single-column or single-row matrix.

Several Muxes are used in this simulation diagram to assemble two or more signals in vector format to form a matrix signal. The content of each signal would not change in this transformation.

➢ *Demux:*

The Demux block extracts the components of an input signal and outputs the components as separate signals. The block accepts either vector (1-D array) signals or bus signals. The Number of output parameters allows people to specify the number and the dimensionality of each output port. If the dimensionality of the outputs is not specified, the block determines the dimensionality of the outputs by itself.

The Demux block operates in either vector or bus selection mode, depending on whether the bus selection mode parameter has been selected. These two modes differ in the type of signals they accept. Vector mode accepts only a vector-like signal, that is, either a scalar (one-element array), vector (1-D array), or a column or row vector (one row or one column 2-D array). Bus selection mode accepts only the output of a Mux block or another Demux block.

The Demux in Figure 6.7 extracts the signal from the S-function and outputs into a triggering signal (4 dimensions) and expected current for compensation (1 dimension).

➢ *Bus Bar*

The Bus Bar block is used to interconnect Power System Blockset blocks. It allows multiple electrical block outputs and inputs to be connected together.

In this simulation for harmonic compensation, the bus bar is the PCC of Figure 6.6, where EAF current, current from STATCOM and current to the system are connected.

➢ *Terminator*

Terminator terminates an unconnected output port, that is to say it can be used to cap blocks whose output ports are not connected to other blocks. If one runs a simulation with blocks having unconnected output ports, Simulink issues warning messages. Using Terminator blocks to cap those blocks avoids warning messages.

➢ *Current Measurement*

The Current Measurement block is used to measure the instantaneous current flowing in any electrical block or connection line. The first output (i) provides a Simulink signal that

can be used by other Simulink blocks such as Scope. The other output (-) is exactly the original input signal.

➢ *Voltage Measurement*

The Voltage Measurement block measures the instantaneous voltage between two electric nodes. The output provides a Simulink signal that can be used by other Simulink blocks such as Scope.

➢ *Scope*

Scope displays signals generated during a simulation. It displays its input with respect to simulation time. The Scope block can have multiple axes (one per port), which have a common time range with independent y-axes. The Scope allows one to adjust the amount of time and the range of input values displayed. It is convenient to move and resize the Scope window and modify the Scope's parameter values during the simulation. When a simulation starts, Simulink does not open Scope windows, although it does write data to connected Scopes. As a result, if one open a Scope during or after a simulation, the Scope's input signal or signals will be displayed.

If the signal is continuous, the Scope produces a point-to-point plot. If the signal is discrete, the Scope produces a stair-case plot. The Scope provides toolbar buttons with functions such as zoom in on displayed data, display all the data input to the Scope, preserve axes settings, limit data displayed, and save data to the workspace.

The Scope in this simulation will display 6 signals, which are divided into 3 groups. Each group has 2 signals to share one x and y axes. These signals are voltage from the STATCOM and voltage at PCC; current derived from the STATCOM and current to be compensated; compensated current and uncompensated EAF current respectively.

6.3 Harmonic Compensation in a Single-phase Circuit

The most challenging things in preparing for EAF current compensation are to get an accurate prediction and set a suitable reference. Based on the function space valued Makov-like model using FFT frequency decomposition methods with 7 harmonics presented in

Section 4.3, one can get the one cycle ahead prediction for EAF current cycle by cycle. Now we will address the problem of setting the reference, that is to say, what the i_{com} is expected to look like. Using a deterministic 60Hz signal is not realistic since this fundamental frequency is shifting randomly, as it is shown in Figure 6.10 (for magnitude) and Figure 6.11 (for phase). The cyclic peak of the EAF current is changing abruptly from time to time. A lot of real power needs to be compensated if a fixed 60Hz magnitude is selected. The phase angle between EAF voltage and current of the 60Hz component is also shifting and shaking (it is jumping up and down), especially when they are close to 180°. If a deterministic sinusoid signal is chosen, it will absolutely lose the synchronization to the actual EAF current and make compensation a difficult process. So it is more practical to use predicted 60Hz, which is component $F_{i-1}(2)$ in Figure 4.5, as the reference for next cycle. Figure 6.12 shows that the predicted reference is not very much different from the actual 60 Hz component.

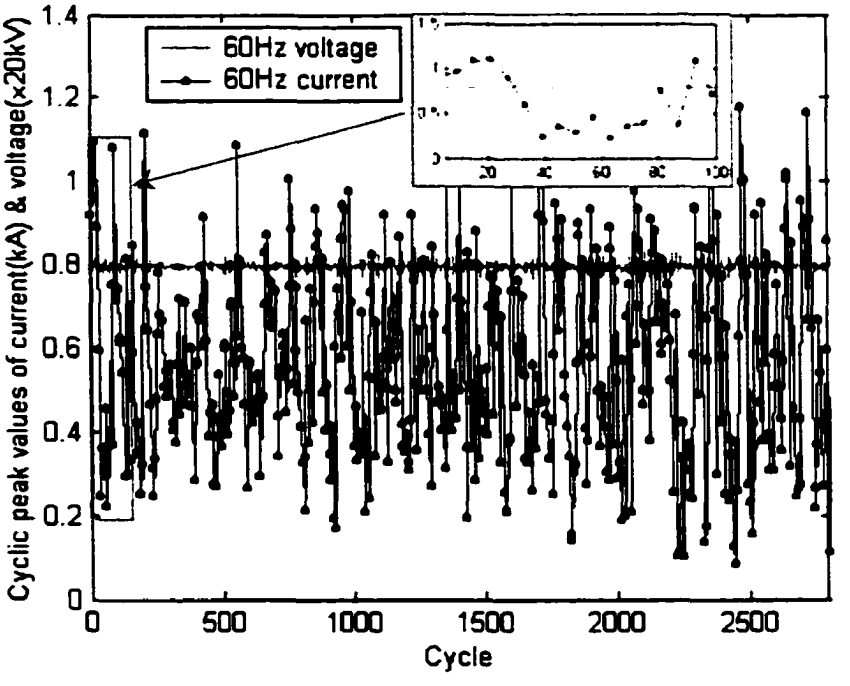

Figure 6.10 Peak values of 60Hz component for EAF current cycle by cycle

The test data used here is 90 seconds to 100 seconds. After obtaining the predicted current and its current reference, one can subtract the former from the later with respect to

each time step and get the expected compensation signal as shown in Figure 6.13. This figure also shows the actual/ideal compensation signal, which is obtained directly from the test data by deducting the actual 60Hz component of EAF current from the test data of this cycle. The real-time compensation is the difference between test data and predicted 60Hz component so that STATCOM can use it for real-time compensation, if the measurement is fast enough.

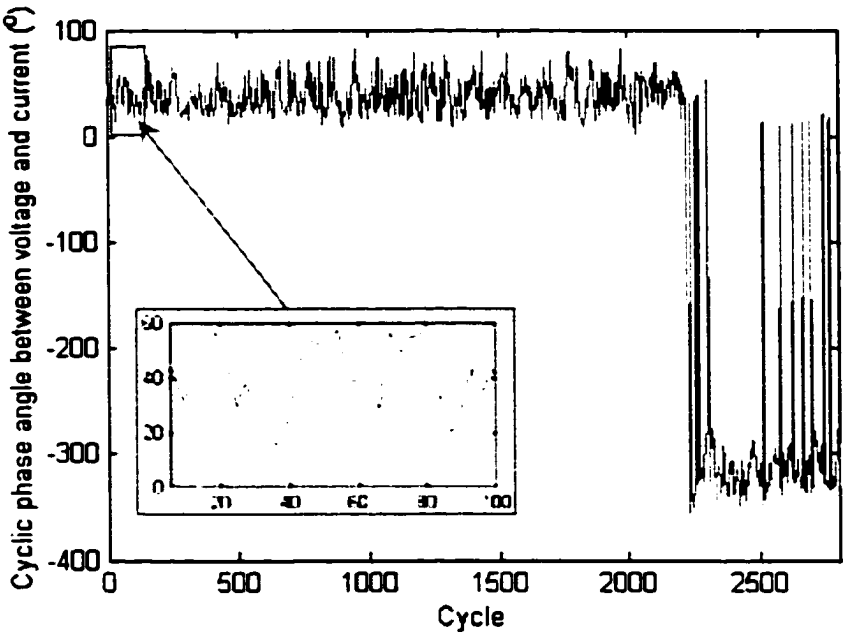

Figure 6.11 Cyclic phase angle between EAF voltage and current of 60Hz component

Figure 6.14 shows the simulation result observed from Scope (picture negative). The figure is divided into three parts. The step-like waveform in the top part is the voltage from STATCOM ($v_{StatCom}$) and the sinusoid-like one is the voltage at PCC(v_{PCC}). In the middle part, one waveform is the actual current output from the STATCOM (i_{diff}), while the other one is the expected compensation current generated by the Markov-like model ($i_{expected}$), as noted. The bottom part shows the uncompensated EAF current (i_{uncom}) and the current after compensation (i_{com}). In the figure, i_{diff} and $i_{expected}$ are very close to each other, which implies that the STATCOM functions very well. There are three major factors that may influence the outcome of the STATCOM: dc voltage source, inductance link and simulation step. This can

be easily seen from the equation $v_{StatCom} - v_{PCC} = L\, di_{diff}/dt$. When $v_{StatCom}$ get larger or the L is selected smaller or the time step is set larger, i_{diff} will change more and versus visa.

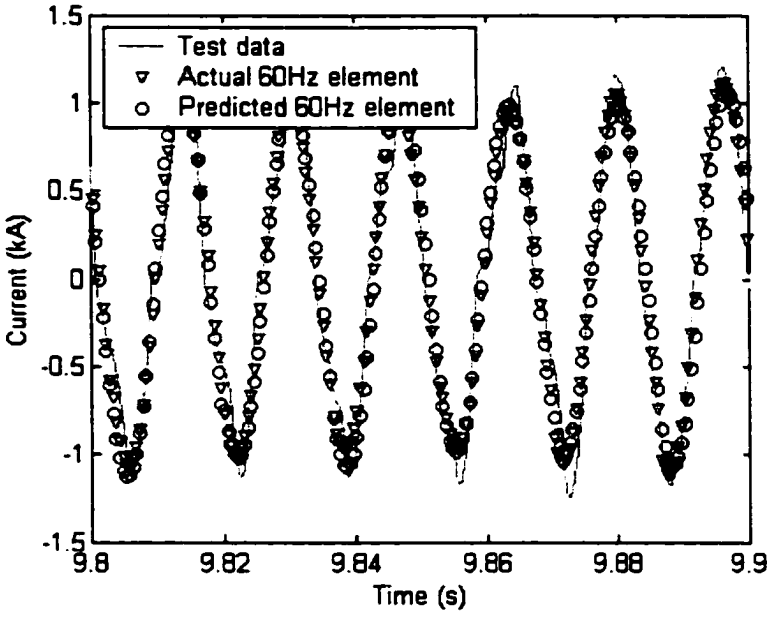

Figure 6.12 Predicted 60Hz element vs. actual one

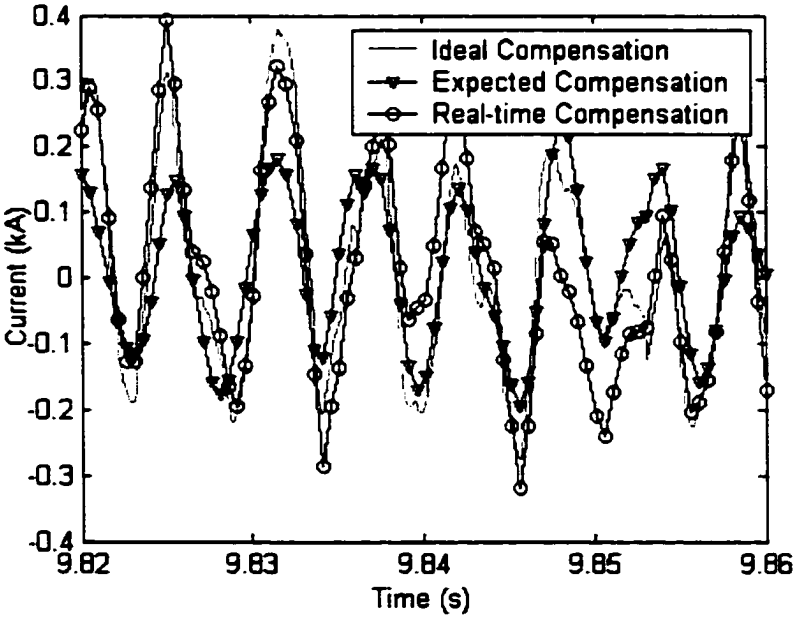

Figure 6.13 The signal derived for compensation

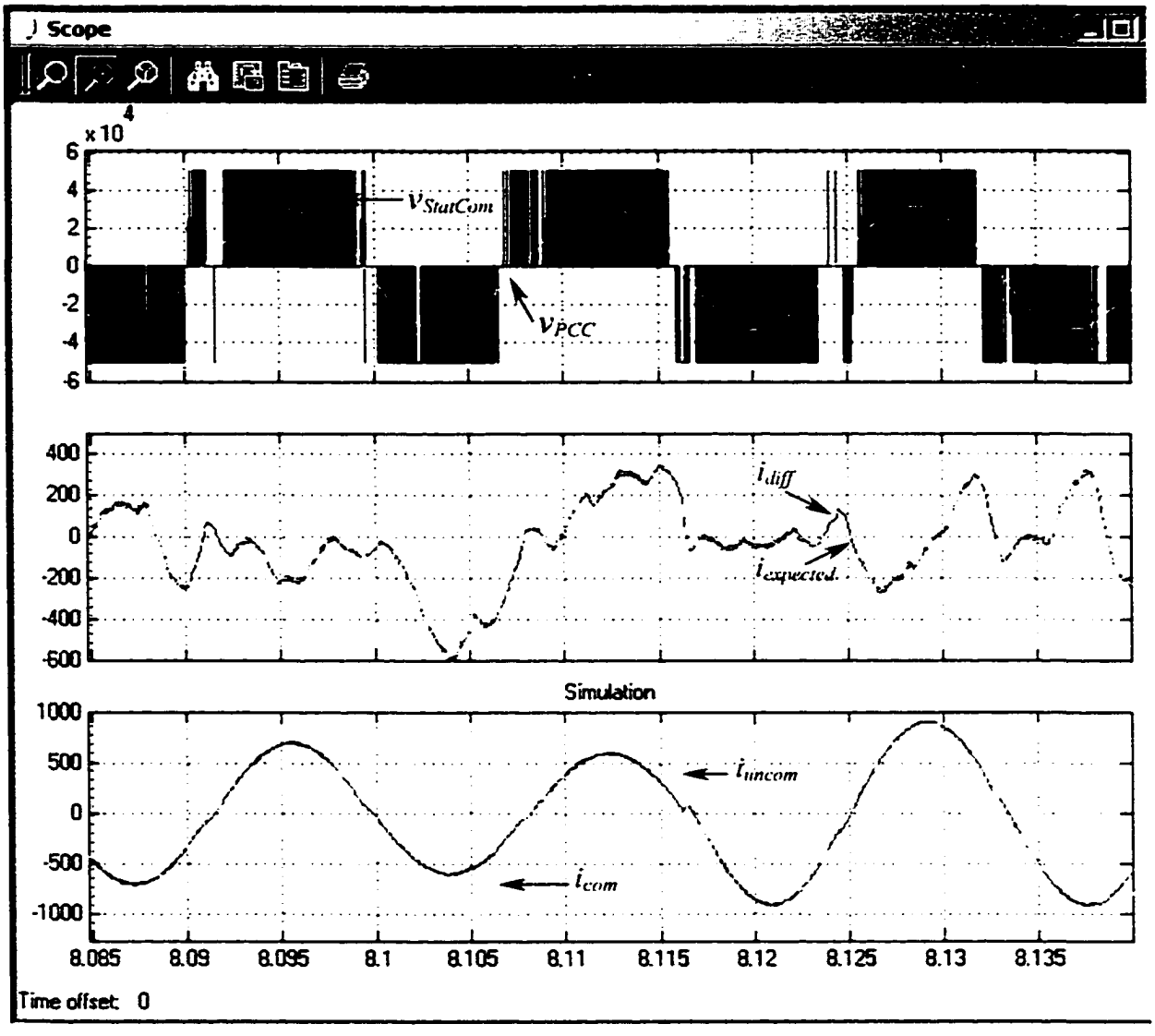

Figure 6.14 Simulation results for EAF current compensation

The period of data in Figure 6.14 is related to the actual data of 98.08~98.14 seconds, with the beginning time at 90 seconds. To look into the waveform to a greater detail, the simulation data was saved and plotted in Figure 6.15. The comparison indicates that the current after compensation does improve to a great extent. It is close to the shape of pure sinusoid. The magnitudes are different from cycle to cycle following the actual condition of EAF current.

To get more information about the effectiveness of the compensation, the currents before compensation and after compensation are processed with FFT to get the information in frequency domain. Figure 6.16 shows the spectrum of the EAF current before compensation while Figure 6.17 is for the current after compensation (the Magnitude of the 60 Hz component is about 500). It can be seen that a large portion of the harmonics are eliminated. But there is still some visible spectrum power around 60 Hz. Some small spectrum appears at second and third harmonics also. The magnitude of fundamental frequency for each cycle is varying and may lead to some leaking to the adjacent frequencies, However, one can clearly see the effect of compensation relating to harmonic currents.

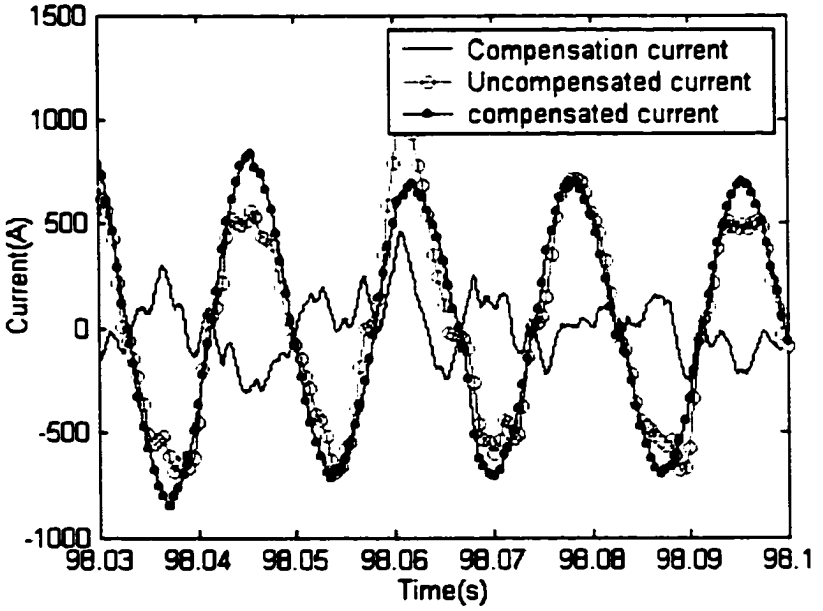

Figure 6.15 Closer look at the various currents

The power quality indices such as THD, K-factor, zero-peak flicker factor and crest factor are also generated from the compensated data. Table 6.1 lists the results from the compensated current as well as from the uncompensated EAF current. The THD limits set by IEEE standard 519 for current distortion [60] is 15% for the actual short circuit ratio of the electric equipment ranging from 100 to 1000, which is common among EAFs. It can be seen that the THD of the compensated current is far less than the limit. In fact, even the strictest

limit of 5% is satisfied for actual short circuit ratio less than 20. When comparing the two columns in Table 6.1, one can find that the power quality has improved a lot: the THD for the actual uncompensated EAF current is more than 5%, but it is only 0.5% here for compensated current.

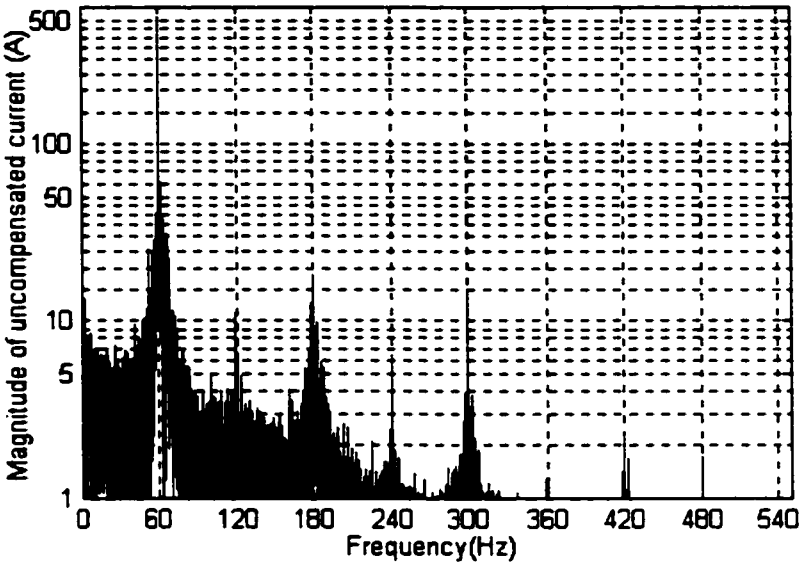

Figure 6.16 Spectrum of the current before compensation

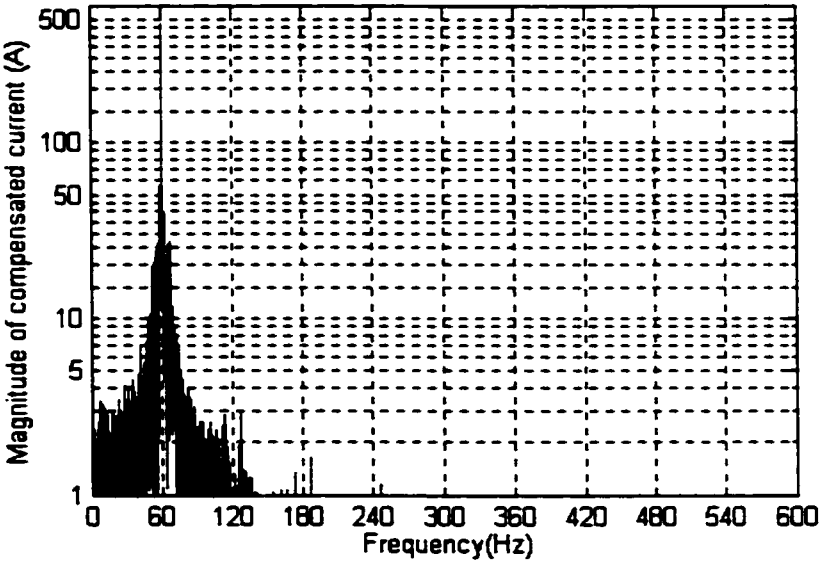

Figure 6.17 Spectrum of the current after compensation

In addition, the other indices such as K-factor also show some improvement. The change of the rest of indices is not so significant because the harmonic compensation is done on a cycle by cycle case and the improvement can hardly be reflected by them. However, the comparison of THD indices reveals that the function space Markov-like model is an accurate approach for the harmonic compensation.

One can notice a problem from the power quality indices by looking at Figure 6.17 again. None of the indices seems to have effectively considered the frequency components which are sub-harmonics (which are not multiples of the fundamental frequency). The discussion of searching for possible effective indices will be left to specialists on power quality and is out of the scope of this dissertation.

Table 6.1 Power quality indices of a current sample for compensation

Power Quality Indices	Uncompensated current	Compensated current
THD (%)	5.0789	0.3278
K-factor	1.0338	1.0046
Zero-peak flicker factor	1.4982	1.4865
Crest factor	3.1019	3.0626

One may notice that there are somewhat strong spectrums among the low frequency range, with the magnitude and phase of them changing from time to time. When data is limited, negative effect may be caused if one just uses the previous information of them for prediction. To consider these frequencies during prediction and compensation, one needs much more data. Fortunately, the power for most of these frequencies is less than 5% of the fundamental frequency. After getting enough data, one can increase the processing unit from one cycle to 3 cycles or more to take care of some low frequencies.

To verify if the simulation is robust, validity of compensation technique for another data sample of EAF current of 100 seconds to 110 seconds is tested. Figure 6.18 shows part of the results for i_{uncom}, i_{com} and i_{diff}. The harmonic compensation is satisfactory by observing the current before compensation and after compensation, which is very close to a sinusoidal waveform.

Thus for a single-phase circuit, the prediction and compensation did demonstrate that the Markov-like model in function space (FFT frequency decomposition) is an effective tool for improving the power quality associated with EAF loads.

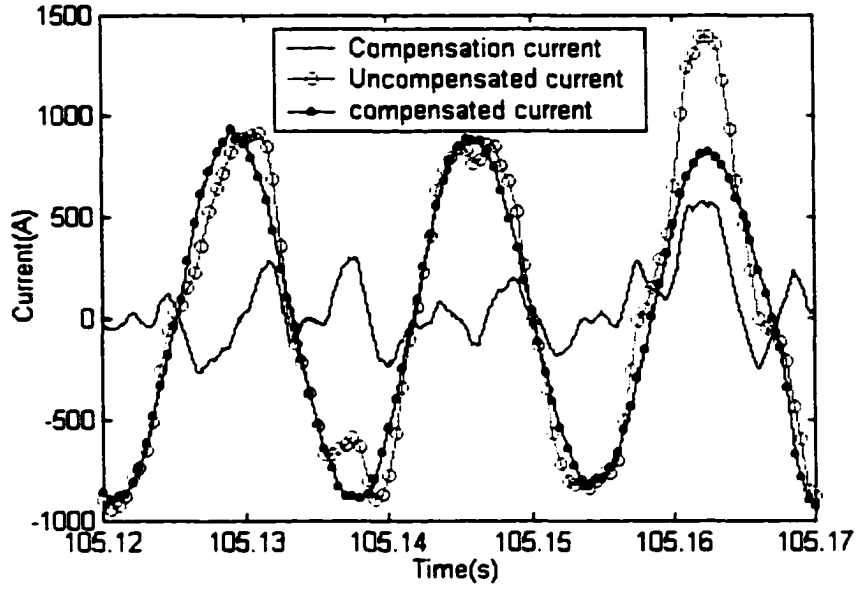

Figure 6.18 Close look at the simulation results for a different sample of data

6.4 Harmonic Compensation for Three-Phase Loads

The Scheme for harmonic compensation presented in Figure 6.7 can be easily extended to a three-phase case by adding two similar sets of blocks for phase B and C. Figure 6.19 gives such a scheme for harmonic compensation in the three phases case. The STATCOM controller mainly performs three steps of work

i) Read the three-phase current from the terminals of the STACOM (GTO Inverter) and test data for actual EAF current at each time step.

ii) At the starting point of each cycle, process the stored EAF current data of one cycle with the Markov-like model in function space with FFT frequency decomposition and

make prediction for the next cycle. Then calculate the current that is expected to be compensated from the STATCOM.

iii) For each time step, compare the current to compensate and the actual current at the STATCOM terminal and decide the action of the GTO switches, which is controlled by the triggering signals generated from Markov model in Statcom controller.

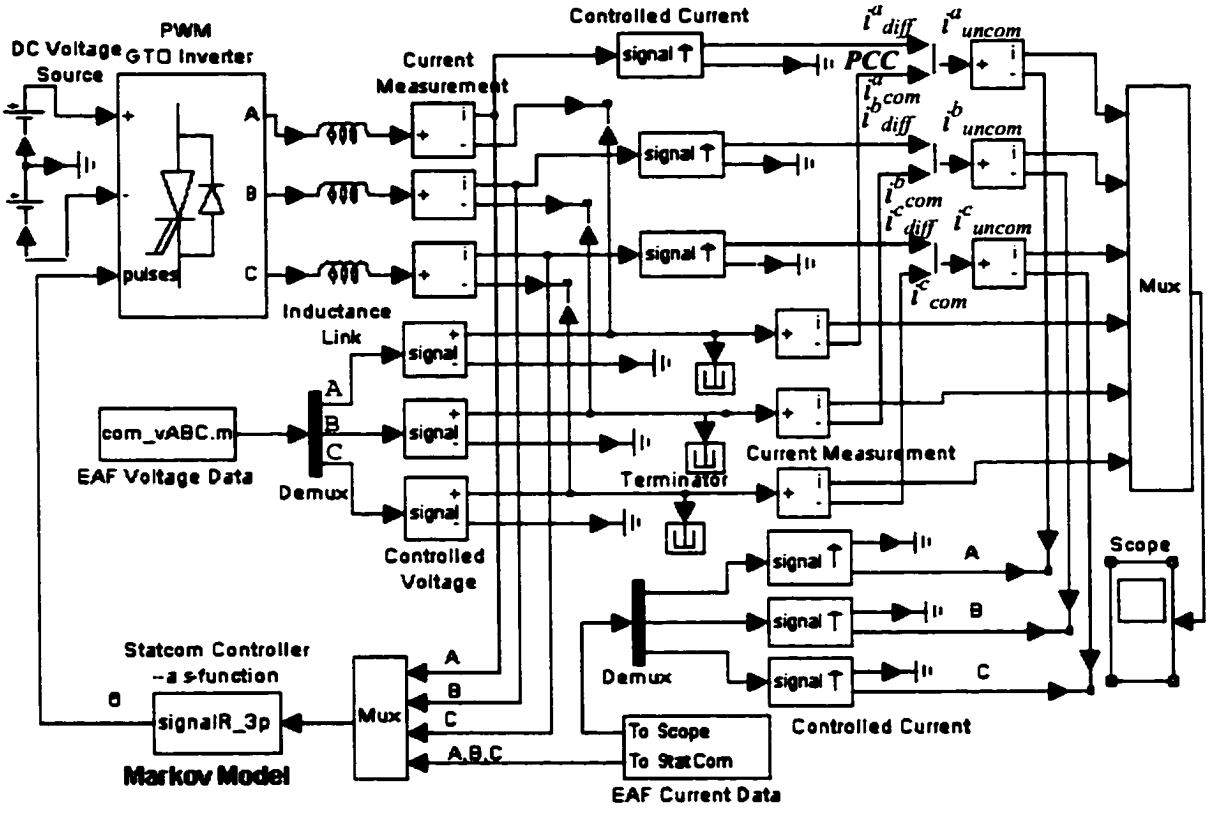

Figure 6.19 Simulink block diagram for STATCOM compensation-three phases

The STACOM device here is a full bridge GTO Inverter, as in Figure 6.9. So there should be 6 triggering signals from the controller for the 6 GTO switches. Another change from the single-phase case is the source that supplies the STATCOM. A neutral point and another similar dc voltage source is added for the three-phase case here.

Figure 6.20 illustrated some simulation results based on the compensation structure discussed above. It can be seen that the compensation is satisfactory. The shape of

make prediction for the next cycle. Then calculate the current that is expected to be compensated from the STATCOM.

iii) For each time step, compare the current to compensate and the actual current at the STATCOM terminal and decide the action of the GTO switches, which is controlled by the triggering signals generated from Markov model in Statcom controller.

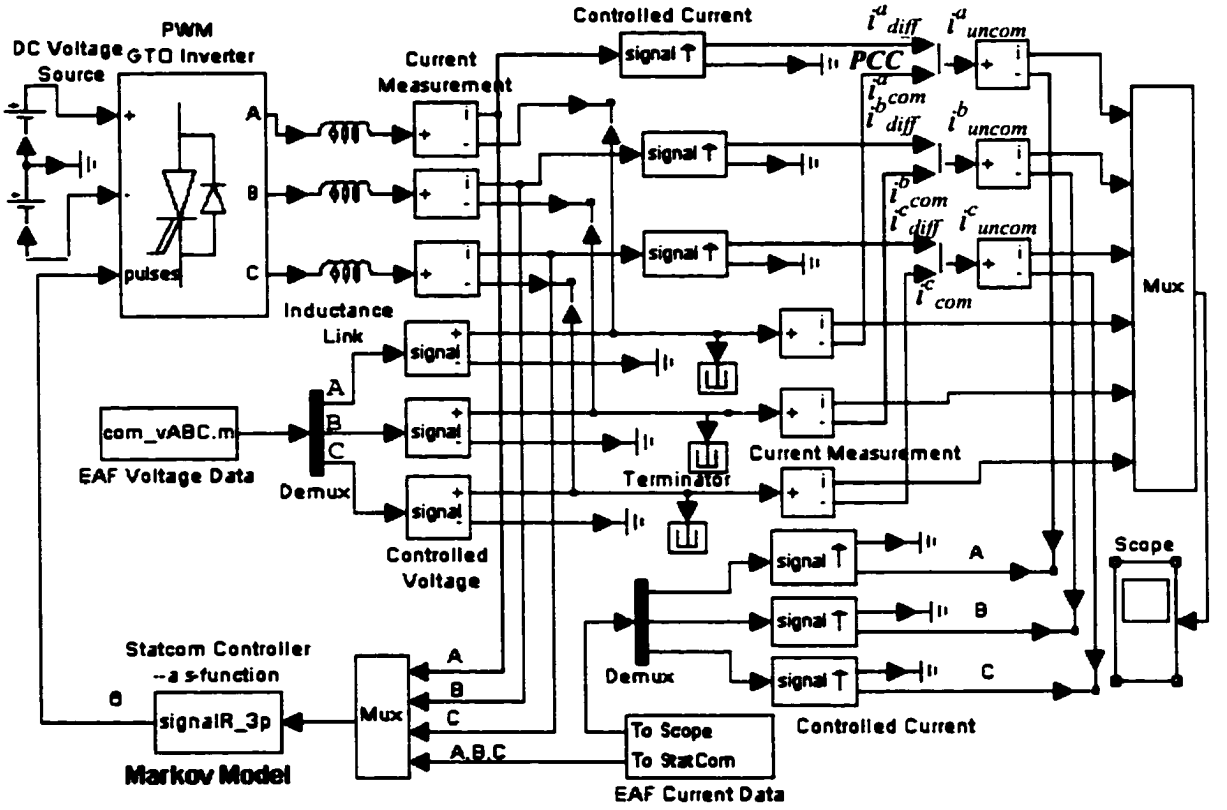

Figure 6.19 Simulink block diagram for STATCOM compensation-three phases

The STACOM device here is a full bridge GTO Inverter, as in Figure 6.9. So there should be 6 triggering signals from the controller for the 6 GTO switches. Another change from the single-phase case is the source that supplies the STATCOM. A neutral point and another similar dc voltage source is added for the three-phase case here.

Figure 6.20 illustrated some simulation results based on the compensation structure discussed above. It can be seen that the compensation is satisfactory. The shape of

compensated current for each cycle is very close to a sinusoid. When compensating each phase separately for the three-phase case, the problem of unbalance may be brought out. That is to say, the current at the system side may not satisfy the equation:

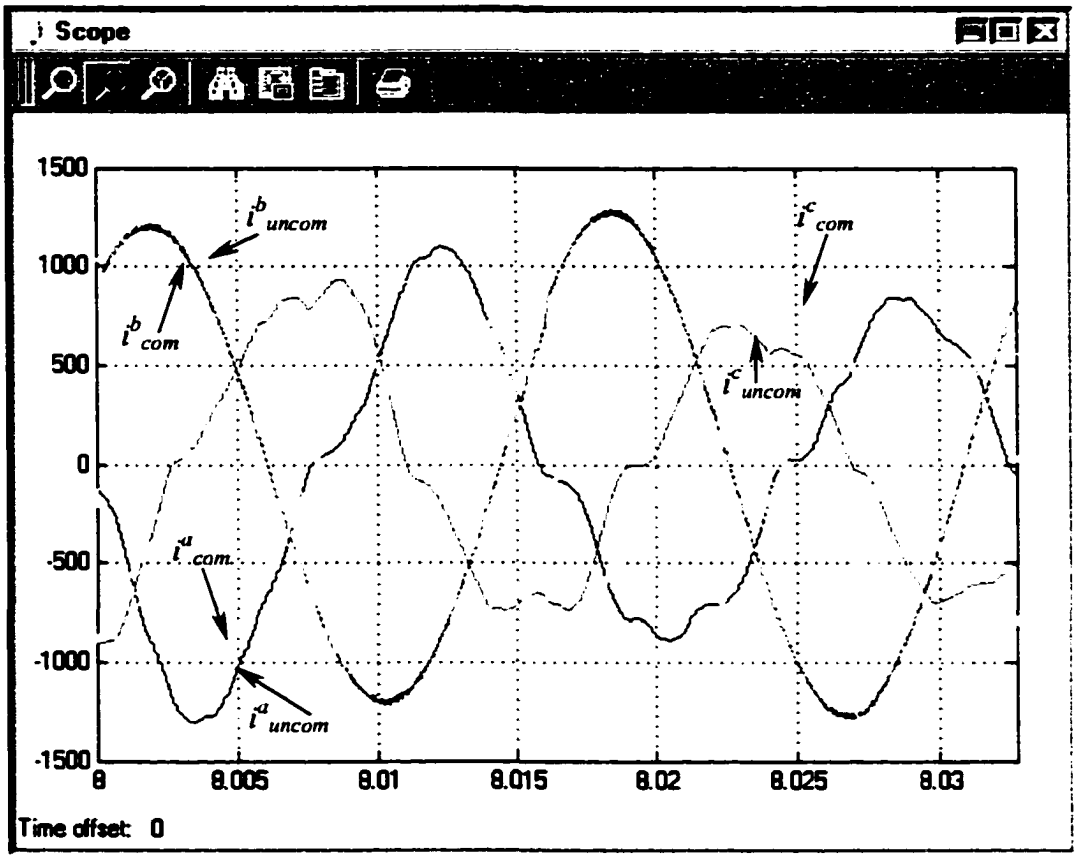

Figure 6.20 Simulation results for three phases EAF current compensation

$$i^a_{com} + i^b_{com} + i^c_{com} = 0 \tag{6.1}$$

To avoid this problem, the current expected to be compensated is forced to validate:

$$i^a_{diff} + i^b_{diff} + i^c_{diff} = 0 \tag{6.2}$$

In practice, the Markov-like model predicts the next cycle and calculate the compensation current only for phase A and B, then derives the compensation current for phase C from

equation 6.2. This will make the unbalance current, if any, very small due to the harmonics by switching poles of the STATCOM. However, in practice this may not be strictly true.

6.5 Summary

The harmonic compensation on the EAF current by a STATCOM device using the function space valued Markov-like model was illustrated in this chapter. Such circuit was simulated with Power System Blockset in Simulink for both single-phase and three-phase loads. It is found with the compensation made, the current near the system side is closer to a smooth sinusoidal waveform of fundamental frequency. A further frequency domain analysis also demonstrated that the proposed compensation decreased the amplitude for harmonics of the EAF current and improved the power quality, confirming that the Markov modeling of the highly nonlinear EAF load and its application for prediction are helpful and applicable to real time operation and control.

7 CONCLUSIONS AND FUTURE WORK

7.1 Conclusions of This Work

Markov-like Models for modeling nonlinear load in power system, using EAF as an example are proposed. The whole system of methodology is presented, including property test, model construction, prediction applications, function space extension and implementation for compensation. A summary of some significant contribution is as follows:

- Markovian property test and stationarity test

Before building a model for a time series using Markov chain, it is important to test if it is Markovian, i.e., if the equations 3.16 or 3.17 are satisfied. For this purpose, the estimate of one step or two step or higher transition probabilities from the historical data are calculated and compared to validate the Markovian property within some error of tolerance. Both a first order chain and a second order chain were tested to be Markovian, with the latter one seems to be more effective.

Stationarity is tested in two ways. As a first approach, one makes use of classic time series theory for stationarity evaluation. One compares, in the second method, the statistical indices generated by the proposed Markov models to the actual EAF data to check stationarity. Both methods demonstrated that EAF current is (weak) stationary, although the plot of the time series looks chaotic. After verifying the stationary features of the EAF time series, the statistical characteristics of the whole system can be easily recognized from an appropriate sample of the historical data.

- Construction of a first and second order Markov model

After identifying the state space, a first order Markov-like model was built from the EAF data by estimating the transition probabilities from EFF of the visits to individual states and state transitions. From this model, one can get the stationary distribution, which portrays the long-term profile of the EAF dynamics. It has also been used for one-step-ahead prediction of EAF current.

But for better accuracy, a second order Markov-like model is suggested. The second order Markov-like model is based on $\{Y_i=(X_i, X_{i+1})\}$, where $\{X_i\}$ is the time series of EAF current. Since it retrieves more instant information from the past, the transition probabilities become sharper (close to 0 or 1) and are more suitable for short-term prediction.

- Extension to function space Markov-like model

In practical situations, the measurement and operation may not be fast enough for controlling purpose with only one-step-ahead accurate prediction, which is within the capability of a second or first order Markov chains. So the Markov-like model was extended to function space, where a vector $\{\eta_j\}$, rather than a single state or a point, is treated as a processing unit. The vector can be a continuous sequence (generally a cycle) of the points from the original time series $\{X_i\}$. While it is not realistic to compute directly with the Markov-like model consisting of these vector states, function approximations were proposed to simplify the calculation as well as to obtain a satisfactory accuracy in prediction. Several methods are tested for the approximation of a cycle of current, such as FFT frequency decomposition, polynomial fit, function of {maximum, minimum and their positions} and function of {maximum, minimum, cycle length and waveform shape}. The FFT frequency decomposition seems to be a more efficient and accurate approximation for the function space Markov model. For most of the approximations, a first order Markov chain is used since it is proven to be sufficient to characterize the dynamics when a whole cycle of EAF data is considered.

- Related EAF current and voltage modeling

In some cases, EAF current and voltage are closely coupled. Thus the modeling accuracy would increase if these two variables are taken into account together. Markov models are built for point case and function space case. Although their performance is not as good as the models for separate current or voltage variables, one cannot generalize that the models on related variables are inferior to the ones on single variable. In fact, this controversy aspect is due to the lack of historical data and plenty of uncertainty for the EAF current. Also, it implies that the variations of current and voltage from the data under study do not have much dependence between each other (the EAF is installed at a lightly loaded

bus). The proposed methodology provides solid basis for modeling of related variables, for example, the current and voltage from an EAF installed at a heavy load bus.

- Short-term and long-term forecasting

For active control or compensation of an EAF to improve the power quality, an accurate prediction of its electrical signals such as current and voltage is indispensable. The basic first order and second order Markov models built for the EAF current have been used to predict the current at least one-step-ahead precisely. After the extension of the models to function space, it could forecast one or more cycles ahead accurately, which allows more time for the power system controllers to react.

The Markov models are also useful for obtaining the long-term prediction, whose results can characterize the statistical features of the EAF current. They are also used to produce power quality indices, which are very close to the actual data.

- Implementation of EAF current compensation

A STATCOM was applied to compensate the EAF current to make each cycle closer to an ideal sinusoidal waveform of fundamental frequency. The effect is visually positive by observing the current waveforms before compensation and after compensation. Further frequency domain analysis also indicated that many harmonics of the EAF current are reduced to a great extent. Extension to a three-phase load is also considered and compensation is proven to be satisfactory. This suggested that the Markov modeling of the highly nonlinear EAF load is helpful and applicable to real time operation and control of EAF for the purpose of improving the power quality in a distribution system.

7.2 Applications to Other Nonlinear Time Series

The time series that was discussed has seasonality, but no significant trend. It is typical for a nonlinear load in a power system, but not for many other time series, such as the monthly power generation in Australia from 1980 to 1991 shown in Figure 7.1. If one plans to apply the models described in this dissertation to such kind of time series, the following procedures is advised.

i. Plot the historical data of this time series in a clear format to check if there is some trend and seasonality. If two or more variables are to be considered, try to plot them into a figure for surveying and check the degree of dependence.

ii. If there is a trend, remove it by some estimation techniques such as least square regression, or transformations such as differencing (if the original time series is X_i, the differencing one is $Y_i = X_i - X_{i-1}$). Figure 7.1 shows such an example.

iii. Test the dependence of the multivariable time series by examining the covariance matrix of the involving variables. If the correlation values are close to zero, separate modeling of each variable is possible. Go to step iv in this case. Otherwise, a correlated model will be more suitable. Chapter 5 discussed the basic approach for modeling of such kind of situation. A first order Markov-like model is constructed by incorporating these variables into the transition matrix. Go to the function space Markov-like model if needed by correspondingly adjusting the transition matrix.

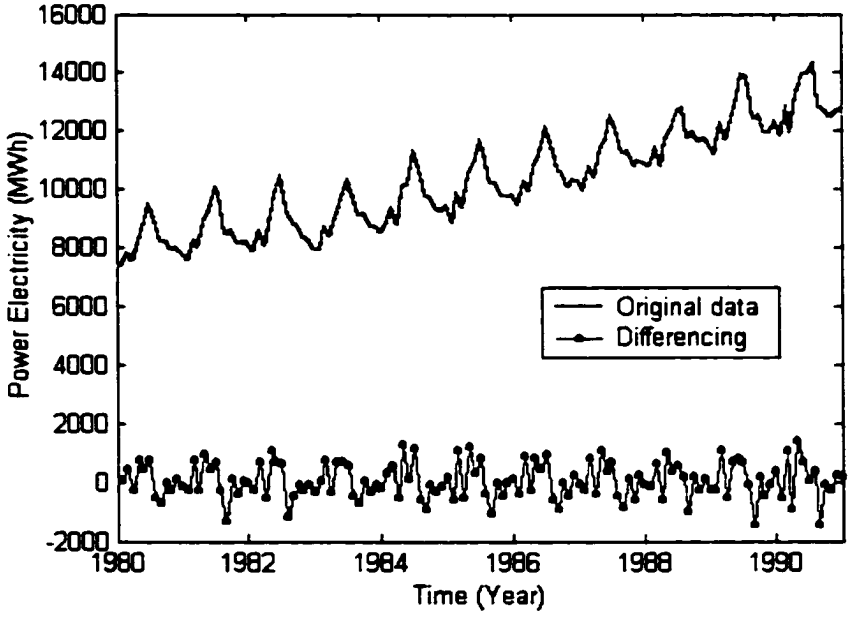

Figure 7.1 Monthly power electricity generation in Australia

iv. Test the first order Markovian property of the residual time series. If it is satisfied within some error of tolerance, go to step v. Otherwise, try the second order Markov

chain. One may resort to other methods if the test as described in Section 3.4 gives too large errors.

v. Construct the model by estimating the transition probabilities from the historical data after identifying the state space. The performance of this model can be further verified by comparing the one-step-ahead prediction results to actual data. Refer to Chapter 3 for detail description.

vi. Function space valued Markov chain maybe necessary for prediction of longer range of time. If computational burden is high, one can try function approximations based on the feature of the time series. Test the effect of approximation by prediction accuracy or comparison to other classic methods. Chapter 4 gives the detailed procedure with examples.

7.3 Suggestions for Future Work

7.3.1 Markov Jump Process Modeling

This addresses the problem in basic Markov modeling that some states have high self-return transition probabilities. Under that circumstance, two or more steps ahead prediction may have some difficulty. Since the prediction may stay at one particular state for a long time, it doesn't have a good chance to jump to the other states.

The Markov jump process [43] may solve this problem. It considers the situation that, at time 0 the system comes into state k and remain in this state until some time $\tau_1>0$, at which time the system jumps to a new state $l\neq k$. This process continues and at time τ_i it is at state a_i. So if $S(t)$ denotes the state of the system at t, it called a jump process by defining

$$S(t)=\begin{cases} k, & 0\le t<\tau_1 \\ l, & \tau_1\le t<\tau_2 \\ \ldots\ldots & \\ a_i, & \tau_i\le t<\tau_{i+1} \\ \ldots & \end{cases} \tag{7.1}$$

In this model, the time of staying at a state is taken into account. The transition probability from state k to l is defined as

$$P_k(\tau_l \le t, X(\tau_l = l) = F_k(t)Q_{kl} \tag{7.2}$$

where $F_k(t)$ is the distribution function that the system remains at state k for a random length of time τ_l. For example, it is $e^{-\lambda t}$ for Poisson process

Q_{kl} is the probability that the system jumps to state l from the current state k, it is like the transition probability P_{kl} of the basic Markov models described in Chapter 3.

Both $F_k(t)$ and Q_{kl} can be estimated empirically from the historical data. By doing this, the model decomposes the transition events into two categories—transit to another state and stay at the same state—and is likely to improve the modeling accuracy.

7.3.2 Compensation for Voltage Flicker

According to the harmonic compensation for EAF current in Section 6.3, the model in function space approximated by FFT techniques is efficient for eliminating higher order harmonics, but not for the low frequency components, as illustrated in Figure 6.17. This is because that the model analyzes one cycle as an object and cannot take care of the frequency components below 60Hz and the ones between 60Hz and 120Hz. To take them into account, it is useful to analyze several cycles at a time. For example, if 5Hz component is of great interest, at least 60/5=12 cycles should be viewed as one object. Since the previous model for harmonic compensation is effective, it is suggested to use this model to predict low frequency components for the associated problem of voltage flicker associated with an arc furnace. This should make the power spectrum below the fundamental frequency cleaner. However, more historic data is required to build the model to make the estimation of the model more accurate. Another solution is to transfer the abc system to dq system and apply the Markov model on the dq components, which take the original fundamental frequency as reference (dc component). In this case, the job is focused on eliminating (or compensation for) the low frequency components as well as high frequency components.

7.3.3 Enrich the Model Through Real-time Operation

Sometimes the historical data may not be enough to estimate the Markov-like model efficiently. One practice to meet this problem is to make the program adaptive, that is to say, collect the data during running the model on a real-time operation of the system and use them to modify the elements of the transition matrix continuously with added information. It is not difficult to realize this in the program. The only thing that should be changed in the program is to adjust the related transition probability corresponding to a new measurement. Of course, it requires a little more memory to remember the number of previous data that fall into each state. For example, currently, the system is in state i and p_{ij} is the transition probability from state i to j with the number of data that visited state i to be n_i. If a new data input makes the system transit to state j, the new p'_{ij} will be $(n_i \times p_{ij}+1)/(1+n_i)$. At the same, p_{i1} , p_{i2} ..., $p_{i(j-1)}$, $p_{i(j-1)}$, ..., p_{iN} will be adjusted accordingly with each of them multiplied by a factor $n_i/(1+n_i)$ to make the transition probabilities from state i sum up to be 1. The adaptive model is likely to be useful for practical application. The longer the model runs, the more accurately it characterizes the system under study.

APPENDIX A LAW OF ITERATED EXPECTATIONS

Law of iterated expectation states that $E(Y/X)$ has the same expectation as the random variable Y. Here is the proof.

The conditional expectation is a function of the value of the random variable X, For different realizations of X, the conditional expectation will be a different number. Suppose we view $E(Y/X)$ as a random variable and take its expectation with respect to the distribution of X:

$$E_X[E_{Y/X}(Y/X)] = \int_{-\infty}^{\infty}[\int_{-\infty}^{\infty} y.f_{Y/X}(y/x)dy]f_X(x)dx \quad \text{(A.1)}$$

A joint density can be written as the product of marginal density and the conditional density:

$$f_{X,Y}(x,y)=f_{Y/X}(y/x)*f_X(x) \quad \text{(A.2)}$$

Also the marginal density $f_X(x)$ is obtained by integrating the joint density $f_{X,Y}(x,y)$ with respect to y:

$$f_X(x) = \int_{-\infty}^{\infty} f_{X,Y}(x,y)dy \quad \text{(A.3)}$$

Then, based on [1.12] and [1.13], [1.10] can be expressed as

$$\int_{-\infty}^{\infty}[\int_{-\infty}^{\infty} y.f_{Y,X}(y,x)dydx = \int_{-\infty}^{\infty} y.f_Y(y)dy \quad \text{(A.4)}$$

Thus

$$E_Y[Y]=E_X[E_{Y/X}(Y/X)] \quad \text{(A.5)}$$

In words, the random variable $E(Y/X)$ has the same expectation as the random variable Y, This is known as the law of iterated expectation.

APPENDIX B ACCOMPANYING DISKETTE AND PROGRAM DESCRIPTION

This appendix describes Matlab programs that are included in the 3.5" floppy disk accompanying this Dissertation. Below are system requirements for running these programs:

- IBM PC or 100% compatibles;
- Hard disk (2GB minimum); Memory (256MB minimum);
- Windows 95 or higher;
- Matlab 5.2, Simulink 4.0 and Power System Blockset 1.0 or higher.

When explaining a program, the *Program name* is stated first, followed by the corresponding sections (if specific) of the Dissertation in which the program is used. Then a brief description of its function will be given, as well as its inputs and outputs.

B.1 Data and Programs for Data Preparation

Original field data—

`Column7.mat` – Recorded data for EAF current of phase A
`Column8.mat` – Recorded data for EAF current of phase B
`Column9.mat` – Recorded data for EAF current of phase C
`Column10.mat` – Recorded data for EAF voltage of phase A
`Column11.mat` – Recorded data for EAF voltage of phase B
`Column12.mat` – Recorded data for EAF voltage of phase C

Note: The ratio between recorded data for current and actual EAF current is 1:400
The ratio between recorded data for voltage and actual EAF voltage is 1:10000
The sampling rate is 10000 samples/second
The time duration of the data is 128 seconds

get_Data.m—

Get samples from the original field data (`Column7` to `Column 12`). The starting point `Data_Start`, the data length `Num_set` and the output file name can be modified in the program.

Input: Any original field data (`Column7` to `Column 12`).

Output: `part_curr*.txt` for current or `part_vol*.txt` for voltage, where * indicates the interval of the data, e.g. * is `30_80` if it is from 30 seconds to 80 seconds of the original field data.

get_testData.m—

Get test data from the original data (`Column7` to `Column 12`). The starting point `Data_Start`, the data length `Num_set` and the output file name can be modified in the program.

Input: Any original field data (`Column7` to `Column 12`).

Output: `test_curr*.txt` for current or `test_vol*.txt` for voltage, where * indicates the interval of the data, e.g. * is `30_80` if it is from 30 seconds to 80 seconds of the original field data.

B.2 Programs for First Order and Second Order Markov Models

Test_Model_1st.m—Section 3.4.1

Test the Markovian property of the EAF current for the first order chain. It can be also use for other data samples by changing the corresponding input file name.

Input: Sample data file such as `part_curr*.txt` or `test_curr*.txt`.

Output: `Test_model1.txt`, which lists the estimates of 2 steps or 3 steps transition probabilities for the EAF current sample.

Test_Model_2nd.m—Section 3.4.1

Test the Markovian property of the EAF current for the second order chain

Input: Sample data file such as `part_curr*.txt` or `test_curr*.txt`.

Output: `Test_model2.txt`, which lists the estimates of 3 steps or 4 steps transition probabilities for the EAF current sample.

Test_Modelv_1st.m— Section 3.4.1

Test the Markov property of the EAF voltage for the first order chain

Input: Sample data file such as `part_vol*.txt` or `test_vol*.txt`.

Output: `Test_model1_v.txt`, which lists the estimates of 3 steps or 4 steps transition probabilities for the EAF current sample.

Markov_1st_a3.m and *Markov_1st_aD.m* (updated for drawing figure)—Section 3.4.2

Basic first order Markov-like model for EAF current. It divides the data into two samples. For each sample, the program first builds the model, then finds the stationary distribution of the model. After that, compares their statistical characteristics through figures and indices. The detail steps for building such a model is described in Section 3.3. Also, Figure 3.4 gives the flow chart for building the model and Figure 3.5 illustrates the procedures to compute the stationary distribution.

Input: Sample current data file such as `part_curr*.txt` or `test_curr*.txt`.

Output: `Markov_i_1st.txt`, which lists all the non-zero elements of the estimates for transition matrix from the EAF current sample and statistical indices for the sample EFFs and stationary distribution for the Markov model.

`Figures` that show the EFFs and ECDFs of the samples and stationary distribution for the Markov model.

Markov_2nd_a3.m & *Markov_2nd_aD.m* (updated for drawing figure)—Section 3.4.5

This program build basic second order Markov-like model for EAF current. It divides the data into two samples. For each sample, the program first builds the model, then finds the stationary distribution of the model. After that, compares their statistical characteristics through figures and indices. The detail steps for building such a model can also be referred to Section 3.3. The flow chart of it is shown in Figure B.1, with the dimension of the transition matrix squared as to the first order model.

Input: Sample current data file such as `part_curr*.txt` or `test_curr*.txt`.

Output: Markov_i_2nd.txt, which lists all the non-zero elements of the estimates for transition matrix from the EAF current sample and statistical indices for the sample EFFs and stationary distribution for the Markov model.

`Figures` that show the EFFs and ECDFs of the samples and stationary distribution for the Markov model.

Markov_1st_v2.m & *Markov_1st_vD.m* (updated for drawing figures)—Section 3.4.2
Basic first order Markov-like model for EAF voltage, It divides the data into two samples. For each sample, the program first builds the model, then finds the stationary distribution of the model. After that, compares their statistical characteristics through figures and indices. Similarly, one can refer to Section 3.3, Figure 3.4 and Figure 3.5 for the detail steps to build such a model.

Input: Sample voltage data file such as `part_vol*.txt` or `test_vol*.txt`.

Output: `Markov_v_1st.txt`, which lists all the non-zero elements of the estimates for transition matrix from the EAF current sample and statistical indices for the sample EFFs and stationary distribution for the Markov model.
`Figures` that show the EFFs and ECDFs of the samples and stationary distribution for the Markov model.

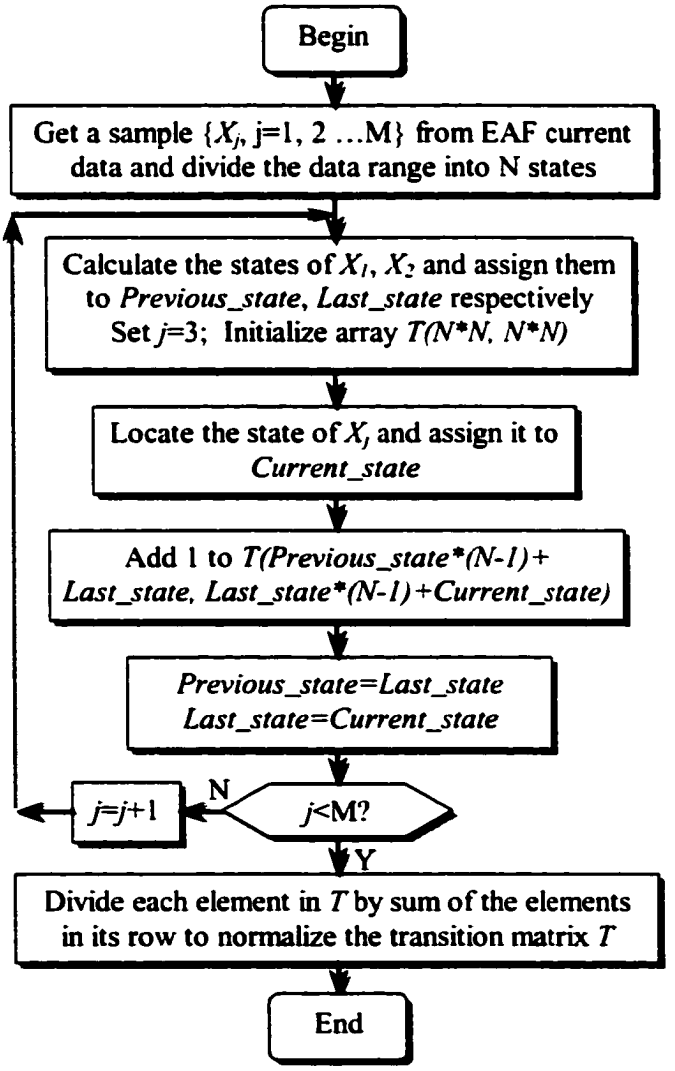

Figure B.1 Flow chart of building a second order Markov model

stationary_test.m — Section 3.4.6

Test the stationarity of the EAF time series in a classic time series framework by evaluating the mean function and auto-covariance for different starting time T_start and shift time/lag H_delay.

Input: Sample current data file such as `part_curr*.txt` or `test_curr*.txt`.

Output: `Stationary_test.txt`, which lists some numeric values for Mean function and Auto-Covariance function at different starting time and shift time.

`Figures` that show the Mean function and Auto-Covariance function for different starting time and shift time.

Markov_1st_pre_E.m— Section 3.5

One-step-ahead prediction using basic first order Markov-like model for EAF current with Conditional Expectation technique. After building the model, the program predicts one point ahead with the information current state at each time step. Then make correction with the new information for prediction of next time step. The detail steps can be found in Figure 3.13.

Input: Sample current data file such as `part_curr*.txt` and `test_curr*.txt`.

Output: `Markov_1i_E.txt`, which is the prediction results related to the period of the actual current measurements `test_curr*.txt`.

`Markov_1i_E_sum.txt`, which generates the statistical indices such as mean, RMSE, %RMSE to judge the performance of one-step-ahead prediction by actual current data `test_curr*.txt`.

`Figures` that show some prediction results compared to the current field data.

Note: For programs used in prediction, some of their names contain "_E", which applied Conditional Expectation technique. While the ones with "_M" uses Maximum Probability technique. If there is no "_E" and "_M", they may use Monte Carlo technique. The corresponding Matlab codes for this are only 2 to 10 lines and are much similar for programs using the same techniques. So there are three programs associated with one prediction method. Only one of them listed in the following.

Markov_1st_prev_E.m— Section 3.5

One-step-ahead prediction using basic first order Markov-like model for EAF voltage with Conditional Expectation technique. The procedure is similar to that for program *Markov_1st_pre_E.m*.

Input: Sample voltage data file such as `part_vol*.txt` and `test_vol*.txt`.

Output: `Markov_1v_E.txt`, which is the prediction results related to the period of the actual voltage measurements `test_vol*.txt`.

`Markov_1v_E_sum.txt`, which generates the statistical indices such as mean, RMSE, %RMSE to judge the performance of one-step-ahead prediction from actual data `test_vol*.txt`.

`Figures` that show some prediction results compared to the actual voltage data.

Markov_1st_pre_vi_M.m— Section 3.5 and Section 5.1

One-step-ahead prediction for related EAF current and voltage using basic first order Markov-like model with maximum probability technique

Input: Sample current data files such as `part_curr*.txt`, `test_curr*.txt` and voltage data files such as `part_vol*.txt`, `test_vol*.txt`

Output: `Markov_1st_pre_vi.txt`, which is the prediction results related to the period of the actual current/voltage measurements `test_curr*.txt` and `test_vol*.txt`.
`Figures` that show some prediction results compared to the actual field data.

Markov_1st_pre_vi_E.m— Section 3.5 and 5.1

Prediction using basic first order Markov-like model for related EAF current and voltage (Conditional Expectation).

One-step-ahead prediction for related EAF current and voltage using basic first order Markov-like model with Conditional Expectation technique

Input: Sample current data files such as `part_curr*.txt`, `test_curr*.txt` and voltage data files such as `part_vol*.txt`, `test_vol*.txt`

Output: `Markov_1st_pre_vi_E.txt`, which is the prediction results related to the period of the actual current/voltage measurements `test_curr*.txt` and `test_vol*.txt`.
`Figures` that show some prediction results compared to the actual field data.

Markov_2nd_pre_E.m— Section 3.5 and 5.1

One-step-ahead prediction using basic second order Markov-like model for EAF voltage with Conditional Expectation technique.

Input: Sample current data file such as `part_curr*.txt` and `test_curr*.txt`.

Output: `Markov_2i_E.txt`, which is the prediction results related to the period of the actual current measurements `test_curr*.txt`.
`Markov_2i_E_sum.txt`, which generates the statistical indices such as mean, RMSE, %RMSE to judge the performance of one-step-ahead prediction by actual current data `test_curr*.txt`.
`Figures` that show some prediction results compared to the current field data.

Draw_previ_Point.m— Section 3.5 and 5.1

Draw the prediction from data basic Markov-like model for related i&v and basic Markov-like model for voltage and current separately.

Input: Sample test current/voltage data `test_curr*.txt` / `test_vol*.txt` and one-step-ahead prediction results `Markov_1i_E.txt` / `Markov_1v_E.txt`.

Output: `Figures` that show some one-step-ahead prediction results from Markov-like model on single voltage or current variable and related current and voltage variables, compared to the current field data.

B.3 Programs for Markov Models in Function Space

Markov_FS20iA.m— Section 4.2.3.1

Get the Fourier sequence (up to 20 order) for the EAF current historical data which is used to build the Markov-like model in function space for EAF current.

Input: Historical current data files such as `part_curr*.txt`.

Output: `partiA_FS20R.txt` and `partiA_FS20I.txt` which are respectively for the real and imaginary part of the Fourier series.

partof_FS20.m— Section 4.2.3.1

Get part of the Fourier sequence (less order) from previous results for EAF current.

Input: `partiA_FS20R.txt` and `partiA_FS20I.txt` which are respectively for the real and imaginary part of the Fourier series from the EAF current data.

Output: `partiA_FSxR.txt` and `partiA_FSxI.txt`, which are respectively for the real and imaginary part of the Fourier series with smaller order (x) of harmonics.

psb_iA_E.m— Section 4.3.1 and Section 4.3.4

One-cycle-ahead prediction EAF current by optimized function space Markov-like model with FFT decomposition using Conditional Expectation technique. Refer to Figure 4.5 for the procedures of this prediction.

Input: `partiA_FS20R.txt` and `partiA_FS20I.txt` which are respectively for the real and imaginary part of the Fourier series from the EAF current data.
Sample test current data such as `test_curr*.txt`

Output: `psb_iA*.txt`, which is the prediction results related to the period of the actual current measurements for test `test_curr*.txt`.
`psb_iA*_E_sum.txt`, which generates the statistical indices such as mean, RMSE, %RMSE to judge the performance of one-cycle-ahead prediction by actual current data `test_curr*.txt`.
`psb_iA*_tm.txt`, which reports the computational resources, such as memory and time, the prediction used.
`ref_iA_*P.txt/ref_iA_*.txt`, which records the predicted/actual fundamental frequency components cycle by cycle.
`psb_iA*_difP.txt/psb_iA*_difR.txt`, which gives the current that should be compensated cycle by cycle to make the current near the system side closer to sinusoidal waveform.
`Figures` that show some prediction results compared to the current field data as well as their spectrum, waveform of fundamental components for each cycle.

Markov_function_FSs_M.m— Section 4.3.1

One-cycle-ahead prediction EAF current by optimized function space Markov-like model with FFT decomposition using Maximum Probability technique. Refer to Figure 4.5 for the procedures of this prediction.

Input: `partiA_FSxR.txt` and `partiA_FSxI.txt` which are respectively for the real and imaginary part of the Fourier series up to x harmonics from the EAF current data.
Sample test current data such as `test_curr*.txt`

Output: `Markov_FSxM.txt`, which is the prediction results related to the period of the actual current measurements for test `test_curr*.txt`.
`Markov_FSxM _sum.txt`, which generates the statistical indices such as mean, RMSE, %RMSE to judge the performance of one-cycle-ahead prediction by actual current data `test_curr*.txt`.
`Markov_FSxM_tm.txt`, which reports the computational resources, such as memory and time, the prediction used.
`Figures` that show some prediction results compared to the current field data.

Markov_FS20v.m— Section 4.2.3.1

Get the Fourier sequence (up to 20 order) for the EAF voltage historical data which is used to build the Markov-like model in function space for it.

Input: Historical voltage data files such as `part_vol*.txt`.

Output: `partv_FS20R.txt` and `partv_FS20I.txt` which are respectively for the real and imaginary part of the Fourier series for EAF voltage.

partof_FS20v.m— Section 4.2.3.1

Get part of the Fourier sequence (less order) from previous results for EAF voltage.

Input: `partv_FS20R.txt` and `partv_FS20I.txt` which are respectively for the real and imaginary part of the Fourier series from the EAF voltage data.

Output: `partv_FSxR.txt` and `partv_FSxI.txt`, which are respectively for the real and imaginary part of the Fourier series with smaller order (x) of harmonics.

psb_vA_E.m — Section 5.2.2

EAF voltage one-cycle-ahead prediction using function space Markov-like model using FFT frequency decomposition with Conditional Expectation technique

Input: `partv_FS20R.txt` and `partv_FS20I.txt` which are respectively for the real and imaginary part of the Fourier series from the EAF current data.

Sample test voltage data such as `test_vol*.txt`

Output: `psb_vA*.txt`, which is the prediction results related to the period of the actual voltage measurements for test `test_vol*.txt`.

`psb_vA*_E_sum.txt`, which generates the statistical indices such as mean, RMSE, %RMSE to judge the performance of one-cycle-ahead prediction by actual voltage data `test_vol*.txt`.

`psb_vA*_tm.txt`, which reports the computational resources, such as memory and time, the prediction used.

`ref_vA_*P.txt/ref_vA_*.txt`, which records the predicted/actual fundamental frequency components cycle by cycle.

`psb_vA*_difP.txt/psb_vA*_difR.txt`, which gives the voltage values that should be compensated cycle by cycle to make the voltage near the system side closer to sinusoidal waveform.

`Figures` that show some prediction results compared to the voltage field data as well as their spectrum, waveform of fundamental components for each cycle.

Markov_function_FSvi_M.m— Section 5.2

One-cycle-ahead prediction by function space valued Model for related current and voltage using FFT decomposition with Maximum Probability technique. Refer to Figure 5.4 for the procedures of this prediction.

Input: `partiA_FSxR.txt` and `partiA_FSxI.txt`, which are respectively for the real and imaginary part of the current Fourier series with up to x of harmonics.

`partv_FSxR.txt` and `partv_FSxI.txt`, which are respectively for the real and imaginary part of the voltage Fourier series with up to x of harmonics.

Sample test current data files such as `test_curr*.txt` and voltage data files such as `test_vol*.txt`.

Output: `markov_FS6Mvi*.txt`, which is the prediction results related to the period of the test current/voltage `test_curr*.txt/test_vol*.txt`.

`markov_FS6Mi*_sum.txt/markov_FS6Mv*_sum.txt`, which generates the statistical indices such as mean, RMSE, %RMSE to judge the performance of one-cycle-ahead prediction by test current/voltage field data `test_curr*.txt/test_vol*.txt`.

markov_FS6Mvi*_tm.txt, which reports the computational resources, such as memory and time, the prediction used.

Markov_function_FSvi_E.m— Section 5.2

One-cycle-ahead prediction by function space valued Model for related current and voltage using FFT decomposition with Conditional Expectation technique. Refer to Figure 5.4 for the procedures of this prediction.

Input: partiA_FSxR.txt and partiA_FSxI.txt, which are respectively for the real and imaginary part of the current Fourier series with up to x of harmonics.

partv_FSxR.txt and partv_FSxI.txt, which are respectively for the real and imaginary part of the voltage Fourier series with up to x of harmonics.

Sample test current data files such as test_curr*.txt and voltage data files such as test_vol*.txt.

Output: markov_FS6Mvi*_E.txt, which is the prediction results related to the period of the test current/voltage test_curr*.txt/test_vol*.txt.

markov_FS6Mi*_E_sum.txt/markov_FS6Mv*_E_sum.txt, which generates the statistical indices such as mean, RMSE, %RMSE to judge the performance of one-cycle-ahead prediction by test current/voltage field data test_curr*.txt/test_vol*.txt.

markov_FS6Mvi*_E_tm.txt, which reports the computational resources, such as memory and time, the prediction used.

Draw_previ.m— Section 5.2

Draw the prediction data by function space valued Model for related current and voltage altogether with prediction results by function space valued Model for voltage and current separately.

Input: Sample test current/voltage data test_curr*.txt/test_vol*.txt and one-cycle-ahead prediction results markov_FS6Mvi*_E.txt for related current and voltage, psb_iA*.txt for current, and psb_vA*.txt for current.

Output: Figures that show some one-cycle-ahead prediction results from Markov-like model on single voltage or current variable and related current and voltage variables, compared to the current field data.

independence_test3.m— Section 5.3

Test the independence of the EAF current and voltage.

Input: partiA_FS20R.txt and partiA_FS20I.txt, which are respectively for the real and imaginary part of the current Fourier series with up to 20 of harmonics.

partv_FS20R.txt and partv_FS20I.txt, which are respectively for the real and imaginary part of the voltage Fourier series with up to 20 of harmonics.

Output: independence_test3.txt, which is the results of independence test for time shift h up to 167.

Markov_abc.m — Section 4.2.3.2 and Section 4.3.1

Obtain the polynomial coefficients sequence from the EAF current (for polynomial fit approximations in function space Markov model) when a cycle is a fixed period (e.g. 167 points)

Input: Historical current data files such as part_curr*.txt.

Output: part_abc.txt, which is the polynomial coefficients for the EAF historical data cycle by cycle where the cycle length is fixed.

Figures that show the sequence of each order of polynomial coefficients.

Markov_abcC.m— Section 4.2.3.2 and Section 4.3.1

Obtain the polynomial coefficients sequence from the EAF current (for polynomial fit approximations in function space Markov model) when a cycle is the interval between two consecutive zero-crossing points which go from negative to positive.

Input: Historical current data files such as part_curr*.txt.

Output: part_abcC.txt, which is the polynomial coefficients for the EAF historical data cycle by cycle, where the cycle length is random.

Figures that show the sequence of each order of polynomial coefficients.

Markov_Frequency.m— Section 4.2.3.4 and Section 4.3.1

Obtain the cycle length sequence from the EAF current (in point) for some approximations in function space Markov model

Input: Historical current data files such as part_curr*.txt.

Output: part_frequency_dots.txt, which is the cycle length for the EAF historical data for two consecutive positive zero-crossing points.

part_frequency_sum.txt, which gives some statistical indices such as mean, variance, maximum and minimum for the part_frequency_dots.txt data.

Figures that show the variation of the cycle length.

Markov_function_abc_M.m/Markov_function_abcC_M.m— Section 4.2.3.2 and Section 4.3.1

Prediction by function space valued Model for current using polynomial fit (without pattern index) with Maximum Probability technique. The first program uses fixed cycle length while the latter one uses random one. The program can be easily modified for Conditional Probability technique by changing 1-2 lines of the related code. Refer to Figure 4.6 for the procedures of this prediction

Input: part_abc.txt/part_abcC.txt from programs *Markov_abc.m /Markov_abcC.m.*

part_frequency_dots.txt from the result of program *Markov_Frequency.m*

test_curr*.txt, which is current test data files.

Output: markov_abcM.txt/markov_abcCM.txt, which are the prediction results related to the period of the actual current measurements for test test_curr*.txt.

markov_abcM_sum.txt/markov_abcCM_sum.txt, which generate the statistical indices such as mean, RMSE, %RMSE to judge the performance of one-cycle-ahead prediction by actual data test_curr*.txt.

Markov_abc_S.m— Section 4.2.3.2 and Section 4.3.1

Obtain the polynomial coefficients sequence from the EAF current (for polynomial fit approximations with pattern index in function space Markov model)

Input: part_abcC.txt from the result of program *Markov_abcC.m.*

Output: abc_u2i.txt, which lists the patterns for polynomial coefficients.

abc_s_u2i.txt, which is the sequence of the polynomial patterns cycle by cycle.

Markov_function_abcP_M.m— Section 4.2.3.2 and Section 4.3.1

Prediction by function space valued Model for current using polynomial fit (with pattern index) with Maximum Probability technique. The program can be modified for Conditional Probability technique by changing 1-2 lines of the related code.

Input: abc_u2i.txt and abc_s_u2i.txt from programs *Markov_abc_S.m.*

part_frequency_dots.txt from the result of program *Markov_Frequency.m*

test_curr*.txt, which is current test data files.

Output: markov_abcPM.txt, which are the prediction results related to the period of the actual current measurements for test test_curr*.txt.

markov_abcPM_sum.txt, which generate the statistical indices such as mean, RMSE, %RMSE to judge the performance of one-cycle-ahead prediction by actual data test_curr*.txt.

markov_abcPM_tm.txt, which reports the computational resources, such as memory and time, the prediction used.

Markov_envelope.m— Section 4.2.3.4 and Section 4.3.1

Obtain the maxima and minima sequence from the EAF current for some approximations in function space Markov-like model such as f(Max,Min,position)

Input: Historical current data files such as part_curr*.txt.

Output: part_maxmini.txt, which records the Maximum and Minimum of each cycle, which is the interval between two consecutive positive zero-crossing points.

part_maxmini_sum.txt which gives some statistical indices such as mean, variance, maximum and minimum for the part_maxmini.txt data.

Figures that show the variation of the maxima and minima.

Markov_function_FS_mc.m— Section 4.2.3.4 and Section 4.3.1

One-cycle-ahead prediction by function space valued Markov-like model with FFT decomposition for EAF current using Monte Carlo technique.

Input: partiA_FSxR.txt and partiA_FSxI.txt, which are respectively for the real and imaginary part of the current Fourier series with up to x of harmonics.

test_curr*.txt, which is current test data files.

Output: markov_FSxh.txt, which are the prediction results related to the period of the actual current measurements for test test_curr*.txt.

markov_FSxh_sum.txt, which generate the statistical indices such as mean, RMSE, %RMSE to judge the performance of one-cycle-ahead prediction by actual data test_curr*.txt.

markov_FSxh_tm.txt, which reports the computational resources, such as memory and time, the prediction used.

Figures that show the performance of prediction results.

Markov_frame2.m/ Markov_frame3.m — Section 4.2.3.4 and Section 4.3.1

Prepare the (Max, Min)/(Max, Min, Cycle Length) sequence for the f{(Min, Max), Cycle length, shape}/ f{(Min, Max, Cycle length), shape} approximations

Input: part_maxmini.txt which is the Maximum and Minimum sequence cyclically.

part_frequency_dots.txt (for *Markov_frame3.m* only), cycle length from *Markov_Frequency.m*

Output: frame_u2i.txt/frame3_u2i.txt, which lists the patterns for Maximum and Minimum (/and Cycle length).

frame_s_u2i.txt/frame3_s_u2i.txt, which is the sequence of (Max, Min)/ (Max, Min, Cycle length) patterns cycle by cycle.

Markov_uniform_data4.m— Section 4.2.3.4 and Section 4.3.1

Make the amplitude of each cycle to be the same (uniform) by multiplying a ratio and modify the time series of this cycle by the ratio accordingly for preparation of shape sequence as described in Table 4.3.

Input: Historical current data files such as `part_curr*.txt`.

Output: `part_uniformi.txt`, which is the modified data for the historical EAF current with the amplitude of each cycle to be the same.

Markov_shape.m— Section 4.2.3.4 and Section 4.3.1

Prepare the shape sequence of each cycle for the f{(Min,Max), length, shape} approximation.

Input: `part_uniformi.txt` which is the result from *Markov_uniform_data4.m.*

Output: `shape_u2i.txt`, which lists the patterns for shape of cycles in the data `part_uniformi.txt`.

`shape_s_u2i.txt`, which is the sequence of the shape patterns cycle by cycle.

Markov_function_1frame_M.m— Section 4.2.3.4 and Section 4.3.1

Prediction using function space valued Markov-like model with f{Min, Max, cycle length, shape} for EAF current (Maximum Probability)

Input: `shape_u2i.txt` and `shape_s_u2i.txt`, shapes from *Markov_shape.m.*

`part_uniformi.txt`, modified data from *Markov_uniform_data4.m.*

`part_frequency_dots.txt`, cycle length from *Markov_Frequency.m*

`test_curr*.txt`, which is current test data files.

Output: `markov_1frame.txt`, which are the prediction results related to the period of the actual current measurements for test `test_curr*.txt`.

`markov_1frame_sum_M.txt`, which generate the statistical indices such as mean, RMSE, %RMSE to judge the performance of one-cycle-ahead prediction by actual data `test_curr*.txt`.

`markov_1frame_tm_M.txt`, which reports the computational resources, such as memory and time, the prediction used.

`Figures` that show the performance of prediction results.

Markov_function_2frame_M.m/ Markov_function_3frame_M.m — Section 4.2.3.4 and Section 4.3.1

Prediction using function space valued Markov-like model with f{(Min, Max), cycle length, shape}/ f{(Min, Max, Cycle length), shape} for EAF current (Maximum Probability)

Input: `shape_u2i.txt` and `shape_s_u2i.txt`, shapes from *Markov_shape.m.*

`frame_u2i.txt/frame3_u2i.txt` and `frame_s_u2i.txt/frame3_s_u2i.txt`, which are the pattern information for f{(Min, Max),cycle length, shape}/f{(Min, Max, cycle length), shape}.

`part_frequency_dots.txt`, cycle length from *Markov_Frequency.m*

`test_curr*.txt`, which is current test data files.

Output: `markov_2fraM.txt/markov_3fraM.txt`, which are the prediction results related to the period of the actual current measurements for test `test_curr*.txt`.

`markov_2fraM_sum.txt/markov_3fraM_sum.txt`, which generate the statistical indices such as mean, RMSE, %RMSE to judge the performance of one-cycle-ahead prediction by actual data `test_curr*.txt`.

`markov_2fraM_tm.txt/markov_3fraM_tm.txt`, which reports the computational resources, such as memory and time, the prediction used.

`Figures` that show the performance of prediction results.

Markov_function_3frame_noC3_M.m/Markov_function_3frame_noC12_M.m— Section 4.2.3.4 and Section 4.3.2

3/12 cycles ahead prediction using function space valued Markov-like model with f{(Min, Max, cycle length), shape} for EAF current (with Maximum Probability prediction technique)

Input: `shape_u2i.txt` and `shape_s_u2i.txt`, shapes from *Markov_shape.m*.

`frame3_u2i.txt` and `frame3_s_u2i.txt`, which are the pattern information for f{(Min, Max),cycle length, shape}/f{(Min, Max, cycle length), shape}.

`part_frequency_dots.txt`, cycle length from *Markov_Frequency.m*

`test_curr*.txt`, which is current test data files.

Output: `markov_3fraM_noC3.txt/ markov_3fraM_noC12.txt`, which are the 3/12 cycles ahead prediction results related to the period of the actual current measurements for test `test_curr*.txt`.

`markov_3fraM_noC3_sum.txt/markov_3fraM_noC12_sum.txt`, which generate the statistical indices such as mean, RMSE, %RMSE to judge the performance of 3/12 cycles ahead prediction by actual data `test_curr*.txt`.

`markov_3fraM_noC3_tm.txt/markov_3fraM_noC12_tm.txt`, which reports the computational resources, such as memory and time, the prediction used.

`Figures` that show the performance of prediction results.

Markov_function_2frame_noC3_M.m/Markov_function_2frame_noC12_M.m— Section 4.2.3.4 and Section 4.3.2

Prediction using function space valued Markov-like model with f{(Min,Max),cycle length, shape} for EAF current 3/12 cycles ahead (with Maximum Probability prediction technique).

Input and Output: They are similar to that for *Markov_function_2frame_M.m*, except that the output is results from 3/12 cycles ahead prediction, which has `_noC3/_noC12` in the file names.

Markov_function_abcP_noC3_M.m/Markov_function_abcP_noC12_M.m— Section 4.2.3.4 and Section 4.3.2

3/12 cycles ahead prediction using function space valued Markov-like model with polynomial fit with pattern index for EAF current (with Maximum Probability prediction technique).

Input and Output: They are similar to that for *Markov_function_abcP_M.m*, except that the output is results from 3/12 cycles ahead prediction, which has `_noC3/_noC12` in the file names.

Markov_function_FSs_noC3_M.m/Markov_function_FSs_noC12_M.m— Section 4.2.3.4 and Section 4.3.2

3/12 cycles ahead prediction using function space valued Markov-like model with FFT frequency decomposition with 7 harmonics for EAF current (with Maximum Probability prediction technique).

Input and Output: They are similar to that for *Markov_function_FSs_M.m*, except that the output is results from 3/12 cycles ahead prediction, which has `_noC3`/`_noC12` in the file names.

trans_ratioI.m— Section 4.3.1

Transfer some results from previous prediction based on recorded data to the actual unit considering the ratio (400:1) of the actual EAF current to recorded data for it. It also generated more indices such as %RMSE.

trans_ratioV.m— Section 4.3.1

Transfer some results from previous prediction based on recorded data to the actual unit considering the ratio (10000:1) of the actual EAF voltage to recorded data for it. It also generated more indices such as %RMSE.

B.4 Programs for Harmonic Compensation

text2matB.m— Section 6.3

Transfer the EAF data from txt format to mat format for sake of compensation in simulink. S-functions in Simulink or power system blockset requires the input file to be .mat format with the first row to be the time steps and the rest rows to be the actual data correspond to the time steps.

Input: Result files from *psb_iA.m* such as `ref_iA_*P.txt` (reference), `psb_iA_difP.txt` (expected compensation) and `psb_iA.txt`(prediction results).
`test_vol*.txt`, which is voltage test data files.
`test_curr*.txt`, which is current test data files.

Output: Mat files for prediction results, such as `ref_iA_*P.mat` and `psb_iA.mat`.
`uncom_v.mat`, which is voltage test data files.
`uncom_i.mat`, which is current test data in .mat format.

Tr_signalR.m— Section 6.3

The s-function used by Simulink for generating the signal to trigger the STACOM based on function space valued Markov-like model with FFT frequency decomposition approximation.

Input: `uncom_i.txt`, which is current test data.

Output: Triggerring signals for the STATCOM (4 poles).
Current that is expected to be compensated by STATCOM.

phaseA_comRR.mdl—Section 6.2

Single-phase simulation module for harmonic compensation.

Input: `uncom_v.mat`, which is voltage test data.
`uncom_i.txt`, which is current test data.

Output: Voltage at PCC and STATCOM terminal, current compensated by the STATCOM and expected to be compensated, current before compensation and after compensation. Their waveforms are shown on Scope.

save_ws.m— Section 6.3

Save some of the data from the Scope in Simulink to a file named `sim_resultR.txt`.

Draw_com_iAR.m— Section 6.3

Draw the detail compensation data based on the simulation results `sim_resultR.txt` and perform frequency domain analysis.

get_DataABC.m, get_testDataABC.m, Markov_FS20iABC.m, psb_E_iABC.m—Section 6.4

These programs are similar to *get_Data.m, get_testData.m, Markov_FS20i.m, psb_iA.m* except that they are for three phases.

text2matABC.m— Section 6.4

Transfer the 3 phases EAF data from txt format to mat format for sake of compensation in simulink.

Input: Result files from *psb_E_iABC.m* such as `psb_A_difP.txt`, expected compensation for phase A.

`test_volA*.txt`, `test_volB*.txt`, `test_volC*.txt`, which are three-phase voltage test data files.

`test_currA*.txt`, `test_currB*.txt`, `test_currC*.txt`, which are three phases current test data files.

Output: Mat files for prediction results, such as `psb_ABC_difR.mat`.

`uncom_vABC.mat`, which is three phases voltage test data.

`uncom_iABC.mat`, which is three phases current test data in .mat format.

signalR_3p.m— Section 6.4

The s-function used by Simulink for generating the signal to trigger the 3 phases STACOM based on function space valued Markov-like model with FFT frequency decomposition approximation.

Input: `uncom_iABC.txt`, which is 3 phases current test data.

Output: Triggerring signals for the STATCOM (6 poles).

Current that is expected to be compensated by STATCOM.

comR_3phase.mdl— Section 6.4

Three phases simulation module for harmonic compensation.

Input: `uncom_vABC.mat`, which is voltage test data.

`uncom_iABC.txt`, which is current test data.

Output: three phases current before compensation and after compensation. Their waveforms are shown on Scope.

save_wsABC.m— Section 6.4

Save some of the three phases data from the Scope in Simulink to a file named `sim_resultABC.txt`.

REFERENCES

[1] G. Chen, X. Dong, *From chaos to order: methodologies, perspectives, and applications*, World Scientific, Singapore; River Edge, NJ, 1998, pp.1-32.

[2] R. Nadira, P. B. Usoro, "Self-Adjusting Model Algorithmic Control Of A Three-Phase Electric Arc Furnace," *J Dyn Syst Meas Control Trans-ASME*, vol. 110, no. 4, Dec. 1988, pp. 361-366.

[3] B. Read, "Reducing Flicker and harmonics from EAFs", *New Steel*, Jan. 1996, pp. 30-34.

[4] P. Kundur, *Power system stability and control*, McGraw-Hill Press, New York, 1994. pp. 272-311.

[5] S. Z. Zhu, Z. Y. Dong, K. P. Wong, Z. H. Wang, "Power system dynamic load identification and stability", *Power System Technology, 2000. Proceedings of International Conference on PowerCon*, Vol. 1, 2000, pp. 13-18.

[6] L. L. Grigsby, *The electric power engineering handbook*, CRC Press, IEEE Press, New York, 2001, pp. (6-1)-(6-20).

[7] A. Sarshar, R. Sharp, R. Iravani, "Analyses of Harmonic and Transient Phenomena Due to Operation of an ac Arc Furnace", *Iron and Steel Engineer*, April 1996, pp. 78-82.

[8] H. Schau, D. Stade, "Mathematical Modeling of Three-phase Arc Furnace", *Proceedings of IEEE International Conference on Harmonics in Power Systems*, vol. 1., Bologna, September 21-23, 1994, pp. 422-428.

[9] G. C. Montanari, M. Loggini, A. Cavallini, L. Pitti, D. Zaninelli, "Arc Furnace Model for the Study of Flicker Compensation in Electrical Networks," *IEEE Transactions on Power Delivery*, vol. 8, no. 4, Oct. 1994, pp. 2026-2036.

[10] E. O'Neill-Carrillo, G. Heydt, E. J. Kostelich, S. S. Venkata, A. Sundaram, "Nonlinear Deterministic Modeling of Highly Varying Loads," *IEEE Transactions on Power Delivery*, vol. 14, no. 2, April, 1999, pp. 537-542.

[11] K. B. Athreya, F. Chen, V. V. Sastry, S. S. Venkata, "A Robust Markov-Like Model For Three-phase Arc Furnaces", submitted to *Technometrics*, February 2002.

[12] G. Manchur and C. C. Erven, "Development of a Model for Predicting Flicker from Electric Arc Furnace", *IEEE Trans. on Power Delivery*, vol. 7, No. 1, January 1992, pp. 416-426.

[13] S. Varadan, E. B. Makram, A. A. Girgis, "A New Time Domain Voltage Source Model for an Arc Furnace using EMTP," *IEEE Transactions on Power Delivery*, vol. 11, no. 3, July 1996, pp. 1685-1691.

[14] R. C. Dugan, "Simulation of Arc Furnace Power Systems", *IEEE Trans. on Industry Applications*, vol. IA-16, no. 6, November 1980, pp. 813-818.

[15] J. G. Mayordomo, L. F. Beites, R. Asensi, M. Izzeddine, L. Zabala, J. Amantegui, "A Frequency Domain Arc Furnace Model For Harmonic Power Flows Under Balanced Conditions", *Proceedings of the 7th International Conference on Harmonics and Quality of Power*, Las Vegas, Oct. 1996, pp. 419-427.

[16] J. G. Mayordomo, L. F. Beites, R. Asensi, M. Izzeddine, L. Zabala, J. Amantegui, "A New Frequency Domain Arc Furnace Model For Iterative Harmonic Analysis," *IEEE Transactions on Power Delivery*, v 12 n 4, Oct 1997, pp. 1771-1778.

[17] T. Wu, W. Song, Y. Zhang, "A New Frequency Domain Method for the Harmonics Analysis of Power System with Arc Furnace", *Proceedings of the 4th International Conference on Advance in Power System Control, Operation and Management, APSCOM-97*, Hong Kong, November 1997, pp.552-555.

[18] A. R. Sadeghian, I. D. Lavers, "Application of Radial Basis Functions to Model Electric Arc Furnace", *Proceeding of International Joint Conference on Neural Networks*, Washington, DC, July 1999, pp. I-115-120.

[19] A. R. Sadeghian, I. D. Lavers, "Nonlinear Black-Box Modeling of Electric Arc Furnace: An Application of Fuzzy Logic Systems", *IEEE 1999 International Fuzzy Systems Conference Proceedings*, Seoul, Korea, August 1999, pp. I-234-239.

[20] P. E. King, T. L. Ochs, A. D. Hartman, "Chaotic Responses in Electric Arc Furnaces," *Journal of Applied Physics*, vol. 76, no. 4, Aug. 1994, pp. 2059-2065.

[21] R. Y. Zhao, "Chaos in electric arc furnaces", MSEE project, Purdue University, West Lafayette, IN, 1994.

[22] C. Tan, M. Verghese, P. Varaiya, F. Wu, "Bifurcation, Chaos, and Voltage Collapse in Power Systems," *Proceedings of the IEEE*, vol. 83, no. 11, Nov. 1995, pp. 1484-1496.

[23] P. Varaiya, F. Wu., H. D. Chiang, *Bifurcations and Chaos in Power Systems: A Survey*, EPRI Report, TR-100834, Aug. 1992.

[24] G. Jang, W. Wang, S. S. Venkata, E. O'Neill-Carrillo, G. T. Heydt, "Electric Arc Furnaces: Chaotic Load Models and Transient Analysis," *Lescope Conference*, Halifax, Nova Scotia, July 1998, pp. 84-88

[25] B. A. Mork, D. L. Stuehm, "Application of Nonlinear Dynamics and Chaos to Ferroresonance in Distribution Systems," *IEEE Transactions on Power Delivery*, vol. 9, no. 2, April 1994, pp. 1009-1017.

[26] E. Acha, A. Semlyen, N. Rajakovic, "A Harmonic Domain Computational Package for Nonlinear Problems and its Application to Electric Arcs", *IEEE Transactions on Power Delivery*, vol. 5, no. 3, July 1990, pp. 1390-1395.

[27] L. Tang, S. Kolluri, M. F. McGranaghan, "Voltage Flicker Prediction For Two Simultaneously Operated ac Arc Furnaces," *IEEE Transactions on Power Delivery*, vol. 12, no. 2, Apr. 1997, pp. 985-992.

[28] A. A. Girgis, B. D. Moss, E. B. Makram, "Reactive Power Compensation and Voltage Flicker Control of an Arc Furnace Load", *Proceedings of the 7th International Conference on Harmonics and Quality of Power(ICHQP)*, Las Vegas, Oct. 1996, pp. 242-247.

[29] Juan Celada S., "Electrical Analysis of the Steel Melting Arc Furnace," *Iron and Steel Engineer*, May 1993, pp. 35-39.

[30] G. T. Heydt, *Electric Power Quality*, 2nd ed., Scottsdale, Stars in a Circle Publication, 1995. pp. 30-55, 194-198.

[31] G. T. Heydt, E. O'Neill-Carrillo, R. Y. Zhao, "The Modeling of Nonlinear Loads as Chaotic Systems in Electric Power Engineering," *Proceedings of the 7th International Conference on Harmonics and Quality of Power*, Las Vegas, Oct. 1996, pp. 704-711.

[32] A. A. Mahmoud, "Modeling of a Resistance Regulated Arc furnace," *IEEE Transaction on Power Apparatus and Systems*, vol. PAS-104, no. 1, Jan. 1985, pp. 58-66.

[33] R. Collantes, T. Gómez, "Identification and Modeling of a Three-phase Arc Furnace for Voltage Disturbance Simulation," *IEEE Transactions on Power Delivery*, vol. 12, no. 4, Oct. 1997, pp. 1812-1817.

[34] VHARM, The Harmonic Verdict, *Power Systems Harmonics and Simulations Program, User Manual*, ver 3.4, Mc-Graw-Edison Power System Div. Of Cooper Industries, Cannonsburg, PA, July 1987.

[35] T. Zheng, E. B. Makram, A. A. Girgis, "Effect of different Arc Furnace Models on Voltage Distortion", *Proceedings of the 8th International Conference on Harmonics and Quality of Power(ICHQP)*, Athens, Greece, Oct. 1998, pp. 1079-1085.

[36] A. V. Mamishev., B. D. Russell, C. L. Benner, "Analysis of High Impedance Faults Using Fractal Techniques," *IEEE Transactions on Power Systems*, vol. 11, no. 1, Feb. 1996, pp. 435-440.

[37] R. L. Devaneg, *A First Course in Chaotic Dynamical Systems*. New York: Addison-Wesley Publishing Company, Inc., 1992, pp. 15-68.

[38] O. Ozgun, A. Abur, "Development of Arc Furnace Model for Power Quality Studies", *IEEE Power Engineering Society Summer Meeting*, Edmonton, Alberta, Canada, vol: 1 , July 1999 , pp. 507–511.

[39] K. B. Athreya, "Random Iterations: An Alternative to Deterministic Chaos Approach to Modeling", Preprint, Department of Mathematics, Iowa State University, 1999.

[40] K. B. Athreya and G. Atuncar, "Kernel Estimation for Real Valued Markov-like Chains, Sankhya", *The Indian Journal of Statistics*, 1009, Vol. 60, Series A, Part 1, pp.1-17, 1998.

[41] A. M. Stankovic and E. A. Marengo, "A Dynamic Characterization of Power System Harmonics Using Markov Chains", *IEEE Trans. On Power Systems*, vol. 13, no.2, May 1998, pp. 441-448.

[42] I. L. MacDonald and W. Zucchini, *Hidden Markov-like and Other Models for Discrete–valued Time Series*, First edition, Chapman & Hall, London, 1997, pp. 12-13.

[43] P. Hoel, S. C. Port, C. J. Stone, *Introduction to stochastic processes*, Houghton Mifflin Company, Boston, 1972, pp. 1-25, 40-52, 85-92.

[44] M. Kijima, *Markov processes for stochastic modeling*, First Edition, Chapman & Hall, London, 1997, pp. 3-6, 13-19.

[45] W. F. Stewart, *Introduction to the Numerical Solution of Markov-like Chain*, Princeton University Press, Princeton, New Jersey, 1994. pp. 5-22.

[46] W. Charytoniuk, M. S. Chen and P. Van Olinda, "Non parametric regression based short-term load forecasting", *IEEE Trans. on Power Systems*, vol. 13, no. 3, Aug 1998, pp. 725-730

[47] IEEE task force on harmonics modeling and simulation," Modeling and simulation of the propagation of harmonics in electric power networks, I. Concepts, models, and simulation techniques, II. Sample systems and examples ", *IEEE Trans. on Power Delivery*, vol. 11, no. 1, Jan. 1996, pp. 452-465.

[48] P. Sprent, *Applied Nonparametric Statistical Methods*, Second Edition, Chapman & Hall, 1993, pp. 1-8.

[49] J. D. Gibbons, *Nonparametric Methods for Quantitative Analysis*, Second Edition, American Sciences Press, Inc., 1985, pp.1-28.

[50] P. J. Brockwell, R. A. Davis, *Introduction To Time Series And Forecasting*, Springer-Verlag, New York, 1996, pp.5-77, 135-169, 222-275, pp. 12-85, 135-169, 260-275.

[51] P. J. Brockwell, R. A. Davis, *ITSM for Windows*, software contained in the text [50], Springer-Verlag, New York, 1996.

[52] J. D. Hamilton, *Time series analysis*, Princeton University Press, Princeton, N.J, 1994, pp. 2-50.

[53] B. L. Bowerman and R. T. O'Connell, *Forecasting and Time Series: an Applied Approach*, Duxbury Press, N. Scituate, MA, 1979, pp. 2-22, 291-330.

[54] R. W. Ramirez, *The FFT, fundamentals and concepts*, Prentice-hall, Inc, London, 1985, pp. 63-82.

[55] C. Gasquet, P. Witomski, *Fourier Analysis and Application: Filtering, Numerical Computation, Wavelets*, Springer-Verlag, New York, Inc, 1998, pp. 68-72.

[56] J. S. Waler, *Fast Fourier Transforms*, CRC Press, Inc, 1991, pp. 49-75.

[57] Y. H. Song, A. T. Johns, Flexible ac transmission systems (FACTS), *Institution of Electrical Engineers*, London, 1999. pp. 159-172.

[58] C. Schauder, STATCOM for compensation of large electric arc furnace installations, *IEEE Power Engineering Society Summer Meeting*, Edmonton, Alberta, Canada, Vol. 2, July 1999, pp. 1109-1112.

[59] N. R. Raju, *A Decoupled Converter Topology for Active Compensation of Power Systems*, PhD Dissertation, University of Washington, 1996. pp.20-22.

[60] IEEE Standard 519-1992, "IEEE Recommended Practices and Requirements for Harmonic Control in Electrical Power Systems," New York, 1992. pp. 5-9.

[61] J. D. Lavers, P. P. Biringer, "Real-Time Measurement of Electric Arc-Furnace Disturbances and Parameter Variations," *IEEE Transactions on Industry Applications*, vol. IA-22, no. 4, July/August 1986, pp. 568-576.

[62] A. Sarshar, M. Sharp, R. M. Iravani, "Analyses of Harmonic and Transient Phenomena due to Operation of an ac Arc Furnace," *Iron and Steel Engineer*, April 1996, pp. 78-82.

[63] A. Nabae, M. Yamaguchi, "Suppression of Flicker in an Arc-Furnace Supply System by an Acive Capacitance-A Novel Voltage Stabilizer in Power Systems," *IEEE Transactions on Industry Applications*, vol. 31, no. 1, Jan./Feb. 1995, pp. 107-111.

[64] C. Gilker, S. R. Mendis, M. T. Bishop, "Harmonic analysis in Electric Arc Furnace Steelmaking Facilities," *Iron and Steel Engineer*, May 1993, pp. 40-44.